



# The komatiite testimony to ancient mantle heterogeneity

Igor Puchtel, Janne Blichert-Toft, Mary Horan, Mathieu Touboul, Richard Walker

## ► To cite this version:

Igor Puchtel, Janne Blichert-Toft, Mary Horan, Mathieu Touboul, Richard Walker. The komatiite testimony to ancient mantle heterogeneity. *Chemical Geology*, 2022, 594, pp.120776. 10.1016/j.chemgeo.2022.120776 . hal-03589592

**HAL Id: hal-03589592**

**<https://hal.science/hal-03589592>**

Submitted on 25 Feb 2022

**HAL** is a multi-disciplinary open access archive for the deposit and dissemination of scientific research documents, whether they are published or not. The documents may come from teaching and research institutions in France or abroad, or from public or private research centers.

L'archive ouverte pluridisciplinaire **HAL**, est destinée au dépôt et à la diffusion de documents scientifiques de niveau recherche, publiés ou non, émanant des établissements d'enseignement et de recherche français ou étrangers, des laboratoires publics ou privés.

# The Komatiite Testimony to Ancient Mantle Heterogeneity

Igor S. Puchtel<sup>1\*</sup>, Janne Blichert-Toft<sup>2</sup>, Mary F. Horan<sup>3</sup>,  
Mathieu Touboul<sup>2</sup>, and Richard J. Walker<sup>1</sup>

<sup>1</sup>Department of Geology, University of Maryland, 8000 Regents Drive, College Park, MD 20742, USA

<sup>2</sup>Laboratoire de Géologie de Lyon, Ecole Normale Supérieure de Lyon, CNRS UMR 5276, Université de  
Lyon, 46 Allée d'Italie, 69007 Lyon, France

<sup>3</sup>Earth and Planets Laboratory, Carnegie Institution for Science, 5241 Broad Branch Road NW, Washington,  
DC 20015, USA

\*Corresponding author: [ipuchtel@umd.edu](mailto:ipuchtel@umd.edu)

Revised for:

*Chemical Geology*

Invited Review Manuscript

Version: February 06, 2022

Keywords: Komatiites; early Earth; mantle heterogeneity; Hf-W, Sm-Nd, Lu-Hf, Re-Os, Pt-Os isotope systems; highly siderophile elements; grainy late accretion; primordial magma ocean, core-mantle interaction; mixing times of the mantle; Nd-Hf-Os isotope paradox.

## Abstract

Komatiites are crystallized samples of high-temperature, high-MgO lavas that were common during the Archean, but became increasingly rarer in the Proterozoic and Phanerozoic. Although the origin of komatiites remains a subject of debate, all komatiites included in this review, ranging in age from 3.6 to 2.0 Ga, are interpreted to have most likely been derived from anhydrous melting in mantle plumes. These plumes are estimated to have been initiated at different depths in the mantle, thus, providing important information about the chemical evolution of the early Earth.

The  $^{142,143}\text{Nd}$ ,  $^{176}\text{Hf}$ ,  $^{182}\text{W}$ ,  $^{187}\text{Os}$ , and  $^{186}\text{Os}$  systematics and trace- and highly siderophile element (HSE) abundances of these komatiites provide strong evidence for the presence of isotopic and chemical heterogeneities in the mantle during the first half of Earth history. These heterogeneities likely reflect the combined effects of: (1) the co-existence of diverse post-magma ocean silicate domains that were characterized by variably-fractionated lithophile and siderophile element abundances; (2) the presence of distinct reservoirs that included mantles and cores of late accreted, differentiated planetesimals; and (3) isotopic exchange across the core-mantle boundary. These data highlight the complexity of komatiite mantle sources, none of which were similar in composition to estimates for the modern bulk silicate Earth (BSE). Moreover, no single petrogenetic model can account for the remarkably diverse chemical and isotopic compositions of komatiites.

The disappearance of resolvable positive and negative  $^{142}\text{Nd}$  anomalies, as well as decoupled  $^{143}\text{Nd}$ - $^{176}\text{Hf}$  isotopic signatures, in the mafic-ultramafic rock record by  $\sim 2.5$  Ga indicate that, by the end of the Archean, the earliest silicate reservoirs, formed through primordial magma ocean crystallization, had been largely destroyed as a result of vigorous convective mantle mixing. This implies that, during the Hadean and Archean, it took the mantle  $\sim 1.5$  Ga to mix away the early formed  $^{142}\text{Nd}$  heterogeneities *via* wholesale mantle convection. Similar to  $^{142}\text{Nd}$  systematics, there appears to have been a shift from mostly positive  $^{182}\text{W}$  anomalies in pre-2.5 Ga komatiite mantle sources to no  $^{182}\text{W}$  offsets in post-2.5 Ga komatiite mantle sources. Coupled with the disappearance of projected HSE depletions in komatiite mantle sources at  $\sim 2.5$  Ga, relative to the modern BSE, this shift may indicate that by the end of the Archean, late accreted planetesimals had become largely homogenized within the mantle, and core-mantle interaction took over as the main driving force of creating  $^{182}\text{W}$  isotope anomalies, possibly coincident with the timing of the onset of modern-style plate tectonics on Earth.

## 1. Introduction

Accurately determining how the distribution of chemical elements within the Earth has changed over time has been, and remains, one of the most fundamental challenges in Earth science; it has far-reaching implications not only for the long-standing debate of how terrestrial planets formed and evolved, but also for understanding ongoing processes on Earth. The information pertaining to the origin and early evolution of Earth comes largely from the geological rock record between ~4.0 and 2.0 Ga, which harbors isotopic and elemental signatures generated in the terrestrial reservoirs *via* early chemical fractionation processes and the radioactive decay of short- and long-lived refractory nuclides, including  $^{146,147}\text{Sm}$ ,  $^{176}\text{Lu}$ ,  $^{182}\text{Hf}$ ,  $^{187}\text{Re}$ , and  $^{190}\text{Pt}$ .

The mantle is the largest of all the terrestrial reservoirs. Its chemically and isotopically heterogeneous nature has long been established by numerous pioneering studies of the Earth's rock record (*e.g.*, Hart and Brooks, 1977; Hofmann and Hart, 1978; Zindler et al., 1982; Hart and Zindler, 1986; Zindler and Hart, 1986; Jacobsen, 1988; Galer and Goldstein, 1991). Some of the heterogeneities have been argued to be primordial in nature, reflecting initial planetary accretion/differentiation and magma ocean crystallization processes (Goldstein and Galer, 1992; Albarède et al., 2000; Drake, 2000; Boyet and Carlson, 2005; Frost et al., 2008; Caro, 2011; Touboul et al., 2012; Carlson et al., 2015; Jacobsen and Yu, 2015; Puchtel et al., 2016a; Rizo et al., 2016; Boyet et al., 2021). Others likely were formed as a result of a protracted terrestrial accretion history (*e.g.*, Willbold et al., 2011; 2015; Dale et al., 2017; Puchtel et al., 2018; Archer et al., 2019) or later processes associated with the dynamic regime of the planet, especially crustal recycling (*e.g.*, DePaolo, 1980; Armstrong, 1981; Hofmann and White, 1982; Patchett et al., 1984; Shirey and Hanson, 1986; Chase and Patchett, 1988; Galer et al., 1989; Bowring and Housh, 1995; Bennett et al., 1996; Salters and White, 1998; Blichert-Toft et al., 2015).

Despite these decades-long research efforts, still limited insights into the terrestrial mantle mixing history mean that the nature, origin, scale, and longevity of early mantle heterogeneities, in terms of different elements and isotopic systems, remain contentious. This review is intended to fill some of the existing gaps in our understanding of early Earth chemical evolution by synthesizing the existing short- and long-lived refractory radiogenic isotopic and elemental abundance data for a representative set of well-preserved and well-characterized komatiite and basalt systems that are especially advantageous for studying processes that occurred within the first 2.5 billion years of Earth history. In parallel, we

address the question of the complex origins of komatiites and their usefulness as proxies for the chemical composition of the early Earth mantle.

Here, we consider komatiite-basalt systems from 13 different localities around the globe: the 3.55 Ga Schapenburg, 3.48 Ga Komati, and 3.26 Ga Weltevreden komatiites in the Kaapvaal Craton of South Africa; the 3.53 Ga Coonterunah, 3.34 Ga Kelly, and 3.18 Ga Ruth Well and Regal komatiites and basalts in the Pilbara Craton of Western Australia; the 2.82 Ga Kostomuksha, 2.41 Ga Vetreny, and 2.05 Ga Lapland komatiites in the Fennoscandian Shield of northern Europe; the 2.72 Ga Pyke Hill-Alexo and Boston Creek komatiites in the Superior Craton of Canada, and the 2.7 Ga Belingwe komatiites in the Rhodesian Craton of South Africa. These komatiite-basalt systems were chosen because of good preservation of their primary mineralogical and textural features and chemical and isotopic compositions, and because complete sets of published high-precision chemical and isotope data, obtained on the same sample sets, are available for these systems. A schematic world map showing the location of these komatiite-basalt systems is provided in the **Electronic Supplement**.

## **2. Komatiites as probes of the early Earth mantle**

Komatiites are ultramafic lavas containing more than 18% MgO in the parental liquid (Arndt and Nisbet, 1982). To be classified as a komatiite, the crystallized lava must either contain spinifex texture, or be genetically related to lavas containing spinifex texture. Spinifex texture is a crucial feature that distinguishes komatiites from other ultramafic lavas, such as picrites, boninites, and meimechites. It is characterized by the presence of large, skeletal crystals of olivine that form during rapid, *in situ* crystallization of high-MgO, superheated (*i.e.*, heated to above liquidus temperatures) silicate liquids. Due to the absence of nucleation sites, superheated liquids display a reluctance to nucleate, and olivine crystals that eventually form do so rapidly upon cooling below the liquidus and are typically large and skeletal, leading to the formation of spinifex texture (*e.g.*, Arndt, 1994; Arndt et al., 2008).

Ever since komatiites were first discovered and described in South Africa (Viljoen and Viljoen, 1969), these rocks have served as a source of valuable information bearing on the chemical and thermal evolution of the mantle (*e.g.*, Arndt et al., 2008). Owing to formation *via* the highest degrees of partial melting of all mantle-derived magmas, komatiites have compositions approaching that of mantle peridotite and, thus, represent the closest available approximation of the chemical characteristics of the mantle among volcanic rocks (*e.g.*, Arndt, 1977; Nesbitt et al., 1979; Herzberg, 1992). As high-degree, superheated, and low-viscosity melts, komatiites extracted large proportions of highly siderophile elements (HSE,

including Re, Os, Ir, Ru, Pt, and Pd) from the mantle, experienced little differentiation prior to emplacement, and likely sampled mantle domains on the order of tens of millions of cubic kilometers, as evidenced by the sheer volumes of komatiitic magmas erupted in a number of Archean terrains. Some of these occurrences are argued to be similar in volume to recent and modern oceanic plateaus, such as the Ontong Java plateau (*e.g.*, Condie, 1975; Schubert and Sandwell, 1989; Storey et al., 1991; Kusky and Kidd, 1992; Desrochers et al., 1993; Kimura et al., 1993; Abbott, 1996; Kent et al., 1996; Puchtel et al., 1998; Arndt et al., 2001). During crystallization of komatiite lava flows, major and trace elements, including HSE, behaved in predictable manners relative to indices of magmatic differentiation, making it possible to obtain precise chronological information, estimate element mobility, and determine HSE abundances in the mantle sources of most komatiites. The ability of komatiites to provide a reliable record of the chemical and isotopic characteristics of mantle domains that existed during the first half of Earth history is the key underlying factor for focusing on komatiites in this review, which is intended to summarize what komatiites have taught us about the evolution of early Earth. On the other hand, although basalts are less informative as probes of the HSE characteristics of the mantle, because of their inherently higher Nd, Hf, and W abundances, they are shown here to be reliable recorders of mantle Nd, Hf, and W isotopic compositions and have also been studied in several komatiite-basalt systems.

### **3. The analytical toolbox to study the chemical evolution of the mantle**

The chemical evolution of the mantle has long been studied using radiogenic isotope systems and lithophile and siderophile element abundances in mantle-derived rocks. The lithophile element-based isotopic systems, particularly  $^{142,143}\text{Nd}$  and  $^{176}\text{Hf}$ , are, by way of their refractory nature and optimal half-lives, powerful tools for examining possible primordial magma ocean processes, as well as subsequent mantle melting and differentiation processes (*e.g.*, DePaolo and Wasserburg, 1976; Jacobsen and Wasserburg, 1979; Patchett and Tatsumoto, 1980; Patchett et al., 1981; White and Patchett, 1984; Zindler and Hart, 1986; Sivell and McCulloch, 1991). Silicate melts have lower Sm/Nd and Lu/Hf than co-existing silicate solids, and after separation, evolve to distinctive  $^{143}\text{Nd}$  and  $^{176}\text{Hf}$  compositions. If Sm/Nd fractionated prior to  $\sim 4.0$  Ga, while  $^{146}\text{Sm}$  was still extant, variations in  $^{142}\text{Nd}$  can also be generated. Hence, application of the combined  $^{142,143}\text{Nd}$  systems provides the temporal resolution necessary for deciphering the timing and mechanisms of the earliest mantle differentiation events (Goldstein and Galer, 1992; Harper and Jacobsen, 1992; Boyet et al., 2003; Caro et al., 2003, 2006, 2017; Boyet and Carlson, 2005, 2006; Bennett et al., 2007;

O'Neil et al., 2008, 2012, 2016; Rizo et al., 2012, 2013, 2016; Roth et al., 2013, 2014). Further combining the  $^{142,143}\text{Nd}$  with the  $^{176}\text{Hf}$  systematics allows identification of specific processes that may have controlled mantle differentiation, including fractionation of the high-pressure bridgmanite (Mg-perovskite) and Ca-perovskite assemblage during crystallization of a primordial magma ocean (Caro et al., 2005; Hoffmann et al., 2011; Rizo et al., 2011; Puchtel et al., 2013; 2016a; Hoffmann and Wilson, 2017; Boyet et al., 2021).

The short-lived  $^{182}\text{Hf}$ - $^{182}\text{W}$  system can be used to detect fractionation of the lithophile trace element Hf from the siderophile trace element W occurring within the first ~60 Ma of Solar System history. This isotope system constitutes a high-resolution tool for identifying magma ocean crystallization, the effects of late accretion, and, by virtue of its dual lithophile and siderophile nature, potentially core-mantle interaction processes (Kleine et al., 2002, 2004, 2009; Yin et al., 2002, Jacobsen and Yu, 2015; Reimink et al., 2020; Willbold et al., 2011, 2015; Touboul et al., 2012; Puchtel et al., 2018, 2020, 2022; Rizo et al., 2019; Mundl-Petermeier et al., 2019, 2020). Further, application of the combined  $^{142}\text{Nd}$  and  $^{182}\text{W}$  tools can help discriminate between early magma ocean differentiation processes and the effects of late accretion (Harper and Jacobsen, 1996; Rizo et al., 2016; 2019; Puchtel et al., 2018; Peters et al., 2021).

Abundances of HSE, combined with  $^{186}\text{Os}$  and  $^{187}\text{Os}$  systematics, provide additional information about the chemical evolution of the mantle and the processes that operated early in Earth history (*e.g.*, Righter et al., 2000; Walker, 2009, 2016; Day, 2013; Puchtel et al., 2014; Day et al., 2016). The behavior of Re, Pt, and Os is governed by their strong partitioning into metal or sulfide liquids relative to silicate melt (Crocket et al., 1997; Righter and Drake, 1997). During mantle melting, Os is moderately to highly compatible with the melting residue, whereas Pt and Re are incompatible to various degrees (*e.g.*, Barnes et al., 1985; Rehkämper et al., 1999; Mallmann and O'Neill, 2007). Thus, the two Os isotopic systems together with HSE abundances provide insight into some primordial processes to which the lithophile element-based isotopic systems are not sensitive, including late-stage planetary accretion and metal-silicate differentiation. Estimates of HSE abundances in komatiite mantle sources can also be used to track the mixing rates of the mantle and the timing of homogenization of late accreted materials within the mantle (*e.g.*, Maier et al., 2009; Puchtel et al., 2018, 2020, 2022). In combination with Os isotope systematics and HSE abundances, the  $^{182}\text{Hf}$ - $^{182}\text{W}$  isotopic system can be used to discriminate between the effects of early planetary differentiation, late accretion, and core-mantle interaction (*e.g.*, Touboul et al.,

2012; Puchtel et al., 2016a, 2018, 2020, 2022; Archer et al., 2019; Rizo et al., 2019; Tusch et al., 2021).

The water content of a komatiitic lava is also an important parameter for assessing where in the mantle the parental melt originated. Water is highly incompatible during mantle melting (*e.g.*, Moore, 1970; Michael, 1995; Saal et al., 2002; Hauri et al., 2006; Cooper et al., 2012). The water content of a given komatiite mantle source can be derived from that of a komatiite lava provided that effects of secondary alteration can be corrected for. For example, correlations between the abundances of water and other lithophile trace elements, *e.g.*, Ce, in submarine basalt glasses have been used in a number of studies to establish H<sub>2</sub>O contents of mantle-derived melts (*e.g.*, Michael, 1995; Saal et al., 2002; Hauri et al., 2006; Cooper et al., 2012). Mid-ocean ridge basalt (MORB) and ocean island basalt (OIB) magmas have H<sub>2</sub>O/Ce  $\leq 370$  (Hauri et al., 2006), similar to the mantle value of  $200 \pm 50$  (Hirschmann, 2018); the rather large range is due to the fact that during anhydrous mantle melting, spinel lherzolite has a bulk solid/melt  $D_{\text{H}_2\text{O}} \approx D_{\text{Ce}}$ , whereas garnet lherzolite has a bulk solid/melt  $D_{\text{H}_2\text{O}} = 0.5 \times D_{\text{Ce}}$ . By contrast, arc magmas have H<sub>2</sub>O/Ce of 2,000 to 3,000, due to variable contributions of H<sub>2</sub>O from the subducting slab (Cooper et al., 2012).

The oxidation state of a komatiite magma and its source reflects important information about the location and processes involved in its generation. For example, knowledge of  $f\text{O}_2$  can potentially be used to distinguish between a hydrous (*i.e.*, subduction) versus anhydrous (*i.e.*, plume) origin of komatiites. Canil (1997, 1999, 2002) and Canil and Fedortchouk (2001) used V partitioning between liquidus olivine and komatiite liquid as a redox indicator. These authors showed that the major factor controlling the distribution of V between olivine and komatiitic melt ( $D_V^{\text{ol/liq}}$ ) was oxygen fugacity,  $f\text{O}_2$ . More oxidized, water-rich island arc magmas (higher  $f\text{O}_2$ ) are invariably characterized by  $D_V^{\text{ol/liq}} < 0.01$ , whereas less oxidized, anhydrous mantle plume-derived magmas (*e.g.*, OIB and MORB) exhibit  $D_V^{\text{ol/liq}} = 0.025 - 0.10$ .

Additional diagnostic features pointing to the origins of komatiites include estimates of potential temperatures of inferred mantle sources and depths of melting initiation. To compare mantle temperatures at various localities, McKenzie and Bickle (1988) proposed the concept of a mantle potential temperature ( $T_p$ ) as a point of reference. Mantle potential temperature is the temperature that the solid adiabatically-convecting asthenospheric mantle would have had at the surface if it ascended without undergoing melting. Mantle potential temperature determines the depth of melting initiation (*e.g.*, Richter, 1988; Herzberg, 1992, 1995;



Herzberg et al., 2007), which, in turn, governs the style of mantle melting and melt segregation (fractional versus batch). The depth of melting initiation and subsequent melt segregation determines the chemical composition of the resultant komatiite melts, including MgO contents. Pressures >8 GPa (240 km depth) stabilize majorite garnet relative to olivine and pyroxene in the source (e.g., Ohtani, 1984; Herzberg and Ohtani, 1988). If the temperature of a plume core is sufficiently high to initiate melting in the majorite garnet stability field, the melting results in the formation of Al-depleted komatiitic melts with subchondritic  $\text{Al}_2\text{O}_3/\text{TiO}_2$  and Gd/Yb, provided the melt separated from the melting residue while still in the majorite garnet stability field. By contrast, melting and melt segregation at lower pressures, within the spinel lherzolite stability field, produces Al-undepleted komatiitic magmas with chondritic  $\text{Al}_2\text{O}_3/\text{TiO}_2$  and Gd/Yb (e.g., Green, 1975; Ohtani, 1984; Kato et al., 1988; Herzberg, 1995).

#### 4. Which parts of the mantle do komatiites sample?

In order to assess the extents of early mantle isotopic and chemical heterogeneities sampled by komatiites, it is important to determine where in the mantle komatiites originate. The location of komatiite magma generation is almost certainly not the same for all komatiites, given the extent of chemical and isotopic heterogeneity inferred for their mantle sources. This, in turn, requires assessment of diverse komatiite formation models.

Komatiites were most common during the Archean and may, during this eon, have been the volumetrically second most significant constituent among volcanic rocks, comprising as much as 25% of the entire volume of volcanic sequences, the rest being composed mostly of basalts (e.g., Condie, 1975, 1981, 1994; de Wit and Ashwal, 1997). Some of these basalts were also derived from komatiites *via* fractional crystallization processes, while others were lower-degree partial melts generated from the same sources as the spatially associated komatiites (Arndt et al., 1977; Campbell et al., 1989; Condie, 2005). The abrupt decline in the abundance of komatiites at the Archean-Proterozoic boundary, as well as the decrease in the MgO contents of emplaced komatiite lavas, have been interpreted as evidence for a significant, up to 300°C, secular cooling of the mantle over the course of Earth history (e.g., Bickle, 1982; Nisbet et al., 1993; Herzberg et al., 2007; Herzberg and Gazel, 2009). Some authors have linked this to a transition from drip to subduction tectonics (Campbell and Griffiths, 2014), arguing that an increasing abundance of subducted slabs allowed for formation of the core-enveloping D'' insulating layer, which they in turn associate with a step-like drop in maximum komatiite magma MgO contents and mantle potential temperatures between 2.7 and 2.0 Ga.

The origin of komatiites has been a subject of studies for the past half century (*e.g.*, Green, 1975, 1981; Allègre, 1982; Arndt et al., 1998, 2008; Parman et al., 2001, 2004; Berry et al., 2008; Sobolev et al., 2016, 2019; Sossi et al., 2016; Asafov et al., 2018). A common interpretation is that the parental magmas to komatiites were produced in unusually hot upwellings of mantle material, termed mantle plumes (*e.g.*, Cawthorn, 1975; Campbell et al., 1989; Griffith and Campbell, 1990; Richards et al., 1991; Loper, 1991; Herzberg, 1995; Richard et al., 1996). The plumes most likely initiated at one of the two major thermal boundary layers in the mantle, *i.e.*, either the core-mantle boundary (CMB) at 2900 km, or the 660 km discontinuity, with the ensuing rise driven by a buoyancy contrast between the less dense, hot plume material and the cooler and denser surrounding mantle (Campbell and Griffiths, 1990, 1992, 1993; Farnetani and Richards, 1995; Farnetani, 1997). The initially solid mantle plume material was partially melted upon reaching shallower depths as a result of decompression. Based on experimental data, Campbell et al. (1989) argued that komatiites were produced in the hotter plume core containing mostly materials derived from near the thermal boundary layer, whereas spatially associated basalts were generated in the cooler plume head which, upon arrival at the surface, would have contained a substantial amount of entrained upper mantle material. However, later studies (*e.g.*, Farnetani and Richards, 1995) argued that such entrainment was unlikely to contribute significantly to the erupted melts.

Two major types of modern mantle plumes have been proposed based on the depth of their initiation, determined using recent high-resolution seismic tomography imaging data (*e.g.*, Courtillot et al., 2003; Montelli et al., 2004; He et al., 2015; Bao et al., 2022). The first type is “primary”, or Morganian, plumes that are commonly thought to originate in the deepest parts of the lower mantle, perhaps from seismically anomalous regions. Early geophysical studies (*e.g.*, Dziewonski et al., 1977) identified seismically anomalous zones along the core-mantle boundary, the so-called Large Low Shear-Wave Velocity Provinces (LLSVP) and Ultra-Low Velocity Zones (ULVZ). The origin of these regions in the mantle is debated. It has been proposed that LLSVPs may be stratified into primordial bottom domains near the core-mantle boundary, often referred to as the D" layer, and mafic shallow domains that extend from ~1100 to 2300 km depths (*e.g.*, Ballmer et al., 2016; Koppers et al., 2021). These regions in the mantle may serve as nurseries for the majority of "primary" mantle plumes (French and Romanovicz, 2015; Totsvik et al., 2016; Koppers et al., 2021). Ocean island basalt systems that have been associated with this type of plume include Azores, Canary, Coral Sea, Easter, Galapagos, Hawaii, Iceland, Samoa, and Tahiti (Courtillot et al., 2003).

The “secondary” type, or Andersonian, plumes have been proposed to originate at the 660 km discontinuity and, hence, would be an upper mantle feature. Ocean island basalt systems that have been associated with this type of plumes include Ascension, Caroline, McDonald, and Pitcairn islands (Courtillot et al., 2003).

Considering the difficulties in determining even present-day mantle plume characteristics (*e.g.*, Fletcher and Wyman, 2015, and references therein), it is not surprising that there are few reliable estimates of Archean plume parameters (Arndt et al., 2008). This is due to the fact that, unlike modern plumes, ancient plumes are extinct mantle features and, therefore, cannot be examined by geophysical methods. Consequently, indirect approaches must be taken, such as geological field observations. For example, the size of postulated plumes can potentially be constrained by the lateral extent of contemporaneous magmatic activity within a given region. Envisioned parental plume heads of up to 2500 km in diameter for large systems, such as the Yilgarn Craton in Western Australia (Campbell and Hill, 1988; Mole et al., 2014; Barnes and Van Kranendonk, 2014; Barnes et al., 2016), have been argued to be indicative of plumes that originated at the CMB. Smaller plume heads, estimated to range from 200 km to 300 km in diameter, and leading to less widespread volcanism, such as the komatiite-basalt systems of the Pilbara Craton in Western Australia and the Superior Craton in Canada (Arndt et al., 2001; Van Kranendonk, 2008; Hickman and Van Kranendonk, 2012; Dostal and Mueller, 2013; Wyman, 2013, 2018, 2020), are likely to be more typical of upper mantle plumes originated at the 660 km discontinuity.

Puchtel et al. (2009b, 2013, 2016a) calculated H<sub>2</sub>O contents of <0.2 wt. % in the Pyke Hill, Belingwe, Schapenburg, Komati, and Weltevreden komatiites, and concluded that their parental magmas were formed under dry, high-temperature melting conditions. Similar estimates of water content have been obtained for the Belingwe komatiites on the basis of the oxidation state of iron in melt inclusions in olivine (*e.g.*, Berry et al., 2008). Thus, it is a common assumption that most komatiites originated from dry, deep-seated mantle sources (Arndt et al., 1998, 2008).

Consistent with the interpretation of an anhydrous, deep mantle origin for most komatiites, Nicklas et al. (2018, 2019) concluded, on the basis of a global survey of partitioning behavior of V between olivine and emplaced komatiitic and picritic melts, that the redox states of a variety of komatiite and OIB sources, ranging in age from 3.48 Ga to present day, were either similar to, or lower than, those of modern MORB.

Recent studies of komatiitic olivine melt inclusions (*e.g.*, Sobolev et al., 2016, 2019; Asafov et al., 2018), while maintaining an anhydrous, deep mantle plume origin for

komatiites, have argued for relatively high water contents in some komatiite magmas, with water being added to rising, dry plume material from a thin hydrous layer located at the top of the mantle transition zone (MTZ), between the 410- and 660- km seismic discontinuities. The origin of these seismic interfaces is attributed to solid- solid phase transitions from olivine to wadsleyite and ringwoodite to perovskite+magnesiowüstite, respectively (*e.g.*, Bina and Helffrich, 1994). The hydrous layer is predicted by Bercovici and Karato (2003) in their MTZ water filter model to occur at the 410 km depth.

Alternatively, it has been argued that komatiites in general, and Komati lavas from the Kaapvaal Craton in South Africa in particular, were produced in a special type of Archean subduction environment *via* hydrous melting of the mantle at shallow depths and at temperatures similar to, or only slightly higher than, those of the ambient upper mantle (*e.g.*, Allègre, 1982; Grove et al., 1997; Parman et al., 1997, 2001, 2004). An important initial condition of this hypothesis is the requirement that the Komati komatiites represent intrusive bodies, since magmatic water escapes outgassing only under pressure (Grove et al., 1997). According to the hydrous komatiite model of Parman et al. (1997, 2001), the presence of water determined both the crystallization sequence and composition of the magmatic minerals of the Komati komatiites. Parman et al. (1997) carried out a detailed experimental study crystallizing material of komatiitic composition under both anhydrous and hydrous conditions, paying particular attention to the composition of the crystallizing pyroxene. Using the pyroxene compositions, these authors estimated that the original Komati komatiite magma contained between 4 and 6 wt. % H<sub>2</sub>O. Such a large amount of water would require the temperature in the Komati source to be ~250°C lower than in anhydrous melting models. In their follow-up review paper, Grove and Parman (2004) argued that the Archean mantle was ≤100°C hotter than the modern mantle, hence, offering a view on the thermal evolution of the Earth that contrasts with those that are based on the traditional assumption of a substantially hotter Archean mantle (*e.g.*, Richter, 1985, 1988; Bickle, 1986; Nisbet et al., 1993; Herzberg et al., 2007, 2010).

The summary of estimates of the mantle potential temperatures ( $T_p$ °C) for the sources of the komatiite systems considered here, as well as the liquidus temperatures of the emplaced komatiite magmas ( $T_{liq}$ °C) and depths of melting initiation in the respective mantle plumes ( $D_{melt\ init}$ ), are presented in **Table 1**. These estimates were generally derived from the studies for the particular komatiite systems referenced in **Table 1** and updated here on the basis of the more recent estimates of the emplaced komatiite lava compositions from Nicklas et al. (2018, 2019), where available, coupled with the previous and more recent mantle melting

parameterization models of McKenzie and Bickle (1988), Herzberg and O'Hara (2002), Herzberg and Asimow (2008), and Herzberg and Gazel (2009).

## 5. Chemical and isotopic data

A summary of the available chemical and isotopic data for the komatiite systems considered in this review are given in **Tables 1 and 2**.

### 5.1. Emplaced lava compositions, mantle potential temperatures, and depths of melting

Estimates of emplaced komatiite lava compositions ( $\text{MgO}_{\text{liq}}$ ), their liquidus temperatures ( $T_{\text{liq}}^{\circ}\text{C}$ ), mantle potential temperatures ( $T_p^{\circ}\text{C}$ ), and depths of mantle melting initiation ( $D_{\text{melt init}}$ ) are listed in **Table 1**. The details of the methodology used for calculating these parameters are provided in the **Electronic Supplement**.

The calculated depths of melting initiation range between 605 and 203 km, while liquidus temperatures vary between 1606°C and 1498°C. There is an apparent tendency for a decrease in depth of melting initiation between 3.6 and 2.0 Ga. This is also reflected in the ~100°C decrease in mantle potential temperatures of komatiite sources from 1841 to 1748°C and a corresponding decrease in MgO contents of emplaced komatiite lavas from ~31 to 25 wt.% over the same period of time. Two exceptions are the Coonterunah and Kelly komatiite systems that are less MgO-rich than the other early Archean systems. Therefore, the data place the depths of onset of melting for all komatiite systems considered here within and above the present-day MTZ and provide minimum estimates for the depths of mantle plume initiation. In the following sections, more clues, as to which parts of the mantle the studied komatiite systems sampled (*i.e.*, depths of mantle plume initiation,  $D_{\text{plume init}}$ ), will be considered using the available geochemical and isotopic data (**Table 2**).

### 5.2. Chemical composition and isotopic systematics

#### 5.2.1. Major and lithophile trace elements

The petrologically most important chemical element in komatiites, along with Mg, is Al; as a result, variations in  $\text{Al}_2\text{O}_3$ , and its rare earth element (REE) behavioral equivalent Yb, form an integral part of all komatiite classifications (*e.g.*, Nesbitt et al., 1979; Jahn et al., 1982). The komatiite systems reviewed here can be subdivided into two major petrological groups on the basis of their  $\text{Al}_2\text{O}_3$  and Yb contents at a given MgO content, namely Al-depleted/enriched and Al-undepleted. The majority of the early Archean komatiite systems, including the Schapenburg, Komati, Weltevreden, Ruth Well, and Regal systems, belong to the Al-depleted/enriched type of lavas characterized by either sub- or supra-chondritic Al/Ti

and Gd/Yb ratios (**Table 1**). Exceptions are the Coonterunah and Kelly systems that belong to the Al-undepleted type of lavas with  $\text{Al}_2\text{O}_3/\text{TiO}_2 = 22.8$  and  $23.1$  and  $\text{Gd}/\text{Yb}_\text{N} = 0.96$  and  $0.91$ , respectively (where N denotes BSE-normalized values of Hofmann, 1988). By contrast, the majority of the late Archean komatiite systems, including the Pyke Hill-Alexo, Belingwe, Vetreny, and Lapland systems, belong to the Al-undepleted type of lavas characterized by generally chondritic Al/Ti and Gd/Yb ratios. The Boston Creek (Puchtel et al., 2018) and Kostomuksha komatiites (Puchtel et al., 1998), with  $\text{Al}_2\text{O}_3/\text{TiO}_2 = 5.1$  and  $17.2$  and  $\text{Gd}/\text{Yb}_\text{N} = 2.0$  and  $1.2$ , respectively, are notable exceptions. Although the Lapland komatiites have low  $\text{Al}_2\text{O}_3/\text{TiO}_2 = 13.2$  and high  $\text{Gd}/\text{Yb}_\text{N} = 1.5$ , these features have been shown to be the result of enrichment in Ti and middle REE (MREE), rather than depletions in Al and heavy REE (Puchtel et al., 2020).

Owing to their high liquidus temperatures and low viscosities during their passage through and/or emplacement onto the continental crust, komatiitic liquids are highly susceptible to contamination by upper crustal rocks (Huppert et al., 1984; Huppert and Sparks, 1985). Archean upper crustal rocks are strongly enriched in Th, U, and light REE (LREE), and relatively depleted in Nb (Rudnick and Gao, 2014) as a result of subduction zone processes involving retention of Nb-rich rutile in the eclogitic residue (Foley et al., 2000; Rudnick et al., 2000). Because of that, upper crustal rocks are characterized by negative Nb anomalies relative to elements with similar incompatibility during mantle melting (Th and La), *i.e.*, their  $\text{Nb}/\text{Nb}^* \ll 1.0$  (where  $\text{Nb}/\text{Nb}^* = \text{Nb}_\text{N}/\sqrt{(\text{Th}_\text{N} \times \text{La}_\text{N})}$ ). By contrast, primary komatiitic magmas are expected to have  $\text{Nb}/\text{Nb}^* \geq 1.0$  (*e.g.*, Hofmann et al., 1986; Jochum et al., 1991). Due to large differences in highly incompatible lithophile trace element concentrations between the upper crust and komatiitic melts, crustal contamination usually leads to sharp increases in the abundances of Th, U, W, and LREE, but much less so of Nb, in the hybrid melts, which acquire negative Nb anomalies in the process. Hence, the  $\text{Nb}/\text{Nb}^*$  ratio represents a diagnostic tool that has been utilized to evaluate and mathematically correct for the effects of crustal contamination (*e.g.*, Puchtel et al., 2016b, 2020, 2022).

The majority of the komatiite systems considered here are variably depleted in highly incompatible lithophile trace elements, with the La/ $\text{Sm}_\text{N}$  ratios ranging between  $0.14$  (the 2.05 Ga Lapland system) and  $0.97$  (the 3.48 Ga Komati system). The 2.72 Ga Boston Creek lavas are the sole exception ( $\text{La}/\text{Sm}_\text{N} = 1.9$ ). Furthermore, all komatiite systems examined here have  $\text{Nb}/\text{Nb}^* \geq 1.0$ , reflecting either a lack of crustal contamination, or that the effects of crustal contamination have been mathematically corrected for, as indicated in **Table 2**. The details of the correction protocol are provided in the **Electronic Supplement**.

### 5.2.2. Isotopic systems of the lithophile elements

**Table 2** presents the initial  $\epsilon^{143}\text{Nd}$  and  $\epsilon^{176}\text{Hf}$  values (defined as the deviation in parts per 10,000 of initial  $^{143}\text{Nd}/^{144}\text{Nd}$  and  $^{176}\text{Hf}/^{177}\text{Hf}$  in a given sample from those in the chondritic reference at the time of lava emplacement) for each komatiite system, which represent compositions of the respective komatiite-basalt mantle sources. These values were derived from the respective Sm-Nd and Lu-Hf isochrons obtained for each komatiite-basalt system and, where appropriate, corrected for crustal contamination, as indicated in **Table 2**, using the lithophile trace element systematics discussed in the previous section. The resultant initial  $\epsilon^{143}\text{Nd}$  and  $\epsilon^{176}\text{Hf}$  values are all positive, ranging between +0.46 and +4.9 and +1.7 and +10.2, respectively, indicating that all the komatiite-basalt systems considered were derived from mantle sources with time-integrated supra-chondritic Sm/Nd and Lu/Hf.

By contrast, Blichert-Toft et al. (2015) reported  $^{143}\text{Nd}$  and  $^{176}\text{Hf}$  data for a suite of heavily altered Komati drill core samples from several flows. That study produced a much greater scatter, and both positive and negative initial  $\epsilon^{143}\text{Nd}$  and  $\epsilon^{176}\text{Hf}$  values for whole-rock samples, than for the initial values obtained from the individual Sm-Nd and Lu-Hf isochrons for the remarkably well preserved Komati komatiite samples from the Puchtel et al. (2013) study reported in **Table 2**. Blichert-Toft et al. (2015) also reported data for variably leached clinopyroxene separates, which yielded initial  $\epsilon^{143}\text{Nd}$  and  $\epsilon^{176}\text{Hf}$  values of  $-2$  and  $+5$ , respectively. This may indicate more complex magmatic and/or alteration history of the samples studied by Blichert-Toft et al. (2015) than for the Komati samples studied by Puchtel et al. (2013).

The time-integrated Sm/Nd and Lu/Hf ratios in the mantle sources of komatiite systems derived from the respective Sm-Nd and Lu-Hf isochron sets are plotted in **Fig. 1**. These ratios were calculated by assuming the minimum-degree fractionation from either the chondritic values or the values defined by the combined  $^{142,143}\text{Nd}$  systematics (where available) to those required to bring the  $\epsilon^{143}\text{Nd}$  and  $\epsilon^{176}\text{Hf}$  to the measured initial  $\epsilon^{143}\text{Nd}$  and  $\epsilon^{176}\text{Hf}$  of the respective mantle sources by the time of komatiite-basalt system formation. All of these komatiite systems were derived from mantle sources having time-integrated  $^{147}\text{Sm}/^{144}\text{Nd}$  and  $^{176}\text{Lu}/^{177}\text{Hf}$  ratios between those of CHUR and DMM. An important feature of the data is that, while all komatiite-basalt systems younger than  $\sim 3.0$  Ga follow the terrestrial Nd-Hf mantle evolution array, indicating long-term “coupled”, or congruent, behavior of the Nd and Hf isotope systematics in the post-3.0 Ga komatiite mantle sources, the komatiite systems older than  $\sim 3.0$  Ga (with the exception of the Pilbara Craton komatiite-basalt systems) plot above

the terrestrial evolution curve, indicating long-term “decoupled”, or incongruent, behavior of the Nd and Hf isotope systematics in their mantle sources. All these early Archean systems are from the Kaapvaal Craton in South Africa. The processes that might have been responsible for producing such Nd-Hf isotope decoupling are discussed in **Section 6.1**.

Relatively limited  $^{142}\text{Nd}$  data are available for the komatiite systems reviewed in this study (**Table 2**). The komatiite systems, for which these data are available, mostly exhibit  $\mu^{142}\text{Nd}$  values indistinguishable from the standard reference value, where  $\mu^{142}\text{Nd}$  is defined as the deviation in parts per million of  $^{142}\text{Nd}/^{144}\text{Nd}$  in a given komatiite sample from the laboratory reference materials (AMES or JNdi), which are considered to represent the composition of the modern BSE. The Schapenburg and Komati komatiite systems have small  $\mu^{142}\text{Nd}$  deficits, averaging  $-5.0 \pm 2.8$  (2SD; Puchtel et al., 2016a) and  $-4.0 \pm 4.1$  (2SD; Boyet et al., 2021), respectively.

### 5.2.3. Tungsten abundance and isotope systematics

The  $^{182}\text{W}$  data are reported as  $\mu^{182}\text{W}$ , which is the deviation in parts per million of  $^{182}\text{W}/^{184}\text{W}$  in a given sample from that of the in-house *Alfa Aesar* laboratory W reference material. The  $\mu^{182}\text{W}$  value of 0 for the reference material is considered to represent the composition of the BSE. This is based on the observation that a limited number of data for modern MORB (Willbold et al., 2011; Rizo et al., 2016; Mundl et al., 2017), numerous data for OIB with low  $^3\text{He}/^4\text{He}$  (Mundl-Petermeier et al., 2020), and data for Proterozoic and Phanerozoic glacial diamictites and granites (Mundl et al., 2018; Nakanishi et al., 2021) are all characterized by  $\mu^{182}\text{W}$  values of  $\sim 0$ .

In contrast to  $^{142}\text{Nd}$ , the majority of komatiite systems examined here exhibit either positive (all the Pilbara, the Kostomuksha, and the Boston Creek komatiite systems), or negative (the Schapenburg and Lapland komatiite systems)  $^{182}\text{W}$  anomalies, with only the Komati and Vetreny komatiite systems lacking an  $^{182}\text{W}$  anomaly.

The behavior of W during magmatic processes is governed mainly by the redox state of the magmatic system in question (Newsom et al., 1996; Arevalo and McDonough, 2008; König et al., 2011). Under reducing conditions, such as those that likely existed during metallic core formation, W behaves as a moderately siderophile element (MSE), concentrating largely in the metal relative to the silicate melt. During mantle melting under relatively oxidizing conditions in the absence of a metal phase, such as typical of the modern upper mantle, W behaves as a highly incompatible element, concentrating in the silicate melt relative to the melting residue, with a degree of incompatibility similar to that of Th and U.



The Archean mantle was recently shown to be only slightly (by  $\sim 1.3$   $\Delta$ FMQ log units) less oxidized than, whereas the Proterozoic mantle was found to be similarly oxidized to, the modern mantle (Nicklas et al., 2018, 2019). Therefore, it is expected that during the mantle melting that produced the komatiite-basalt systems considered in this review, W behaved similarly to Th and U and, hence, that in undisturbed komatiite-basalt systems,  $W/Th \approx W/Th_{BSE}$ , where  $W/Th_{BSE} = 0.19$  (McDonough and Sun, 1995). Indeed, in modern OIB and MORB, for which W is characterized by a primary, magmatic distribution, the W/Th ratios are similar to the BSE value of 0.19 (*e.g.*, König et al., 2008, 2011; Jenner and O'Neill, 2012). Modern island arc lavas, on the other hand, show uniformly elevated W/Th ratios relative to the BSE value attributed to various contributions of fluid-borne W to the arc mantle from the subducted slab (König et al., 2008, 2011). Although some komatiite systems (*e.g.*, the Komati, Vetreny, and Lapland systems) have average W/Th ratios within the uncertainty limits of the BSE value, and in that respect are similar to modern OIB and MORB, others are variably either enriched (most common) or depleted in W over Th (**Table 1**). In addition, the lack of correlation between W concentrations and indices of magmatic differentiation, such as MgO content, indicates either W mobility after lava emplacement in most komatiite-basalt systems (*e.g.*, Touboul et al., 2012; Puchtel et al., 2016a, 2018, 2020, 2022; Tusch et al., 2021) or involvement of a yet-unaccounted-for magmatic process.

The issue of the origin of W in Archean and Proterozoic komatiite-basalt systems is, therefore, controversial. Recent studies have shown that W abundance and isotopic systematics can be affected by crustal contamination, hydrothermal alteration, and metamorphism (*e.g.*, Touboul et al., 2014; Liu et al., 2016; Puchtel et al., 2016a,b, 2018, 2020, 2022; Tusch et al., 2019, 2021), resulting mostly in W enrichments relative to immobile trace elements with similar degree of incompatibility, *e.g.*, Th. Two mechanisms, based on the origin of W, have been proposed to account for the elevated W/Th ratios in komatiites and basalts. The first mechanism advocates derivation of W from an endogenous source, whereby W originated within the komatiite-basalt system. The second mechanism assumes an exogeneous origin, whereby W is introduced into the komatiite-basalt systems from genetically unrelated sources. We address these two mechanisms in more detail below.

**Endogenous** origin of W in komatiite-basalt systems have been advocated for the Kostomuksha (Touboul et al., 2012), Schapenburg (Puchtel et al., 2016a), Boston Creek (Puchtel et al., 2018), and the Coonterunah and Kelly systems (Puchtel et al., 2022). In case of the two Pilbara komatiite-basalt systems, the komatiites are characterized by high W/Th ratios, whereas the basalts, that are spatially associated and genetically related to komatiites,

are depleted to only slightly enriched in W relative to Th. In these komatiite-basalt systems, and also in many other Archean komatiite-basalt systems around the globe, komatiites constitute 5-10% of the sequence by volume, the rest consisting of basalts (Condie, 1981; de Wit and Ashwal, 1997; Smithies et al., 2007). Originally, basalts contain significantly higher abundances of all highly incompatible trace elements, including W, compared to komatiites. During secondary alteration, komatiites are turned into serpentinites, whereas basalts are transformed into amphibolites. Serpentine is a major host for W and can accommodate several orders of magnitude more W than the precursor mineral olivine, whereas W shows a lower affinity for amphibole (Liu et al., 2016). Therefore, if W is mobilized and redistributed within a komatiite-basalt volcanic sequence, it is expected to be preferentially captured by komatiites during serpentinization of the primary mineral assemblage. The effect of this relative W enrichment is amplified by the low trace element concentrations in komatiites, resulting in high W/Th ratios (Puchtel et al., 2022).

In the case of the Boston Creek system, samples collected across a differentiated lava flow have remarkably uniform  $^{182}\text{W}$  compositions, but show a wide range of W/Th ratios, from enriched in the lower olivine cumulate part to BSE-like in the low-Mg basaltic layer, with strong inverse correlation between MgO content (*i.e.*, amount of modal serpentine) and W/Th (Puchtel et al., 2018). The above features were argued by these authors to reflect an endogenous nature of W in the Boston Creek system, with isotopically uniform W having been redistributed within the lava flow and hence reflecting the primary magmatic signature.

The above scenarios have been argued to be applicable to several other komatiite-basalt systems, including the Kostomuksha (Touboul et al., 2012), and the Schapenburg (Puchtel et al., 2016a) systems.

**Exogenous** W in the komatiite-basalt systems considered in this review has been shown to be derived from upper crustal rocks either during passage of mafic-ultramafic magmas through the continental crust *en route* to the surface (the Vetreny and Lapland systems: Puchtel et al., 2016b, 2020), or as a result of interaction with upper crustal rocks during both the magmatic stage *via* crustal contamination, and the post-magmatic stage *via* fluid-rock interaction (the Ruth Well and Regal systems: Puchtel et al., 2022).

Due to the generally high W abundances in upper crustal rocks (*e.g.*, Rudnick and Gao, 2014), crustal contamination has the potential to modify both W concentrations and  $^{182}\text{W}$  compositions of komatiite-basalt magmas during ascent, as has been argued to be the case for the Vetreny, Lapland, Ruth Well, and Regal systems on the basis of studies of lithophile trace element systematics (Puchtel et al., 2016b, 2020, 2022). In order to mathematically correct for

the effects of magmatic crustal contamination, these authors performed un-mixing calculations using the degrees of crustal contamination estimated on the basis of trace element systematics and assumptions about the W isotopic composition and abundances in the most likely potential crustal contaminant.

Being a highly fluid-mobile element (*e.g.*, König et al., 2008), W can be transferred from spatially associated granitic rocks to komatiite-basalt sequences *via* W-rich fluids. Such a mechanism has been proposed to affect the W isotopic composition of the Ruth Well and Regal komatiite systems on the basis of the high W/Th ratios in both komatiites and basalts and the similarity in  $^{182}\text{W}$  compositions between the most W-enriched komatiites and the spatially associated 3.5 Ga tonalites of the Pilbara Craton (Puchtel et al., 2022). These authors were able to evaluate the W isotopic composition of the primary lavas by assuming that their  $^{182}\text{W}$  composition was similar to that of the least affected basalts from Tusch et al. (2021) and Puchtel et al. (2022), with W/Th ratios closest to that in the BSE estimate.

After corrections have been applied where needed, the  $\mu^{182}\text{W}$  values reported in **Table 2** are considered to reflect those in the sources of the respective komatiite-basalt systems.

### 5.3. Os isotope systematics and HSE abundances

The  $^{186,187}\text{Os}$  data are listed in **Table 2** and plotted in **Fig. 2**. The majority of the komatiite systems have  $\gamma^{187}\text{Os}$  values (defined as percent deviation of the  $^{187}\text{Os}/^{188}\text{Os}$  ratio in a given komatiite sample from a chondritic reference value at the time of komatiite lava emplacement) plotting within the chondritic range, indicating evolution of their mantle sources with time-integrated near-chondritic Re/Os ratios. The only exceptions are the Schapenburg and Kostomuksha komatiite systems that have more radiogenic  $\gamma^{187}\text{Os}$  values of +3.7 and +2.5, respectively, implying that their mantle sources evolved with long-term slightly suprachondritic Re/Os.

The limited  $^{186}\text{Os}$  data available indicate that, out of the seven systems studied, only three (the Pyke Hill, Belingwe, and Vetreny systems) have initial  $\mu^{186}\text{Os}$  values (defined as the deviation in ppm of the  $^{186}\text{Os}/^{188}\text{Os}$  ratio in a given komatiite sample from a chondritic reference value at the time of the komatiite lava emplacement) that plot within the chondritic range, indicating that their mantle sources evolved with time-integrated near-chondritic Pt/Os ratios. The other four komatiite systems have non-chondritic initial  $\mu^{186}\text{Os}$  values and, thus, evolved with either suprachondritic (the Weltevreden, Kostomuksha, and Lapland systems) or subchondritic (the Komati system) time-integrated Pt/Os ratios. Importantly, among the mantle sources with non-chondritic Re-Os and/or Pt-Os systematics, only in the Kostomuksha

komatiite source are these isotope systematics coupled, whereas in the others, they are decoupled.

The total HSE abundances in the komatiite mantle sources have been calculated using the bootstrap method of Puchtel et al. (2004b) that was refined in subsequent studies (*e.g.*, Puchtel et al., 2020, 2022). This method combines the  $^{186,187}\text{Os}$  isotopic and HSE abundance data for a suite of komatiitic lavas derived from a common primary magma and related by fractional crystallization of olivine after lava emplacement. The details of the analytical protocol used in the bootstrap method of Puchtel et al. (2004b) are provided in the **Electronic Supplement**.

The total HSE abundances in the sources of the komatiite systems considered in this review, calculated as percent of those in the estimates of the modern BSE of Becker et al. (2006), are presented in **Table 2** and plotted as a function of their age in **Fig. 3**. The calculated total HSE abundances range from ~30% in the 3.55 Ga Schapenburg and 3.53 Ga Coonterunah systems to ~120% in the 2.05 Ga Lapland system. Overall, the entire dataset, except for the obvious outliers (*e.g.*, the 2.72 Ga Boston Creek, 2.69 Ga Belingwe, and 2.41 Ga Vetreny systems), exhibits a broad trend of increasing HSE abundances in the komatiite mantle sources with time. This trend is generally consistent with that defined by the much more scattered data of Maier et al. (2009).

In the following sections, the data reviewed in **Section 5** will be discussed in light of the possible mechanisms responsible for creating these early chemical and isotopic heterogeneities in the mantle.

## **6. Mechanisms for creating early mantle heterogeneities**

### **6.1. Primordial differentiation of the mantle**

Crystallization of a primordial magma ocean(s) is one possible mechanism for generating early chemical and isotopic heterogeneities in the mantle (*e.g.*, Boyet et al., 2003, 2021; Boyet and Carlson, 2005, 2006; Caro et al., 2005, 2017; Brown et al., 2014; Puchtel et al., 2016a; Byerly et al., 2017; Morino et al., 2017). Periodic magma oceans are likely a direct consequence of planetary growth due to gravitational energy release from core formation and high-energy collisions during final stages of accretion (*e.g.*, Tonks and Melosh, 1993; Bottke et al., 2010; Rubie et al., 2011). Crystallization of a magma ocean results in stratification controlled by fractionation of mineral assemblages, the composition of which depends on the depth of the magma ocean and the composition of the melted domain. Some studies have argued for occasional, near-complete melting of the silicate Earth, such as may have occurred

during the putative giant impact that led to formation of the Moon (Rubie et al., 2011; Canup, 2012; Elkins-Tanton, 2012; Young et al., 2016). The pressures and temperatures near the bottom of such a magma ocean would have stabilized bridgmanite (Mg-perovskite) and Ca-perovskite (Kato et al., 1988; Abe, 1997; Walter et al., 2004). Because most trace elements are variably compatible in Ca-perovskite, with the degree of compatibility decreasing in the order Lu>Hf>Sm>Nd (Corgne et al., 2005), the presence of Ca-perovskite in the fractionating assemblage would result in stronger fractionation of Lu/Hf relative to Sm/Nd than that observed under upper mantle conditions. Over time, this would result in Nd-Hf isotopic decoupling in the mantle domains derived from magma ocean differentiation products, relative to the coupling of these two isotope systems observed in the sources of modern MORB and most OIB, which together define the modern Nd-Hf mantle array, or terrestrial evolution curve (e.g., Salters and White, 1998).

The Nd-Hf mantle array owes its origin to the coupled, or congruent, Nd-Hf isotope systematics of most terrestrial rocks that arise from similar partitioning behavior of the parent ( $^{147}\text{Sm}$ ,  $^{176}\text{Lu}$ ) and daughter ( $^{143}\text{Nd}$ ,  $^{176}\text{Hf}$ ) isotopes of the Sm-Nd and Lu-Hf systems during upper mantle differentiation and crust-forming processes (e.g., Patchett et al., 1981; Salters and White, 1998; Vervoort and Blichert-Toft, 1999; Vervoort et al., 1999, 2000). During mantle melting, both parent isotopes are less incompatible with the melt fraction than the daughter isotopes, which results in higher Sm/Nd and Lu/Hf ratios in the melting residue compared to the melt; over time, the residual mantle evolves to more radiogenic Nd and Hf isotopic compositions than the extracted melts. Both isotope systems are lithophile, refractory, insensitive to redox conditions, and largely immobile during alteration and metamorphism. These properties make them useful for investigating the interplay between the formation and recycling of oceanic and continental crust in driving the geochemical evolution of the mantle.

The decoupling of the Nd and Hf isotope systematics (and, thus, deviation from the terrestrial Nd-Hf array) in the early Archean komatiite-basalt systems from the Kaapvaal Craton, such as Schapenburg, Weltevreden, and Komati, have been interpreted to reflect the involvement of primordial magma ocean processes.

Based on the combined  $^{142,143}\text{Nd}$  and  $^{176}\text{Hf}$  systematics, Puchtel et al. (2013) developed a model of formation of the mantle silicate reservoirs that gave rise to the Komati and Weltevreden komatiites *via* crystallization of a primordial magma ocean. According to their model, during magma ocean differentiation, the lower three quarters of the magma column (from depths of ~2900 to ~700 km) were largely dominated by bridgmanite, with subordinate amounts of ferropericlase and Ca-perovskite, Ca-Pv (Trønnes and Frost, 2002; Ito et al., 2004;

Caro et al., 2005; Elkins-Tanton, 2008). Puchtel et al. (2013) used an equilibrium crystallization model based on the high-pressure and -temperature partitioning studies of Corgne and Wood (2002; 2004), Corgne et al. (2005), Liebske et al. (2005), and Walter et al. (2004), and assumed a completely molten mantle with a composition corresponding to that of the early depleted reservoir (EDR) of Boyet and Carlson (2006) that crystallized within the first 150 Ma of the Solar System history, i.e., by 4400 Ma.

Since the study of Puchtel et al. (2013) has been published, the EDR model of Boyet et al. (2006) has been proven untenable. This model was based on the data available at the time that the accessible Earth has a greater  $^{142}\text{Nd}/^{144}\text{Nd}$  ratio than chondrites (Carlson et al., 2007). This  $^{142}\text{Nd}$  difference required a higher-than-chondritic Sm/Nd ratio for the accessible Earth. This ratio must have been acquired during global silicate differentiation within the first 30 million years of Solar System formation (Boyet and Carlson, 2006) and implied the formation of a complementary  $^{142}\text{Nd}$ -depleted reservoir that is either hidden in the deep Earth, or lost to space by impact erosion (Caro et al., 2008). However, Burkhardt et al. (2016) showed that, compared to chondrites, Earth's building blocks were enriched in  $^{142}\text{Nd}$  that was produced by the s-process of nucleosynthesis, which leads to higher  $^{142}\text{Nd}/^{144}\text{Nd}$  ratios. After these authors corrected for this effect, the  $^{142}\text{Nd}$  composition of chondrites and the accessible Earth were shown to be indistinguishable. The results of Burkhardt et al. (2016), therefore, obviate the need for a hidden-reservoir or  $^{142}\text{Nd}$ -superchondritic Earth models and imply a chondritic Sm/Nd ratio for the BSE.

In view of the new data of Burkhardt et al. (2016), we have modified the model of Puchtel et al. (2013), as illustrated in **Fig. 4**; the methodology used in these model calculations are available as an **Electronic Supplement**. The composition of the primordial magma ocean, unlike in our previous model, is now represented by that of the chondritic uniform reservoir (CHUR).

**Figure 4** shows the time-integrated  $^{147}\text{Sm}/^{144}\text{Nd}$  and  $^{176}\text{Lu}/^{177}\text{Hf}$  ratios in the sources of the Komati and Weltevreden komatiite systems formed as a result of the 4400 Ma magma ocean differentiation and crystallization event specified above, depending on the relative proportions of fractionating bridgmanite and Ca-Pv. The upper panel of the diagram represents aggregate compositions of the magma ocean cumulates, while the lower panel represents the compositions of the residual liquids. As mentioned in the previous model, the contrasting partitioning behavior of Lu and Hf between bridgmanite and Ca-Pv results in differentiation trends that are highly affected by the relative proportions of these two phases. According to this model, the Komati and Weltevreden mantle domains represent solidification

products of a bridgmanite-Ca-Pv cumulate that was derived from ~20% and 12% accumulation of a bridgmanite:Ca-Pv assemblage in the proportions of 93:7 and 80:20, respectively. These proportions and the degrees of magma ocean crystallization are within the range of those envisaged for lower mantle conditions during the Hadean (*e.g.*, Caro et al., 2005). If the modified model of Puchtel et al. (2013) presented here is correct, the mantle plumes that gave rise to the Komati and Weltevreden komatiites must have originated in the lower mantle (**Table 1**).

Boyet et al. (2021) obtained a slightly negative average  $\mu^{142}\text{Nd}$  value of  $-4.0 \pm 4.1$  for a set of Komati drill core samples. As noted above, that study combined their  $^{142}\text{Nd}$  results with the  $^{143}\text{Nd}$  and  $^{176}\text{Hf}$  data of Blichert-Toft et al. (2015) for clinopyroxene separates from the same rocks. In order to explain the negative  $\mu^{142}\text{Nd}$  and  $\epsilon^{143}\text{Nd}$  values and the corresponding positive  $\epsilon^{176}\text{Hf}$  value, Boyet et al. (2021) proposed a four-stage model for the formation of these lavas, whereby the negative  $\mu^{142}\text{Nd}$  value and low Hf/Sm ratios developed during the crystallization of a deep magma ocean soon after Earth accretion. The material that ultimately became the source of the komatiites was a residual liquid produced by 50% crystallization of a bridgmanite/ferropericlase/Ca-Pv mineral assemblage in the proportions 79:16:5, which resulted in decoupling of the Nd and Hf isotope systematics. Thus, the model of Boyet et al. (2021) also supports a lower mantle origin for the plume that gave rise to the Komati komatiites.

Metal-silicate fractionation processes operating at the high temperatures and pressures characterizing the first ~60 Ma of Solar System history at the base of an early transient magma ocean, or in a partially molten zone at or near the core-mantle boundary (Labrosse et al., 2007), while  $^{182}\text{Hf}$  was still extant, have also been argued to be capable of generating coupled  $^{182}\text{W}$  and  $^{186,187}\text{Os}$  heterogeneities in the mantle (Touboul et al., 2012). To explain the enriched  $^{182}\text{W}$  and  $^{186,187}\text{Os}$  compositions of the Kostomuksha komatiite system, Touboul et al. (2012) envisioned a lower mantle magma ocean reservoir where silicate melt could potentially equilibrate with metal that represented either the growing core or the metal passing through the molten region on its way to the core. This model is based on experimental data of substantially reduced metal-silicate partitioning for Re and Pt, relative to Os, at high temperatures and pressures (Righter and Drake, 1997; Cottrell and Walker, 2006; Fortenfant et al., 2006; Yokoyama et al., 2009; Brenan and McDonough, 2009), and on the more siderophile behavior of W under the somewhat more reducing conditions that likely existed in the lower mantle during core formation compared to the present-day upper mantle (Wade and

Wood, 2005). The model of Touboul et al. (2012) requires the long-term survival of some portion of the mantle in which HSE and MSE were set by high-temperature and -pressure metal-silicate partitioning under reducing conditions. In order to achieve the  $^{186, 187}\text{Os}$  and  $^{182}\text{W}$  isotopic and elemental characteristics of the Kostomuksha komatiite source, Touboul et al. (2012) envisioned a mantle plume tapping this reservoir and mixing material from it with overlying mantle characterized by Os isotopic compositions and HSE concentrations similar to those in estimates of the BSE of Meisel et al. (2001) and Becker et al. (2006), in the proportions of ~1:1 (**Fig. 5**). If the model of Touboul et al. (2012) is correct, it implies that the plume, which gave rise to the Kostomuksha komatiites, originated in the lowermost mantle.

Isotopic heterogeneities involving the HSE-based isotopic systems have also been argued to be related to primordial magma ocean crystallization processes by Puchtel et al. (2014) in their study of the HSE abundances and  $^{186, 187}\text{Os}$  compositions of the Komati and Weltevreden komatiite systems considered above. These authors used the experimental partitioning data of Borisov and Palme (1997) and Mallmann and O'Neill (2007) indicating that under the highly reducing conditions that may have existed during crystallization of a primordial magma ocean immediately following the main stage of core formation (Frost et al., 2008), solubility of Pt in silicate melts, unlike the other HSE, may have been low and Pt, hence, would have had a strong tendency to form alloys. Fractionation and subsequent heterogeneous dispersal of Pt alloys within the mantle could have resulted in the formation of both Pt-enriched and -depleted domains. These would then have evolved with supra- and subchondritic Pt/Os ratios, respectively, which over time would have resulted in the decoupling of the  $^{186}\text{Os}$  and  $^{187}\text{Os}$  systems in these domains (Puchtel et al., 2014).

A model of silicate-silicate fractionation during primordial mantle magma ocean crystallization, involving early removal of bridgmanite and Ca-Pv, was also proposed by Puchtel et al. (2016a) to explain the coupled  $^{182}\text{W}$ ,  $^{142, 143}\text{Nd}$ , and  $^{176}\text{Hf}$  isotope systematics of the Schapenburg komatiite source. In their model, the authors recognized that crystal-liquid fractionation in a purely silicate system of a global primordial magma ocean would lead to high Hf/W, Sm/Nd, and Lu/Hf in early-formed cumulates and low Hf/W, Sm/Nd, and Lu/Hf in the residual liquid. If these fractionation processes occurred while  $^{182}\text{Hf}$  and  $^{146}\text{Sm}$  were still extant, the residual silicate liquid would have developed a coupled deficit in  $^{182}\text{W}$  and  $^{142}\text{Nd}$ , compared to the ambient mantle, which is what has been observed in the 3.55 Ga Schapenburg komatiites. If the model of Puchtel et al. (2016a) is applicable, it places the mantle domain that served as the sources for the Schapenburg mantle plume in the lowermost mantle.



## 6.2. Late accretion

The term “late veneer” was first introduced by Turekian and Clark (1969) and later elaborated on by Chou et al. (1978; 1983) to explain the excess of HSE abundances in the terrestrial mantle compared to what would otherwise be expected after core formation on the basis of the low pressure and -temperature metal-silicate experimental partitioning data available at the time (*e.g.*, Kimura et al., 1974). Late accretion is defined as the accretion of 0.5-1% (Walker, 2009) of Earth's mass of a chondritic component after cessation of core formation. In earlier studies, it was assumed that this chondritic component was added to the surface of the Earth in the form of relatively small objects to create a thin layer initially coating the entire planet (thus the term “veneer”). It has also been proposed that a slow downward mixing of this putative thin layer into the mantle was responsible for the apparent trend of increasing HSE abundances in Archean komatiites over time (Maier et al., 2009). Studies by Bottke et al. (2002, 2007), however, have concluded that it is unlikely that late accretion in the form of small objects could have achieved an Earth/Moon late accretionary mass influx ratio of ~1200 required on the basis of the Re-Os isotopic and HSE abundance studies of terrestrial (Meisel et al., 2001; Becker et al., 2006; Fischer-Gödde et al., 2011) and lunar (Walker et al., 2004, 2014; Day et al., 2007; Day and Walker, 2015) samples. Bottke et al. (2010) proposed that late accretion to Earth was dominated by addition of a few large projectiles, with a mean diameter of ~2500 km, and that HSE were added to the Moon through the accretion of much smaller bodies, ~250 km in diameter. Projectiles with a diameter of 2500 km hitting the Earth likely have been differentiated into HSE-rich cores and HSE-stripped silicate mantles (Marchi et al., 2018). As a result, mantle domains with low HSE abundances and positive  $^{182}\text{W}$  anomalies, on the one hand, and high HSE abundances and negative  $^{182}\text{W}$  anomalies, on the other hand, would have been generated. In the absence of modern-style plate tectonics prior to ~2.5 Ga (*e.g.*, Brown and Johnson, 2018), these mantle domains would be expected to survive for extended periods of time before eventually becoming homogenized within the mantle *via* wholesale mantle convection.

Heterogeneous distribution of HSE in the early Earth's mantle has been recognized from  $^{186,187}\text{Os}$  and HSE abundance studies of komatiites (*e.g.*, Maier et al., 2009; Puchtel et al., 2004a,b, 2005, 2009a,b, 2014, 2016a,b, 2018, 2020, 2022). As noted in **Section 5**, available high-precision  $^{187}\text{Os}$  data for komatiitic systems worldwide indicate that most komatiite sources were characterized by initial  $\gamma^{187}\text{Os}$  values ranging from only -0.1 to +1.3, implying that these komatiitic systems evolved with long-term Re/Os well within the range of chondritic meteorites (**Fig. 2a**). Only two exceptions have been identified so far, which are

the Schapenburg and Kostomuksha komatiite systems. The more limited  $^{186}\text{Os}$  dataset indicates a somewhat greater variability outside of the chondritic range, but, nevertheless, suggests that the mantle sources of the late Archean Pyke Hill, Belingwe, and Vetreny komatiite systems evolved with time-integrated Pt/Os within the chondritic range (**Fig. 2b**). By contrast, the high initial  $\mu^{186}\text{Os}$  and  $\gamma^{187}\text{Os}$  values in the mantle source of the Kostomuksha komatiites require long-term suprachondritic Pt/Os and Re/Os ratios. Originally, these coupled  $^{186,187}\text{Os}$  enrichments were interpreted to be the result of core-mantle interaction processes (Puchtel et al., 2005). However, the  $^{182}\text{W}$  data obtained by Touboul et al. (2012) for these komatiites rendered this interpretation implausible and these authors instead proposed that the combined  $^{186,187}\text{Os}$  and  $^{182}\text{W}$  systematics were the result of metal-silicate fractionation in a primordial magma ocean, as discussed earlier. Additional contrasts are the Komati and Weltevreden (Puchtel et al., 2014) and the Lapland (Puchtel et al., 2020) komatiite systems, which evolved with non-chondritic time-integrated Pt/Os ratios and chondritic time-integrated Re/Os ratios, thereby displaying decoupling of the  $^{186}\text{Os}$  and  $^{187}\text{Os}$  systematics. For the Komati and Weltevreden komatiite systems, this decoupled behavior has been interpreted to be the result of fractionation of Pt-Fe alloys in a primordial magma ocean during the first 150 Ma of Earth history, followed by slow homogenization of the crystallized post-magma ocean mantle domains characterized by fractionated Pt/Os ratios (Puchtel et al., 2014). For the Lapland komatiite system, derivation from a mantle domain characterized by an excess of late accreted, differentiated planetesimal core metal, the so-called “grainy” late accretion (Walker, 2016), were considered to be one of the two plausible models for explaining the decoupled  $^{186}\text{Os}$  and  $^{187}\text{Os}$  systematics (Puchtel et al., 2020).

On the basis of variable Pt and Ru contents in komatiites of various ages, Maier et al. (2009) argued for a gradual increase in HSE abundances in the presumed deep mantle sources of komatiites between ~3.5 and ~2.9 Ga due to slow downward mixing of a “late veneer” of chondritic materials. However, the  $^{186,187}\text{Os}$  and  $^{182}\text{W}$  isotopic and HSE abundance studies of Puchtel et al. (2020; 2022, and references therein) of the best preserved early Archean to early Proterozoic komatiite systems worldwide revealed a somewhat more complex picture. As attested to by the plot of the calculated total HSE abundances in the sources of these komatiite systems as percent of those in the estimates of the modern BSE of Becker et al. (2006) versus age (**Fig. 3**), this trend has been argued unlikely to be the result of simple “slow downward mixing of a late veneer of chondritic materials”, although a broad trend of increasing HSE abundances in komatiite sources over time is apparent (*e.g.*, Puchtel et al., 2016a, 2018, 2020, 2022). The argument is two-fold. First, as is evident from **Fig. 3**, the total HSE abundances in

the sources of some late Archean komatiite systems were even lower than those in some early Archean komatiite systems. Second, for some of the komatiite systems considered here, *e.g.*, the Schapenburg and Kostomuksha komatiites, the calculated total HSE abundances were shown to be inconsistent with the proportion of late accreted materials estimated to have been added to their sources based on the  $^{186,187}\text{Os}$  and  $^{182}\text{W}$  data (Touboul et al., 2012; Puchtel et al., 2016a).

These observations are illustrated in **Fig. 6**, where the  $\mu^{182}\text{W}$  values of komatiite systems are plotted against the calculated total HSE abundances in their mantle sources normalized to those in the estimates for the modern BSE of Becker et al. (2006). This proportion corresponds to the fraction of the total HSE budget of the modern BSE added during late accretion, assuming an essentially HSE-free BSE immediately following core formation. According to this model, the HSE budgets, taking into account their respective uncertainties, of those komatiitic systems that plot within the segment constrained by the blue lines in **Fig. 6**, are consistent with having been established *via* addition of late accreted materials to their mantle source regions. By contrast, the HSE budgets of the komatiite systems that plot outside this segment are presumed to have been affected by additional primordial processes, such as metal-silicate (*e.g.*, the Kostomuksha komatiites: Touboul et al., 2012) or silicate-silicate (*e.g.*, the Schapenburg komatiites: Puchtel et al., 2016a) fractionation in a primordial magma ocean within the first 60 Ma of Solar System history. Furthermore, the combined  $^{187,186}\text{Os}$ - $^{182}\text{W}$  and HSE abundance data for the Lapland komatiite system (**Fig. 6**) are consistent with involvement of fractionated metal derived from cores of differentiated planetesimals during late accretion processes and formation of Os-W isotope and HSE abundance heterogeneities in the early mantle (Puchtel et al., 2020).

It has been argued that the impactors that created the largest impact basins on the Moon, Mars, and presumably also the Earth, were hundreds of km in diameter (Ryder, 2002; Strom et al., 2005; Bottke et al., 2010) and possibly dominated by differentiated planetesimals. Impacts of such bodies would be capable of generating large  $^{182}\text{W}$  and HSE anomalies in portions of the mantle as a result of such “grainy” late accretion (Walker, 2016; Marchi et al., 2018; 2020). Cores of differentiated planetesimals would have up to two orders of magnitude higher W abundances, and up to 350 ppm less radiogenic  $^{182}\text{W}/^{184}\text{W}$ , than the modern BSE (Kleine et al., 2002, 2004; Schoenberg et al., 2002; Yin et al., 2002). Hence, any mantle domain to which an excess of this material was added would be  $^{182}\text{W}$ -depleted and would also be expected to be enriched in HSE, compared to BSE, as is observed for the Lapland komatiite system (Puchtel et al., 2020). On the other hand, the mantle domain to which less of

a late accretionary HSE component was added, *e.g.*, in the form of the HSE-stripped silicate mantles of differentiated planetesimals, would be  $^{182}\text{W}$ -enriched, compared to those mantle domains to which a full HSE complement of late accretionary material was added, and would also be depleted in HSE relative to BSE. A typical example of a komatiite system derived from such a mantle domain is the Boston Creek komatiites (Puchtel et al., 2018).

Using the data for the komatiite systems, for which late accretion has been argued to be the main cause for the observed  $^{182}\text{W}$  versus source HSE abundance relationships (**Fig. 6**), and assuming that the  $^{182}\text{W}$  excesses were due entirely to a deficit of late accreted materials in their mantle sources, Puchtel et al. (2022) estimated  $\mu^{182}\text{W}$  of the pre-late accretionary BSE to be  $+17\pm7$  (**Fig. 6**). This estimate is consistent with the  $^{182}\text{W}$  excess in the pre-late accretion BSE of  $+18\pm9$  ppm obtained by Kleine and Walker (2017) using an independent approach and to the estimates for the  $^{182}\text{W}$  composition of the pre-late accretionary Moon of  $+25\pm5$  ppm (Kruijer et al., 2015; Touboul et al., 2015; Kruijer and Kleine, 2017). These similarities provide further support to the hypothesis that the Earth and the Moon formed from material with identical W isotopic compositions (Kleine and Walker, 2017), in concert with earlier observations of similarity of O, Si, and Ti isotopic compositions between the Earth and the Moon (*e.g.*, Dauphas et al., 2014), as well as additional evidence that the Moon likely formed mainly from terrestrial, rather than impactor, material.

### 6.3. Core-mantle boundary processes

Core-mantle exchange is yet another process that may have been responsible for creating large  $^{182}\text{W}$  and  $^{186,187}\text{Os}$  isotope and HSE abundance heterogeneities in the mantle. Originally, the idea was proposed by Walker et al. (1995) based on their studies of the Re, Pt, and Os partitioning behavior in group IIAB magmatic iron meteorites. Walker et al. (1995) noted that during magmatic differentiation, solid metal – liquid metal partition coefficients decrease in the order  $D_{\text{Os}} > D_{\text{Re}} > D_{\text{Pt}}$ , so that after crystallization of the inner core, the liquid outer core would end up with supra-chondritic Re/Os and Pt/Os and, given enough time, would develop coupled  $^{186,187}\text{Os}$  enrichments. Walker et al. (1997) observed a coupled radiogenic  $^{186,187}\text{Os}$  signature in the Noril'sk sulfide ores, which they interpreted as having originated from interaction of the starting 251 Ma Siberian superplume (*e.g.*, Campbell, 2007) with the liquid outer core at the CMB.

The concept of core-mantle interaction was further elaborated upon by Brandon et al. (1998, 1999, 2003) and Puchtel et al. (2005) in their studies of plume-derived ocean island basalts and komatiites. These authors proposed that the type of correlation between the initial

$\mu^{186}\text{Os}$  and  $\gamma^{187}\text{Os}$  values observed in plume-derived Hawaiian picrites and Gorgona Island and Kostomuksha komatiites is unique to mixtures with fractionated liquid outer core metal (Pt/Re  $\sim$ 100), whereas common crustal materials have Pt/Re  $<$ 30.

The major drawback of the original core-mantle interaction model stems from the fact that the onset of inner core crystallization is poorly constrained, ranging from  $<$ 1.0 to 3.5 Ga given the uncertainties in estimates of present-day heat flux at the CMB which vary from 3 to 10 TW (see review in Nakagawa, 2020, and references therein), as well as currently insufficient knowledge of the partition coefficients of radioactive elements (*e.g.*, K) under the CMB conditions. Another issue concerns the fact that the core-mantle interaction model of Walker et al. (1995) and Brandon et al. (1998, 1999) calls for physical addition of  $\sim$ 1% of the outer core liquid metal to the silicate lower mantle. Because the liquid outer core has up to three orders of magnitude higher HSE abundances compared to the mantle, the  $^{186}, ^{187}\text{Os}$  composition of the resulting hybrid mantle source would be dominated by that of the outer core, and this source would also have had an order of magnitude higher HSE abundances compared to those in the BSE. Most OIB, including Hawaiian picrites, are sulfur-saturated melts and likely to have lost a significant part of their HSE inventory to either immiscible sulfide liquid fractionation or to retaining residual sulfide in their melting source regions (*e.g.*, Shirey and Walker, 1998; Bennett et al., 2000; Jamais et al., 2008; Ireland et al., 2009). Such loss of HSE during magma generation and ascent would not be the case for komatiites, however, which are strongly sulfur-undersaturated magmas and, therefore, reliably record the HSE abundances in their mantle source regions upon emplacement. Yet, those komatiites for which input from the outer core has been advocated to explain their coupled  $^{186}, ^{187}\text{Os}$  enrichments, *e.g.*, Gorgona Island (Brandon et al., 2003) and Kostomuksha (Puchtel et al., 2005) komatiites, have calculated HSE abundances in their mantle source regions similar to those in estimates for the modern BSE.

To reconcile the  $^{186}, ^{187}\text{Os}$  and HSE abundance data for the Kostomuksha komatiites with this apparent inconsistency, Puchtel and Humayun (2000) proposed a mechanism of core-mantle interaction *via* isotopic exchange at the core-mantle interface, without any significant mass transfer from the core to the mantle. This idea has been further advanced by Humayun (2011). The mechanism of core-mantle interaction of Humayun (2011) requires the outer core liquid to be trapped in a cumulate pile of Fe-rich non-metallic precipitates (FeO, FeS, Fe<sub>3</sub>Si) at the top of the core, then undergo fractional crystallization by precipitating solid metal grains and leaving behind the residual metallic liquid. The residual liquid is then incorporated into the base of the mantle, where it subsequently may be entrained by mantle plumes.

Based on the discovery of negative  $\mu^{182}\text{W}$  values in some modern ocean island basalts, Mundl et al. (2017), Rizo et al. (2019), and Mundl-Petermeier et al. (2019, 2020) have also argued for some form of core-mantle exchange/equilibration in order to transfer the inferred negative  $\mu^{182}\text{W}$  value of the core of  $-220$  to plumes rising from the CMB. Although the  $^{186,187}\text{Os}$  and  $^{182}\text{W}$  data obtained on the same samples are still limited, all Hawaiian lavas with negative  $\mu^{182}\text{W}$  (ranging between  $-7.8$  and  $-20.2$ ) are also characterized by positive  $\mu^{186}\text{Os}$  (ranging between  $+18.6$  and  $+62.8$ ) and positive  $\gamma^{187}\text{Os}$  (ranging between  $+2.0$  and  $+7.2$ ). Furthermore, Puchtel et al. (2020) obtained a negative  $\mu^{182}\text{W}$  value of  $-10$  for the Lapland komatiites, which is within the range of the  $\mu^{182}\text{W}$  values obtained for Hawaii, and proposed that Lapland komatiites could be early Proterozoic equivalents of Hawaiian picrites. A core-mantle interaction process, as put forward by Puchtel et al. (2020), would be expected to have decreased the  $^{182}\text{W}$  value in the Lapland komatiite source relative to the ambient mantle, and also have increased the HSE abundances in this source over ambient mantle levels, which is consistent with the observations (**Fig. 6**). That study further proposed that if the residual metal in the model of Humayun (2011) had a composition similar to that of fractionated iron meteorites, its entrainment into the mantle plume that gave rise to the Lapland komatiites could explain the decoupled  $^{186,187}\text{Os}$  systematics of these komatiites.

#### 6.4. Crustal recycling processes

Yet another important mechanism for creating mantle chemical heterogeneities is recycling of Earth's mantle lithosphere, oceanic crust, and sedimentary layers back into the mantle (Hofmann and White, 1982; Shirey and Hanson, 1986; Chase and Patchett, 1988; Campbell and Griffiths, 1992; Hart et al., 1992; Carlson, 1994; Roy-Barman and Allègre, 1995; Widom, 1997; Lassiter and Hauri, 1998; Blichert-Toft et al., 1999; Lassiter, 2006). This recycling may occur via subduction – a process by which one tectonic plate moves under another and sinks into the mantle as the plates converge; subduction is the driving force behind modern plate tectonics. The subducted material may age in the mantle for hundreds of millions of years until entrained in mantle plumes. Although there is little agreement on the timing of the onset or even existence of modern-style plate tectonics in the Hadean and Archean (e.g., Brown, 2007; Shirey et al., 2008; Gerya, 2014; Sizova et al., 2015; Johnson et al., 2017; Bédard, 2018), several lines of geochemical evidence put forward by Shirey et al. (2008) require that some version of modern-style plate tectonics already operated as far back in Earth history as 3.5 billion years ago, followed by a transition from the stagnant-lid to mobile-lid plate tectonic regimes sometime in the late Archean (O'Neill and Debaille, 2014).

Crustal recycling, e.g., in the form of subduction of pelagic sediments into the mantle, may also cause decoupling of Nd and Hf isotope systematics of lavas from the Nd-Hf mantle array, as has been argued to be the case for a suite of drill core Komati komatiite samples (Blichert-Toft et al., 2015). This is due to the fact that the Lu/Hf ratio is strongly fractionated relative to Sm/Nd in the Earth's sedimentary system (Patchett et al., 1984). This is caused by high resistance to chemical weathering of the mineral zircon, which contains most of the Hf budget of continental crustal rocks. During weathering of continental crustal rocks, they break down into zircon-bearing sandy sediments with very low Lu/Hf and fine-grained clay material with up to three times the chondritic Lu/Hf ratio. During sediment transport via turbidity currents, sandy sediments stay on or near the continent, while the pelagic material is carried out onto the ocean floor, where it may eventually be subducted into the mantle.

## 7. The Nd-Hf-Os isotope paradox and its implications for early Earth history

As noted above, there is evidence for decoupling between the radiogenic lithophile  $^{143}\text{Nd}$  and  $^{176}\text{Hf}$  systems in certain komatiites mantle sources, but there is also apparent decoupling between these lithophile isotope systems and the highly siderophile  $^{187}\text{Os}$  system in some komatiite mantle sources. The majority of the Archean and Proterozoic komatiite systems are characterized by variable, and generally strong, long-term depletions in more incompatible lithophile trace elements relative to less incompatible elements, e.g., Nd versus Sm and Hf versus Lu (**Fig. 1**), yet they retain chondritic time-integrated Re/Os (**Fig. 2**). These komatiite mantle sources must have experienced relatively early melt depletion events that fractionated the Sm/Nd and Lu/Hf ratios to suprachondritic values high enough to bring the  $^{143}\text{Nd}$  and  $^{176}\text{Hf}$  compositions to the variably positive  $\epsilon^{143}\text{Nd}$  and  $\epsilon^{176}\text{Hf}$  values. Since Re is generally moderately to highly incompatible during mantle melting, whereas Os is moderately to highly compatible (e.g., Barnes et al., 1985; Mallmann and O'Neill, 2007), these melt extraction events should have also decreased the Re/Os ratio in the komatiite-basalt mantle sources. This would have resulted in retardation of  $^{187}\text{Os}$  ingrowth and, thus, evolution of the sources to variably negative  $\gamma^{187}\text{Os}$  values. However, such isotopic relationships are not observed in the global komatiite record.

Puchtel et al. (2022) named this phenomenon the Nd-Hf-Os isotope paradox, to which Puchtel et al. (2020, 2022) offered a solution by developing a model whereby the komatiite-basalt mantle sources underwent early (~100 Ma into Solar System history), low-degree ( $F = 1.5\text{-}2.0\%$ ) partial melting and melt extraction events that would have sufficiently fractionated the Sm/Nd and Lu/Hf ratios in the mantle sources, but would have had little effect on the

Re/Os ratio due to the significantly lower incompatibility of Re compared to Nd and Hf during low-degrees of partial mantle melting.

Because this depleted reservoir is apparently persistent throughout the Archean and is globally distributed, it requires early formation and subsequent complete isolation of a complementary basaltic crust enriched in incompatible lithophile trace elements. Calculations by Puchtel et al. (2022) indicate that such crust formed as a result of 1.5-2.0% batch melting of a BSE-like mantle would contain 31-27 ppm Nd, 7.1-6.5 ppm Sm, 0.62-0.59 ppm Lu, and 5.2-4.7 ppm Hf, and would have  $^{147}\text{Sm}/^{144}\text{Nd} = 0.140\text{-}0.145$  and  $^{176}\text{Lu}/^{177}\text{Hf} = 0.0166\text{-}0.0174$  (compared to 0.1967 and 0.0336 in the BSE, respectively). Based on these estimates of Sm and Nd concentrations in the early crust, the mass of this reservoir must have represented  $\leq 2.0\%$  of the mass of the BSE, which is consistent with this reservoir being the size of the D'' layer. The existence of such crust has been previously advocated for by Galer and Goldstein (1991). Alternatively, this earliest mafic crust could have served as the source of the oldest tonalite-trondhjemite-granodiorite (TTG) complexes (Carlson et al., 2019), such as those from the Nuvvuagittuq Greenstone Belt in Québec (O'Neil et al., 2008, 2016) or the Vodla Block TTG complex in the Fennoscandian Shield (Puchtel et al., 2016b).

The residence time of this early mafic crust in the mantle is difficult to constrain. The available komatiite-basalt record would require its isolation through at least the late Archean, *i.e.*, when the  $^{142}\text{Nd}$  anomalies were still present in the mantle (Debaille et al., 2013). However, there is no evidence that this crust was stored in the mantle until the present day, based on the generally chondritic  $^{138}\text{Ce}$ ,  $^{142,143}\text{Nd}$ , and  $^{176}\text{Hf}$  composition estimates for the BSE (Jackson and Carlson, 2012; Horan et al., 2018; Willig and Stracke, 2019; Willig et al., 2020; Hyung and Jacobsen, 2020).

## 8. Komatiite constraints on early mixing rates of the terrestrial mantle

It has been proposed that the mixing rates of the mantle, or the average time of mantle homogenization, can be evaluated through studies of short-lived radiogenic isotope systematics and HSE abundances in mantle-derived rocks (*e.g.*, Jacobsen and Yu, 2015; Carlson et al., 2019; Hyung and Jacobsen, 2020; Tusch et al., 2021; Puchtel et al., 2022). Isotopic variations due to the decay of the now extinct  $^{146}\text{Sm}$  and  $^{182}\text{Hf}$  nuclides recorded processes in the Earth that fractionated Sm/Nd and Hf/W ratios between different terrestrial reservoirs at the times when these parent nuclides were still alive. When these events occurred during the first ~600 and ~60 Ma of Earth history, respectively, the differentiation processes resulted in formation of  $^{142}\text{Nd}$  and  $^{182}\text{W}$  anomalies in these terrestrial reservoirs. Due to the



protracted, violent accretion history of the Earth accompanied by vigorous convective mixing during the Hadean and Archean eons, these reservoirs and, thus, the isotopic anomalies they hosted, were gradually erased from the geological record. Hence, tracing the variations in the magnitude of these isotopic anomalies over geological time can be used to determine the mixing rates of the terrestrial mantle (*e.g.*, Jacobsen and Yu, 2015; Hyung and Jacobsen, 2020).

Early mantle convection models (*e.g.*, Blichert-Toft and Albarède, 1994; Coltice and Schmalz, 2006) concluded that the mixing times in the hot Hadean and Archean mantle were 10 times faster than today, and that any large-scale primordial chemical and isotopic heterogeneities in the mantle would have been erased within ~100 Ma of their creation. However, during the past two decades, numerous  $^{142}\text{Nd}$  and  $^{182}\text{W}$  anomalies have been discovered in the terrestrial mantle-derived rock record (**Fig. 7**). The largest  $^{142}\text{Nd}$  anomalies ( $\mu^{142}\text{Nd}$  up to +20 ppm and down to -20 ppm) have been reported for Eo- to Paleoarchean supracrustal rocks from the Isua Greenstone Belt, Greenland (Boyet et al., 2003; Caro et al., 2006; Bennett et al., 2007; Rizo et al., 2011; 2012; 2013; O'Neil et al., 2016), the Nuvvuagittuq Greenstone Belt, Québec (O'Neil et al., 2008; 2012; Roth et al., 2013), the Acasta Gneiss Complex, Canada (Roth et al., 2014; Reimink et al., 2018), and the Barberton Greenstone Belt, Kaapvaal Craton, South Africa (Puchtel et al., 2016a; Boyet et al., 2021). These isotopic anomalies must have been created before ~4.0 Ga by silicate-silicate differentiation and, thus, have survived for >1.0 Ga, implying much slower mixing times of the mantle for  $^{142}\text{Nd}$  than was predicted by the early mantle convection models. Following these discoveries, more recent mantle convection models argue for complete homogenization of the mantle by the end of the Archean (*e.g.*, Rosas and Korenaga, 2018; Korenaga, 2021). Only few terrestrial samples with ages between 3.0 and 2.7 Ga have  $\mu^{142}\text{Nd}$  values deviating from the terrestrial standard by more than  $\pm 5$  ppm, the only known exception being 2.72 Ga tholeiites from the Abitibi Greenstone Belt, Canada (Debaille et al., 2013). Although there is a significant gap in the mafic-ultramafic rock record for  $^{142}\text{Nd}$  data between ~2.7 Ga and the present day, it indeed appears that  $^{142}\text{Nd}$  anomalies largely disappeared by the end of the Archean (**Fig. 7**). As a result, on the basis of the now much larger  $^{142}\text{Nd}$  record and using a mathematical mantle mixing box model, Hyung and Jacobsen (2020) concluded that the relationships in **Fig. 7** are consistent with mantle mixing rates of ~400 Ma that operated since the early Hadean. These authors further argued that such fast mixing rates are consistent with Earth's thermal and chemical evolution having been largely regulated by plate tectonics for most of its history.

Nonetheless, recent studies have shown that some modern plume-derived OIB (**Fig. 7**) have  $^{142}\text{Nd}$  compositions resolved, albeit marginally, from the terrestrial standard (*e.g.*, Horan et al., 2018; Peters et al., 2018), indicating that some  $^{142}\text{Nd}$  isotopic signatures dating back to Earth's earliest differentiation events may still be preserved in deepest parts of the modern mantle.

In contrast to the earliest  $^{142}\text{Nd}$  record, mostly positive  $^{182}\text{W}$  anomalies, of up to  $\sim +20$  ppm, have been reported for mafic-ultramafic rocks ranging in age from 4.0 to 2.7 Ga (**Fig. 7b**). The only exceptions are komatiites from the Schapenburg system (Puchtel et al., 2016a), which have a negative  $^{182}\text{W}$  anomaly of  $-8$  ppm. On the other hand, some recent and modern OIB, such as Hawaii, Samoa, Iceland, Galapagos, Heard, Pitcairn (Mundl et al., 2017; Mundl-Petermeier et al., 2019, 2020), and Kerguelen and Reunion (Rizo et al., 2019) are characterized by negative  $^{182}\text{W}$  anomalies down to  $-25$  ppm, although the volumetrically dominant signature in OIB is most likely  $^{182}\text{W} = 0$ . The very limited data available (Puchtel et al., 2016b, 2020) provide a hint that there may be a transition at  $\sim 2.5$  Ga from mostly positive  $\mu^{182}\text{W}$ -dominated to no-anomaly  $\mu^{182}\text{W}$ -dominated mantle (**Fig. 7b**). With the relatively young 2.05 Ga Lapland komatiites already registering a negative  $^{182}\text{W}$  anomaly of  $-10$  ppm (Puchtel et al., 2020), and some OIB sources registering negative  $^{182}\text{W}$  anomalies down to  $-25$  ppm, this transition may indicate the combined effects of the onset of modern-style plate tectonics and core-mantle interaction taking over as the main driving forces controlling the W isotopic composition of the deep plume mantle sources (*e.g.*, Rizo et al., 2019; Carlson et al., 2019).

The different behavior of the two short-lived isotopic systems in the mantle may be possible to reconcile when the mechanisms behind the origin of  $^{142}\text{Nd}$  and  $^{182}\text{W}$  anomalies are considered. Because both Sm and Nd are uniformly strongly lithophile elements under the redox conditions applicable to Earth's formation,  $^{142}\text{Nd}$  anomalies are solely the result of primordial silicate-silicate planetary differentiation (*e.g.*, Boyet and Carlson, 2005). No new  $^{142}\text{Nd}$  anomalies could have been created in the BSE after  $\sim 4.0$  Ga, when  $^{146}\text{Sm}$  became extinct. In contrast to the  $^{146}\text{Sm}$ - $^{142}\text{Nd}$  system, Hf is strongly lithophile, while W is moderately siderophile. Hafnium, therefore, can be fractionated from W during metal-silicate differentiation, such as that which occurred during planetary core segregation. During silicate-silicate differentiation, W is more incompatible than Hf, which can result in fractionation of Hf from W in purely silicate systems. Both processes are considered to be capable of creating  $^{182}\text{W}$  anomalies within the first 60 Ma of Earth's history, while  $^{182}\text{Hf}$  was still extant. The additional processes that are thought to be capable of introducing  $^{182}\text{W}$  heterogeneities to the

mantle and to which the  $^{142}\text{Nd}$  system was insensitive, were late accretion and core-mantle interaction, as discussed in **Section 6**. As a result of the combination of all these factors in variable, and generally unconstrained, proportions, the use of the  $^{182}\text{Hf}$ - $^{182}\text{W}$  isotopic system for tracing mixing times of the mantle appears to be of lesser value than the  $^{146}\text{Sm}$ - $^{142}\text{Nd}$  systematics.

Mantle mixing rates in terms of HSE have been studied *via* tracing the changes in HSE abundances in the mantle over the span of geological time (*e.g.*, Maier et al., 2009; Puchtel et al., 2018, 2020, 2022). Because the lunar highland crust, which was formed at  $\sim 4.4$  Ga (*e.g.*, Borg et al., 2014), is only negligibly contaminated by meteoritic material (*e.g.*, Day et al., 2010), late accretion must have been largely complete prior to 4.4 Ga, *i.e.*, within the first  $\sim 150$  Ma of the Solar System history. Puchtel et al. (2022) used the estimated HSE abundances in the sources of the Archean and Proterozoic komatiite systems plotted in **Fig. 3** as a function of their ages and *Isoplot* regression analysis to calculate the average time by which the late accreted materials would have been completely homogenized within the mantle, and found  $2.5 \pm 0.2$  Ga. These data require that survival times of the late accreted planetesimals within the mantle, before complete homogenization, were on average  $1.9 \pm 0.2$  Ga (*i.e.*, the time interval between 4.4 and 2.5 Ga), thus constraining the average mixing rates of the terrestrial mantle in terms of siderophile element abundances in the Hadean and the Archean. This period in time coincides with the timing of onset of modern-style plate tectonics on Earth, as argued by some (Brown, 2007; Brown and Johnson, 2018), and with the near-complete disappearance of all  $^{142}\text{Nd}$  and positive  $^{182}\text{W}$  anomalies in the mantle (Carlson et al., 2019; Reimink et al., 2020; Tusch et al., 2021).

It is possible that some inefficient mixing could be due to early Earth tectonic regimes differing from those of modern-style plate tectonics (O'Neill and Debaille, 2014). A stagnant-lid, or episodic, subduction regime in the Hadean is consistent with the persistence of short-lived isotopic anomalies and compositional heterogeneities, although more recent modeling indicates that such mantle heterogeneities can survive for billions of years, even under a mobile-lid tectonic regime (Foley and Rizo, 2017).

## **9. The diverse nature of komatiite sources reflects on the complexity of the terrestrial mantle**

As is evident from the chemical and isotopic data summarized in **Tables 1** and **2** and discussed throughout this review, komatiite mantle sources were characterized by extreme diversity throughout the Archean and early Proterozoic in terms of both trace- and HSE

abundances and radiogenic isotope systematics. Early Archean komatiites were likely derived from lower mantle domains that were created very early in Earth history as a result of deep-seated magma ocean crystallization processes. These mantle domains were characterized by highly variable, and often strong, long-term depletions in the highly incompatible lithophile trace elements and generally large deficits in the late accreted component, as attested to by their HSE abundance and  $^{182}\text{W}$  systematics.

The late Archean and Proterozoic komatiites show evidence in their mantle sources for limited variability of long-term depletions in highly incompatible lithophile trace elements as a result of prior melt extractions. With the exception of the Kostomuksha and possibly Lapland systems, these komatiites were derived from mantle plumes that originated in the upper mantle, most likely in the MTZ. These komatiite sources were characterized by smaller deficits to excesses in the late accreted component, as testified to by their HSE abundance and  $^{182}\text{W}$  systematics.

Finally, our compilation of the geochemical data relevant to the mantle sources of Archean and early Proterozoic komatiites reveals that none of the projected sources were similar in composition to estimates for the BSE. The komatiite systems considered here, which span wide geographical and temporal distributions, further demonstrate that no single petrogenetic model can account for all the diverse chemical compositions of komatiites.

## 10. Conclusions

Komatiites, due to their unique properties and, with a few exceptions, very old ages, are among the best samples to constrain the evolution of the chemical composition of the early Earth's mantle. Isotopic and elemental signatures created in early-formed silicate reservoirs *via* radioactive decay of short- and long-lived nuclides, including  $^{146,147}\text{Sm}$ ,  $^{176}\text{Lu}$ ,  $^{182}\text{Hf}$ ,  $^{187}\text{Re}$ , and  $^{190}\text{Pt}$ , have been sampled by komatiitic magmas and preserved in the geological rock record. These signatures have been used here to constrain the nature and timing of formation of these, by now largely vanished, mantle reservoirs.

The komatiites considered in the present review are interpreted to have been derived from anhydrous melting in mantle plumes that were initiated in both the lower and upper mantle, although, in contrast to modern plumes, all evidence for the depths of ancient mantle plume initiation is circumstantial in nature.

The data for the existing 3.6-2.0 Ga komatiite record provide robust evidence for the presence of remarkably ancient isotopic and chemical heterogeneities in the mantle at that time interval in Earth history. These heterogeneities have been shown here to reflect the

combined effects of (i) the co-existence of diverse post-magma ocean silicate domains characterized by variably-fractionated lithophile and siderophile element abundances; (ii) the presence of distinct reservoirs representing mantles and cores of large, differentiated planetesimals delivered to Earth during late accretion; and (iii) isotopic exchange across the core-mantle boundary.

The near-complete disappearance of resolvable  $^{142}\text{Nd}$  anomalies and of decoupled  $^{143}\text{Nd}$ - $^{176}\text{Hf}$  isotopic signatures in the mafic-ultramafic rock record by  $\sim 2.5$  Ga indicates that the earliest silicate reservoirs, formed as a result of primordial magma ocean crystallization, had been largely destroyed by that time through vigorous, convective mantle mixing, implying mixing rates of the mantle on the order of  $\sim 1.5$  Ga. The shift from mostly positive  $^{182}\text{W}$  offsets in the pre-2.5 Ga mantle sources of mafic-ultramafic lavas to no  $^{182}\text{W}$  offsets at  $\sim 2.5$  Ga, as well as disappearance of HSE abundance anomalies at  $\sim 2.5$  Ga, may indicate the combined effects of the onset of modern-style plate tectonics and core-mantle interaction that took over as the main driving force of creating  $^{182}\text{W}$  isotopic heterogeneities in the mantle.

This review further emphasizes the great compositional complexity of early Archean to early Proterozoic komatiite mantle sources in terms of both lithophile and siderophile element abundances and isotope systematics; apparently, none of these sources were similar in composition to that of the BSE. Obviously, no single petrogenetic model can fully account for the chemical and isotopic diversity of komatiites.

## Acknowledgements

This work was supported by NSF Petrology and Geochemistry grant EAR 1754186 to ISP. We are grateful to Al Hofmann and Maud Boyet for thorough and constructive reviews of the initial version of this manuscript and to Catherine Chauvel for editorial handling. This work greatly benefitted from close collaborations with Carl Anhaeusser, Nick Arndt, Gary Byerly, Eero Hanski, Al Hofmann, Munir Humayun, Vyacheslav and Victoria Kulikov, Mike Leshner, Marek Locmelis, Euan Nisbet, and Andi Mundl-Petermeier.

- 1201 Abbott, D., 1996. Plumes and hotspots as sources of greenstone belts. *Lithos* 37 (2-3): 113-  
1202 127.
- 1203 Abe, Y., 1997. Thermal and chemical evolution of the terrestrial magma ocean. *Physics of the*  
1204 *Earth and Planetary Interiors* 100 (1-4): 27-39.
- 1205 Agee, C.B. and Walker, D., 1988. Static compression and olivine flotation in ultrabasic  
1206 silicate liquid. *Journal of Geophysical Research* 93 (B4): 3437-3449.
- 1207 Albarède, F., Blichert-Toft, J., Vervoort, J. D., Gleason, J. D., Rosing, M., 2000. Hf-Nd  
1208 isotope evidence for a transient dynamic regime in the early terrestrial mantle. *Nature* **404**  
1209 (6777): 488-490.
- 1210 Allègre, C.J., 1982. Genesis of Archaean komatiites in a wet ultramafic subducted plate. In:  
1211 Arndt, N.T. and Nisbet, E.G. (Eds.), *Komatiites*, George Allen and Unwin, London, pp.  
1212 495-500.
- 1213 Andreasen, R., Sharma, M., Subbarao, K.V., and Viladkar, S.G., 2008. Where on Earth is the  
1214 enriched Hadean reservoir? *Earth and Planetary Science Letters* 266 (1-2): 14-28.
- 1215 Archer, G.J., Brennecka, G.A., Gleißner, P., Stracke, A., Becker, H., and Kleine, T., 2019.  
1216 Lack of late-accreted material as the origin of  $^{182}\text{W}$  excesses in the Archaean mantle:  
1217 Evidence from the Pilbara Craton, Western Australia. *Earth and Planetary Science Letters*,  
1218 528: 115841.
- 1219 Arevalo, R., McDonough, W. F., 2008. Tungsten geochemistry and implications for  
1220 understanding the Earth's interior. *Earth and Planetary Science Letters* **272** (3-4): 656-665.
- 1221 Armstrong, R. L., 1981. Radiogenic isotopes: the case for crustal recycling on a near-steady-  
1222 state no-continental-growth. *Philosophical Transactions of the Royal Society of London*  
1223 **A301**: 443-472.
- 1224 Arndt, N.T., 1994. Archaean Komatiites. In: Condie, K.C. (Ed.). *Archaean Crustal Evolution*,  
1225 Elsevier, Amsterdam, pp. 11-44.
- 1226 Arndt, N.T. and Nisbet, E.G., 1982. *Komatiites*. Allen and Unwin, London, 582 pp.
- 1227 Arndt, N.T., Leshar, C.M., and Barnes, S.J., 2008. *Komatiite*. Cambridge University Press,  
1228 Cambridge, UK, 467 pp.
- 1229 Arndt, N.T., Naldrett, A.J., Pyke, D.R., 1977. Komatiitic and iron-rich tholeiitic lavas of  
1230 Munro Township, northeast Ontario. *Journal of Petrology* **18**: 319-369.
- 1231 Arndt, N.T., 1977. Ultrabasic magmas and high-degree melting of the mantle. *Contributions*  
1232 *to Mineralogy and Petrology* 64 (2): 205-221.
- 1233 Arndt, N.T., Ginibre, C., Chauvel, C., Albarède, F., Cheadle, M., Herzberg, C., Jenner, G.,  
1234 and Lahaye, Y., 1998. Were komatiites wet? *Geology* 26 (8): 739-742.
- 1235 Arndt, N., Bruzak, G., and Reischmann, T., 2001. The oldest continental and oceanic  
1236 plateaus: Geochemistry of basalts and komatiites of the Pilbara Craton, Australia.  
1237 *Geological Society of America Special Paper* 352: 359-387.
- 1238 Asafov, E.V., Sobolev, A.V., Gurenko, A.A., Arndt, N.T., Batanova, V.G., Portnyagin, M.V.,  
1239 Garbe-Schönberg, D., and Krashennnikov, S.P., 2018. Belingwe komatiites (2.7 Ga)  
1240 originate from a plume with moderate water content, as inferred from inclusions in  
1241 olivine. *Chemical Geology* 478: 39-59.

1242 Ballmer, M.D., Schumacher, L., Lekic, V., Thomas, C., and Ito, G., 2016. Compositional  
1243 layering within the large low shear-wave velocity provinces in the lower mantle.  
1244 *Geochemistry, Geophysics, Geosystems* 17 (12): 5056-5077.

1245 Bao, X., Lithgow-Bertelloni, C.R., Jackson, M.G., and Romanowicz, B., 2022. On the relative  
1246 temperatures of Earth's volcanic hotspots and mid-ocean ridges. *Science* 373 (6576): 57-  
1247 61.

1248 Barnes, S.-J., Naldrett, A.J., Gorton, M.P., 1985. The origin of the fractionation of platinum-  
1249 group elements in terrestrial magmas. *Chemical Geology* 53 (3-4): 303-323.

1250 Barnes, S.J. and Van Kranendonk, M.J., 2014. Archean andesites in the east Yilgarn craton,  
1251 Australia: Products of plume-crust interaction? *Lithosphere* 6 (2): 80-92.

1252 Barnes, S.J., Mole, D., Wyche, S., and Dering, G., 2016. Komatiites and associated rocks of  
1253 the Kalgoorlie–Leonora region. *Geological Survey of Western Australia Record* 2016/12,  
1254 70 pp.

1255 Becker, H., Horan, M.F., Walker, R.J., Gao, S., Lorand, J.-P., and Rudnick, R.L., 2006.  
1256 Highly siderophile element composition of the Earth's primitive upper mantle: Constraints  
1257 from new data on peridotite massifs and xenoliths. *Geochimica et Cosmochimica Acta* 70  
1258 (17): 4528-4550.

1259 Bédard, J.H., 2018. Stagnant lids and mantle overturns: Implications for Archaean tectonics,  
1260 magmagenesis, crustal growth, mantle evolution, and the start of plate tectonics.  
1261 *Geoscience Frontiers* 9 (1): 19-49.

1262 Bennett, V.C., Esat, T.M., and Norman, M.D., 1996. Two mantle-plume components in  
1263 Hawaiian picrites inferred from correlated Os-Pb isotopes. *Nature* **381** (6579): 221-224.

1264 Bennett, V.C., Norman, M.D., and Garcia, M.O., 2000. Rhenium and platinum group element  
1265 abundances correlated with mantle source components in Hawaiian picrites: sulphides in  
1266 the plume. *Earth and Planetary Science Letters* 183 (3-4): 513-526.

1267 Bennett, V.C., Brandon, A.D., and Nutman, A.P., 2007. Coupled  $^{142}\text{Nd}$ - $^{143}\text{Nd}$  isotopic  
1268 evidence for Hadean mantle dynamics. *Science* 318 (5858): 1907-1910.

1269 Bercovici, D. and Karato, S., 2003. Whole-mantle convection and the transition-zone water  
1270 filter. *Nature* 425 (6953): 39-44.

1271 Berry, A.J., Danyushevsky, L.V., O'Neill, H.S.C., Newville, M., and Sutton, S.R., 2008.  
1272 Oxidation state of iron in komatiitic melt inclusions indicates hot Archaean mantle.  
1273 *Nature* 455 (7215): 960-963.

1274 Bickle, M.J., 1982. The magnesium contents of komatiitic liquids. In: *Komatiites*. George  
1275 Allen and Unwin, London, pp. 479-494.

1276 Bickle, M.J., 1986. Implications of melting for stabilisation of lithosphere and heat loss in the  
1277 Archaean. *Earth and Planetary Science Letters* 80 (3-4): 314-324.

1278 Bina, C.R. and Helffrich, G., 1994. Phase transition Clapeyron slopes and transition zone  
1279 seismic discontinuity topography. *Journal of Geophysical Research* 99 (B8): 15853-  
1280 15860.

1281 Blichert-Toft, J. and Albarède, F., 1994. Short-lived chemical heterogeneities in the Archaean  
1282 mantle with implications for mantle convection. *Science* 263: 1593-1596.

1283 Blichert-Toft, J. and Arndt, N.T., 1999. Hf isotope compositions of komatiites. *Earth and*  
1284 *Planetary Science Letters* 171(3): 439-451.

1285 Blichert-Toft, J., Frey, F.A., and Albarède, F., 1999. Hf isotope evidence for pelagic  
1286 sediments in the source of Hawaiian basalts. *Science* **285**: 879-882.

1287 Blichert-Toft, J. and Puchtel, I.S., 2010. Depleted mantle sources through time: Evidence  
1288 from Lu-Hf and Sm-Nd isotope systematics of Archean komatiites. *Earth and Planetary*  
1289 *Science Letters* 297 (3-4): 598-606.

1290 Blichert-Toft, J., Arndt, N.T., Wilson, A., and Coetzee, G., 2015. Hf and Nd isotope  
1291 systematics of early Archean komatiites from surface sampling and ICDP drilling in the  
1292 Barberton Greenstone Belt, South Africa. *American Mineralogist* 100: 2396-2411.

1293 Borg, L.E., Gaffney, A.M., and Shearer, C.K., 2014. A review of lunar chronology revealing  
1294 a preponderance of 4.34–4.37 Ga ages. *Meteoritics and Planetary Science* **50** (4): 715-732.

1295 Borisov, A. and Palme, H., 1997. Experimental determination of the solubility of platinum in  
1296 silicate melts. *Geochimica et Cosmochimica Acta* 61 (20): 4349-4357.

1297 Botke, W.F., Morbidelli, A., Jedicke, R., Petit, J.-M., Levison, H.F., Michel, P., Metcalfe,  
1298 T.S., 2002. Debaised Orbital and Absolute Magnitude Distribution of the Near-Earth  
1299 Objects. *Icarus* 156 (2): 399-433.

1300 Botke, W.F., Levison, H.F., Nesvorny, D., Dones, L., 2007. Can planetesimals left over from  
1301 terrestrial planet formation produce the lunar Late Heavy Bombardment? *Icarus* 190 (1):  
1302 203-223.

1303 Botke, W.F., Walker, R.J., Day, J.M.D., Nesvorny, D., and Elkins-Tanton, L., 2010.  
1304 Stochastic Late Accretion to Earth, the Moon, and Mars. *Science* 330 (6010): 1527-1530.

1305 Bouvier, A., Vervoort, J.D., and Patchett, P.J., 2008. The Lu-Hf and Sm-Nd isotopic  
1306 composition of CHUR: Constraints from unequilibrated chondrites and implications for  
1307 the bulk composition of terrestrial planets. *Earth and Planetary Science Letters* 273 (1-2):  
1308 48-57.

1309 Boyet, M., Blichert-Toft, J., Rosing, M., Storey, M., Télouk, P., and Albarède, F., 2003. <sup>142</sup>Nd  
1310 evidence for early Earth differentiation. *Earth and Planetary Science Letters* 214 (3-4):  
1311 427-442.

1312 Boyet, M., and Carlson, R.W., 2005. <sup>142</sup>Nd evidence for early (>4.53 Ga) global  
1313 differentiation of the silicate Earth. *Science* **309** (5734): 576-581.

1314 Boyet, M., and Carlson, R.W., 2006. A new geochemical model for the Earth's mantle  
1315 inferred from <sup>146</sup>Sm-<sup>142</sup>Nd systematics. *Earth and Planetary Science Letters* 250 (1-2):  
1316 254-268.

1317 Boyet, M., Garçon, M., Arndt, N.T., Carlson, R. W., and Konc, Z., 2021. Residual liquid from  
1318 deep magma ocean crystallization in the source of komatiites from the ICDP drill core in  
1319 the Barberton Greenstone Belt. *Geochimica et Cosmochimica Acta* 304: 141-159.

1320 Brenan, J.M. and McDonough, W.F., 2009. Core formation and metal-silicate fractionation of  
1321 osmium and iridium from gold. *Nature Geoscience* 2: 798-801.

1322 Brown, M. and Johnson, T., 2018. Secular change in metamorphism and the onset of global  
1323 plate tectonics. *American Mineralogist* 103 (2): 181-196.

1324 Brown, M., 2007. Metamorphism, Plate Tectonics, and the Supercontinent Cycle. *Earth*  
1325 *Science Frontiers* 14 (1): 1-18.

1326 Brown, S.M., Elkins-Tanton, L.T., and Walker, R.J., 2014. Effects of magma ocean  
1327 crystallization and overturn on the development of <sup>142</sup>Nd and <sup>182</sup>W isotopic



1328 heterogeneities in the primordial mantle. *Earth and Planetary Science Letters* 408: 319-  
1329 330.

1330 Bowring, S. A., Housh, T., 1995. The Earth's early evolution. *Science* **269** (5230): 1535-1540.

1331 Boyet, M., Blichert-Toft, J., Rosing, M., Storey, M., Télouk, P., Albarède, F., 2003.  $^{142}\text{Nd}$   
1332 evidence for early Earth differentiation. *Earth and Planetary Science Letters* **214**: 427-442.

1333 Brandon, A.D., Walker, R.J., Morgan, J.W., Norman, M.D., and Prichard, H.M., 1998.  
1334 Coupled  $^{186}\text{Os}$  and  $^{187}\text{Os}$  evidence for core-mantle interaction. *Science* 280 (5369): 1570-  
1335 1573.

1336 Brandon, A.D., Norman, M.D., Walker, R.J., and Morgan, J.W., 1999.  $^{186}\text{Os}$ - $^{187}\text{Os}$   
1337 systematics of Hawaiian picrites. *Earth and Planetary Science Letters* 174 (1-2): 25-42.

1338 Brandon, A.D., Walker, R.J., Puchtel, I.S., Becker, H., Humayun, M., and Revillon, S., 2003.  
1339  $^{186}\text{Os}$ - $^{187}\text{Os}$  systematics of Gorgona Island komatiites: Implications for early growth of the  
1340 inner core. *Earth and Planetary Science Letters* 206 (3-4): 411-426.

1341 Brandon, A.D., Humayun, M., Puchtel, I.S., and Zolensky, M., 2005. Re-Os isotopic  
1342 systematics and platinum group element composition of the Tagish Lake carbonaceous  
1343 chondrite. *Geochimica et Cosmochimica Acta* **69** (6): 1619-1631.

1344 Brandon, A.D., Walker, R.J., and Puchtel, I.S., 2006. Platinum-osmium isotope evolution of  
1345 the Earth's mantle: Constraints from chondrites and Os-rich alloys. *Geochimica et*  
1346 *Cosmochimica Acta* 70 (8): 2093-2103.

1347 Burkhardt, C., Borg, L.E., Brennecka, G.A., Shollenberger, Q.R., Dauphas, N., and Kleine,  
1348 T., 2016. A nucleosynthetic origin for the Earth's anomalous  $^{142}\text{Nd}$  composition. *Nature*  
1349 537: 394-398.

1350 Byerly, B.L., Kareem, K., Bao, H., and Byerly, G.R., 2017. Early Earth mantle heterogeneity  
1351 revealed by light oxygen isotopes of Archaean komatiites. *Nature Geoscience* 10: 871-  
1352 876.

1353 Campbell, I.H., Griffiths, R.W., and Hill, R.I., 1989. Melting in an Archaean mantle plume:  
1354 head it's basalts, tails it's komatiites. *Nature* 339 (6227): 697-699.

1355 Campbell, I.H. and Hill, R.I., 1988. A two stage model for the formation of the granite-  
1356 greenstone terrains of the Kalgoorlie-Norseman area, Western Australia. *Earth and*  
1357 *Planetary Science Letters* 90 (1): 11-25.

1358 Campbell, I.H. and Griffiths, R.W., 1990. Implications of mantle plume structure for the  
1359 evolution of flood basalts. *Earth and Planetary Science Letters* 99 (1-2): 79-93.

1360 Campbell, I.H. and Griffiths, R.W., 1992. The changing nature of mantle hotspots through  
1361 time: Implications for the chemical evolution of the mantle. *Journal of Geology* 92 (5):  
1362 497-523.

1363 Campbell, I.H. and Griffiths, R.W., 1993. The evolution of the mantle's chemical structure.  
1364 *Lithos* 30 (3): 389-399.

1365 Campbell, I.H., 2007. Testing the plume theory. *Chemical Geology* 241 (3-4): 153-176.

1366 Campbell, I.H. and Griffiths, R.W., 2014. Did the formation of D" cause the Archaean-  
1367 Proterozoic transition? *Earth and Planetary Science Letters* 388: 1-8.

1368 Canil, D., 1997. Vanadium partitioning and the oxidation state of Archaean komatiite  
1369 magmas. *Nature* 389 (6653): 842-845.

- Canil, D., 1999. Vanadium partitioning between orthopyroxene, spinel and silicate melt and the redox states of mantle source regions for primary magmas. *Geochimica et Cosmochimica Acta* 63 (3-4): 557-572.
- Canil, D., 2002. Vanadium in peridotites, mantle redox and tectonic environments: Archean to present. *Earth and Planetary Science Letters* 195 (1-2): 75-90.
- Canil, D. and Fedortchouk, Y., 2001. Olivine-liquid partitioning of vanadium and other trace elements, with applications to modern and ancient picrites. *Canadian Mineralogist* 39: 319-330.
- Canup, R.M., 2012. Forming a Moon with an Earth-like Composition via a Giant Impact. *Science* 338 (6110): 1052-1055.
- Carlson, R.W., 1994. Mechanisms of Earth differentiation: consequences for the chemical structure of the mantle. *Review of Geophysics* 32 (4): 337-361.
- Carlson, R.W., Boyet, M., and Horan, M., 2007. Chondrite barium, neodymium, and samarium isotopic heterogeneity and early earth differentiation. *Science* 316 (5828): 1175-1178.
- Carlson, R. W., Boyet, M., O'Neil, J., Rizo, H., and Walker, R. J., 2015. Early Differentiation and Its Long-Term Consequences for Earth Evolution. In: *The Early Earth*. Hoboken, New Jersey, John Wiley & Sons, Inc.: 143-172.
- Carlson, R.W., Garçon, M., O'Neil, J., Reimink, J., and Rizo, H., 2019. The nature of Earth's first crust. *Chemical Geology* 530: 119321.
- Caro, G., Bourdon, B., Birck, J.-L., and Moorbath, S., 2003.  $^{146}\text{Sm}$ - $^{142}\text{Nd}$  evidence from Isua metamorphosed sediments for early differentiation of the Earth's mantle. *Nature* 423 (6938): 428-432.
- Caro, G., Bourdon, B., Wood, B.J., and Corgne, A., 2005. Trace-element fractionation in Hadean mantle generated by melt segregation from a magma ocean. *Nature* 436 (7048): 246-249.
- Caro, G., Bourdon, B., Birck, J.-L., and Moorbath, S., 2006. High-precision  $^{142}\text{Nd}/^{144}\text{Nd}$  measurements in terrestrial rocks: Constraints on the early differentiation of the Earth's mantle. *Geochimica et Cosmochimica Acta* 70 (1): 164-191.
- Caro, G., Bourdon, B., Halliday, A.N., and Quitte, G., 2008. Super-chondritic Sm/Nd ratios in Mars, the Earth and the Moon. *Nature* 452 (7185): 336-339.
- Caro, G., 2011. Early Silicate Earth Differentiation. *Annual Review of Earth and Planetary Sciences* 39 (1): 31-58.
- Caro, G., Morino, P., Mojzsis, S.J., Cates, N.L., and Bleeker, W., 2017. Sluggish Hadean geodynamics: Evidence from coupled  $^{146,147}\text{Sm}$ - $^{142,143}\text{Nd}$  systematics in Eoarchean supracrustal rocks of the Inukjuak domain (Québec). *Earth and Planetary Science Letters* 457: 23-37.
- Cawthorn, R.G, 1975. Degrees of melting in mantle diapirs and the origin of ultrabasic liquids. *Earth and Planetary Science Letters* 27 (1): 113-120.
- Chase, C.G., Patchett, P.J., 1988. Stored mafic/ultramafic crust and early Archaean mantle differentiation. *Earth and Planetary Science Letters* 91 (1-2): 66-72.
- Chou, C.-L., 1978. Fractionation of siderophile elements in the earth's upper mantle. *Proceedings of the 9th Lunar and Planetary Science Conference*, pp. 219-230.

1413 Chou, C.-L., Shaw, D.M., Crocket, J.H., 1983. Siderophile trace elements in the Earth's  
1414 oceanic crust and upper mantle. *Journal of Geophysical Research* 88 (S2): A507-A518.

1415 Coltice, N. and Schmalzl, J., 2006. Mixing times in the mantle of the early Earth derived from  
1416 2-D and 3-D numerical simulations of convection. *Geophysical Research Letters* 33 (23):  
1417 L23304.

1418 Condie, K.C., 1975. Mantle-plume model for the origin of Archaean greenstone belts based  
1419 on trace element distributions. *Nature* 258 (5534): 413-414.

1420 Condie, K.C., 1981. Archaean greenstone belts. Elsevier, Amsterdam, 434 pp.

1421 Condie, K.C., 1994. Greenstones through time. In: Condie, K.C. (Ed.). *Archean Crustal*  
1422 *Evolution*. Elsevier, Amsterdam, pp. 85-120.

1423 Condie, K.C., 2005. High field strength element ratios in Archean basalts: a window to  
1424 evolving sources of mantle plumes? *Lithos* 79 (3-4): 491-504.

1425 Cooper, L.B., Ruscitto, D.M., Plank, T., Wallace, P.J., Syracuse, E.M., and Manning, C.E.,  
1426 2012. Global variations in H<sub>2</sub>O/Ce: 1. Slab surface temperatures beneath volcanic arcs.  
1427 *Geochemistry Geophysics Geosystems* 13 (3): Q03024.

1428 Corgne, A. and Wood, B.J., 2002. CaSiO<sub>3</sub> and CaTiO<sub>3</sub> perovskite-melt partitioning of trace  
1429 elements: Implications for gross mantle differentiation. *Geophysical Research Letters* 29  
1430 (19): 39.1-39.4.

1431 Corgne, A. and Wood, B.J., 2004. Trace element partitioning between majoritic garnet and  
1432 silicate melt at 25 GPa. *Physics of the Earth and Planetary Interiors* 143: 407-419.

1433 Corgne, A., Liebske, C., Wood, B.J., Rubie, D.C., and Frost, D.J., 2005. Silicate perovskite-  
1434 melt partitioning of trace elements and geochemical signature of a deep perovskitic  
1435 reservoir. *Geochimica et Cosmochimica Acta* 69 (2): 485-496.

1436 Cottrell, E. and Walker, D., 2006. Constraints on core formation from Pt partitioning in mafic  
1437 silicate liquids at high temperatures. *Geochimica et Cosmochimica Acta* 70 (6): 1565-  
1438 1580.

1439 Courtillot, V., Davaille, A., Besse, J., and Stock, J., 2003. Three distinct types of hotspots in  
1440 the Earth's mantle. *Earth and Planetary Science Letters* 205 (3): 295-308.

1441 Crocket, J.H., Fleet, M.E., and Stone, W.E., 1997. Implications of composition for  
1442 experimental partitioning of platinum-group elements and gold between sulfide liquid and  
1443 basalt melt: The significance of nickel content. *Geochimica et Cosmochimica Acta* 61  
1444 (19): 4139-4149.

1445 Dale, C.W., Kruijer, T.S., and Burton, K.W., 2017. Highly siderophile element and <sup>182</sup>W  
1446 evidence for a partial late veneer in the source of 3.8 Ga rocks from Isua, Greenland.  
1447 *Earth and Planetary Science Letters* 458: 394-404.

1448 Dauphas, N., Burkhardt, C., Warren, P. H., Fang-Zhen, T., 2014. Geochemical arguments for  
1449 an Earth-like Moon-forming impactor. *Philosophical Transactions of the Royal Society:*  
1450 **372** (2024): 20130244.

1451 Day, J.M.D., Walker, R.J., James, O.B., and Puchtel, I.S., 2010. Osmium isotope and highly  
1452 siderophile element systematics of the lunar crust. *Earth and Planetary Science Letters*  
1453 289 (3-4): 595-605.

1454 Day, J.M.D., 2013. Hotspot volcanism and highly siderophile elements. *Chemical Geology*  
1455 341: 50-74.

Day, J.M.D., Pearson, D.G., Taylor, L.A., 2007. Highly siderophile element constraints on accretion and differentiation of the Earth-Moon system. *Science* 315 (5809): 217-219.

Day, J.M.D. and Walker, R.J., 2015. Highly siderophile element depletion in the Moon. *Earth and Planetary Science Letters* 423: 114-124.

Day, J.M.D., Brandon, A.D., and Walker, R.J., 2016. Highly Siderophile Elements in Earth, Mars, the Moon, and Asteroids. *Reviews in Mineralogy and Geochemistry* 81 (1): 161-238.

Debaille, V., O'Neill, C., Brandon, A.D., Haenecour, P., Yin, Q.-Z., Mattielli, N., and Treiman, A.H., 2013. Stagnant-lid tectonics in early Earth revealed by <sup>142</sup>Nd variations in late Archean rocks. *Earth and Planetary Science Letters* 373: 83-92.

DePaolo, D. J., 1980. Crustal growth and mantle evolution: inferences from models of element transport and Nd and Sr isotopes. *Geochimica et Cosmochimica Acta* 44 (8): 1185-1196.

DePaolo, D.J. and Wasserburg, G.J., 1976. Nd isotopic variations and petrogenetic models. *Geophysical Research Letters* 3 (5): 249-252.

Desrochers, J.-P., Hubert, C., Ludden, J.N., and Pilote, P., 1993. Accretion of Archean oceanic plateau fragments in the Abitibi greenstone belt, Canada. *Geology* 21 (5): 451-454.

De Wit, M.J. and Ashwal, L.D., 1997. *Greenstone Belts*. Clarendon Press, Oxford, 809 pp.

Dostal, J. and Mueller, W.U., 2013. Deciphering an Archean mantle plume: Abitibi greenstone belt, Canada. *Gondwana Research* 23 (2): 493-505.

Drake, M. J., 2000. Accretion and primary differentiation of the Earth: A personal journey. *Geochimica et Cosmochimica Acta* 64 (14): 2363-2370.

Dupré, B., Chauvel, C., and Arndt, N.T., 1984. Pb and Nd isotopic study of two Archean komatiitic flows from Alexo, Ontario. *Geochimica et Cosmochimica Acta* 48 (10): 1965-1972.

Dziewonski, A.M., Hager, B.H., and O'Connell, R.J., 1977. Large-scale heterogeneities in the lower mantle. *Journal of Geophysical Research* 82 (2): 239-255.

Elkins-Tanton, L.T., Parmentier, E.M., and Hess, P.C., 2003. Magma ocean fractional crystallization and cumulate overturn in terrestrial planets: Implications for Mars. *Meteoritics & Planetary Science* 38 (12): 1753-1771.

Elkins-Tanton, L.T., 2008. Linked magma ocean solidification and atmospheric growth for Earth and Mars. *Earth and Planetary Science Letters* 271 (1-4): 181-191.

Elkins-Tanton, L.T., 2012. Magma Oceans in the Inner Solar System. *Annual Review of Earth and Planetary Sciences* 40 (1): 113-139.

Farnetani, C.G. and Richards, M.A., 1995. Thermal entrainment and melting in mantle plumes. *Earth and Planetary Science Letters* 136 (4): 251-267.

Farnetani, C.G., 1997. Excess temperature of mantle plumes: the role of chemical stratification across "D". *Geophysical Research Letters* 24 (13): 1583-1586.

Fischer-Gödde, M., Becker, H., and Wombacher, F., 2010. Rhodium, gold and other highly siderophile element abundances in chondritic meteorites. *Geochimica et Cosmochimica Acta* 74 (1): 356-379.

1498 Fischer-Gödde, M., Becker, H., Wombacher, F., 2011. Rhodium, gold and other highly  
 1499 siderophile elements in orogenic peridotites and peridotite xenoliths. *Chemical Geology*  
 1500 280 (3-4): 365-383.

1501 Fletcher, M. and Wyman, D.A., 2015. Mantle plume-subduction zone interactions over the  
 1502 past 60 Ma. *Lithos* 233: 162-173.

1503 Foley, S.F., Barth, M.G., and Jenner, G.A., 2000. Rutile/melt partition coefficients for trace  
 1504 elements and an assessment of the influence of rutile on the trace element characteristics  
 1505 of subduction zone magmas. *Geochimica et Cosmochimica Acta* 64 (5): 933-938.

1506 Foley, B.J. and Rizo, H., 2017. Long-term preservation of early formed mantle heterogeneity  
 1507 by mobile lid convection: Importance of grainsize evolution. *Earth and Planetary Science*  
 1508 *Letters* 475: 94-105.

1509 Fortenfant, S.S., Gunther, D., Dingwell, D.B., and Rubie, D.C., 2003. Temperature  
 1510 dependence of Pt and Rh solubilities in a haplobasaltic melt. *Geochimica et*  
 1511 *Cosmochimica Acta* 67 (1): 123-131.

1512 French, S.W. and Romanowicz, B., 2015. Broad plumes rooted at the base of the Earth's  
 1513 mantle beneath major hotspots. *Nature* 525 (7567): 95-99.

1514 Frost, D. J., Mann, U., Asahara, Y., Rubie, D. C., 2008. The redox state of the mantle during  
 1515 and just after core formation. *Philosophical Transactions of the Royal Society* **366** (1883):  
 1516 4315-4337.

1517 Galer, S. J. G., Goldstein, S. L., O'Nions, R. K., 1989. Limits on chemical and convective  
 1518 isolation in the Earth's interior. *Chemical Geology* **75** (4): 257-290.

1519 Galer, S. J. G., Goldstein, S. L., 1991. Early mantle differentiation and its thermal  
 1520 consequences. *Geochimica et Cosmochimica Acta* **55** (1-2): 227-239.

1521 Gerya, T., 2014. Precambrian geodynamics: Concepts and models. *Gondwana Research* 25  
 1522 (2): 442-463.

1523 Gangopadhyay, A. and Walker, R.J., 2003. Re-Os systematics of the ca. 2.7 Ga komatiites  
 1524 from Alexo, Ontario, Canada. *Chemical Geology* 196 (1-4): 147-162.

1525 Goldstein, S.L., O'Nions, R.K., and Hamilton, P.J., 1984. A Sm-Nd Isotopic Study of  
 1526 Atmospheric Dusts and Particulates from Major River Systems. *Earth and Planetary*  
 1527 *Science Letters* 70 (2): 221-236.

1528 Goldstein, S.L., Galer, S.J.G., 1992. On the trail of early mantle differentiation:  $^{142}\text{Nd}/^{144}\text{Nd}$   
 1529 ratios of early Archean rocks. *Eos* **73** (30): 323.

1530 Green, D.H., 1975. Genesis of Archean peridotitic magmas and constraints on Archean  
 1531 geothermal gradients and tectonics. *Geology* 3 (1): 15-18.

1532 Green, D.H., 1981. Petrogenesis of Archean ultramafic magmas and implications for Archean  
 1533 tectonics. In: *Precambrian Plate Tectonics*, Kröner, A. (Ed.), Elsevier, Amsterdam, pp.  
 1534 469-480.

1535 Grove, T.L., de Wit, M.J., and Dann, J., 1997. Komatiites from the Komati type section,  
 1536 Barberton, South Africa. In: de Wit, M.J. and Ashwal, L.D. (Eds.). *Greenstone Belts*.  
 1537 Oxford Science Publications, Oxford, pp. 422-437.

1538 Grove, T.L. and Parman, S.W., 2004. Thermal evolution of the Earth as recorded by  
 1539 komatiites. *Earth and Planetary Science Letters* 219 (3-4): 173-187.

1540 Hamilton, P.J., O'Nions, R.K., Bridgwater, D., and Nutman, A.P., 1983. Sm-Nd studies of  
 1541 Archaean metasediments and metavolcanics from West Greenland and their implications  
 1542 for the Earth's early history. *Earth and Planetary Science Letters* 62 (2): 263-272.

1543 Harper, C.L. and Jacobsen, S.B., 1992. Evidence from coupled  $^{147}\text{Sm}$ - $^{143}\text{Nd}$  and  $^{146}\text{Sm}$ - $^{142}\text{Nd}$   
 1544 systematics for very early (4.5-Gyr) differentiation of the Earth's mantle. *Nature* 360  
 1545 (6406): 728-732.

1546 Harper, C.L. and Jacobsen, S.B., 1996. Evidence for  $^{182}\text{Hf}$  in the early Solar System and  
 1547 constraints on the timescale of terrestrial accretion and core formation. *Geochimica et*  
 1548 *Cosmochimica Acta* 60 (7): 1131-1153.

1549 Hart, S. R., Brooks, S., 1977. The geochemistry and evolution of Early Precambrian mantle.  
 1550 *Contributions to Mineralogy and Petrology* 61 (2): 109-128.

1551 Hart, S. R., Zindler, A., 1986. In search of a bulk-earth composition. *Chemical Geology* 57  
 1552 (3-4): 247-267.

1553 Hart, S.R., Hauri, E.H., Oschmann, L.A., and Whitehead, J.A., 1992. Mantle plumes and  
 1554 entrainment: isotopic evidence. *Science* 256 (5056): 517-520.

1555 Hauri, E.H., Gaetani, G.A., and Green, T.H., 2006. Partitioning of water during melting of the  
 1556 Earth's upper mantle at  $\text{H}_2\text{O}$ -undersaturated conditions. 248 (3-4): 715-734.

1557 He, Y., Wen, L., Capdeville, Y., and Zhao, L., 2015. Seismic evidence for an Iceland thermo-  
 1558 chemical plume in the Earth's lowermost mantle. *Earth and Planetary Science Letters* 417:  
 1559 19-27.

1560 Herzberg, C.T. and Ohtani, E., 1988. Origin of komatiite at high pressures. *Earth and*  
 1561 *Planetary Science Letters* 88 (3-4): 321-329.

1562 Herzberg, C.T., 1992. Depth and degree of melting of komatiites. *Journal of Geophysical*  
 1563 *Research* 97 (B4): 4521-4540.

1564 Herzberg, C.T., 1995. Generation of plume magmas through time: an experimental  
 1565 perspective. *Chemical Geology* 126 (1): 1-16.

1566 Herzberg, C. and O'Hara, M.J., 2002. Plume-associated ultramafic magmas of Phanerozoic  
 1567 age. *Journal of Petrology* 43 (10): 1857-1883.

1568 Herzberg, C., Asimow, P.D., Arndt, N.T., Niu, Y.L., Leshner, C.M., Fitton, J.G., Cheadle,  
 1569 M.J., and Saunders, A.D., 2007. Temperatures in ambient mantle and plumes: Constraints  
 1570 from basalts, picrites, and komatiites. *Geochemistry Geophysics Geosystems* 8: Q02006.

1571 Herzberg, C. and Gazel, E., 2009. Petrological evidence for secular cooling in mantle plumes.  
 1572 *Nature* 458 (7238): 619-622.

1573 Herzberg, C., Condie, K., and Korenaga, J., 2010. Thermal history of the Earth and its  
 1574 petrological expression. *Earth and Planetary Science Letters* 292 (1-2): 79-88.

1575 Hickman, A. and Kranendonk, M.V., 2012. Early Earth Evolution: Evidence from the 3.5-1.8  
 1576 Ga Geological History of the Pilbara Region of Western Australia. *Episodes* 35 (1): 283-  
 1577 297.

1578 Hirschmann, M.M., 2018. Comparative deep Earth volatile cycles: The case for C recycling  
 1579 from exosphere/mantle fractionation of major ( $\text{H}_2\text{O}$ , C, N) volatiles and from  $\text{H}_2\text{O}/\text{Ce}$ ,  
 1580  $\text{CO}_2/\text{Ba}$ , and  $\text{CO}_2/\text{Nb}$  exosphere ratios. *Earth and Planetary Science Letters* 502: 262-273.

1581 Hoffmann, J.E., Münker, C., Polat, A., Rosing, M.T., and Schulz, T., 2011. The origin of  
 1582 decoupled Hf-Nd isotope compositions in Eoarchean rocks from southern West  
 1583 Greenland. *Geochimica et Cosmochimica Acta* 75 (21): 6610-6628.

1584 Hoffmann, J.E. and Wilson, A.H., 2017. The origin of highly radiogenic Hf isotope  
1585 compositions in 3.33 Ga Comondale komatiite lavas (South Africa). *Chemical Geology*  
1586 455: 6-21.

1587 Hofmann, A.W. and Hart, S., 1978. An assessment of local and regional isotopic equilibrium  
1588 in the mantle. *Earth and Planetary Science Letters* 38 (1): 44-62.

1589 Hofmann, A.W. and White, W.M., 1982. Mantle plumes from ancient oceanic crust. *Earth*  
1590 *and Planetary Science Letters* 57 (2): 421-436.

1591 Hofmann, A.W., Jochum, K.P., Seufert, M., and White, W.M., 1986. Nb and Pb in oceanic  
1592 basalts: New constraints on mantle evolution. *Earth and Planetary Science Letters* 79 (1-  
1593 2): 33-45.

1594 Hofmann, A.W., 1988. Chemical differentiation of the Earth: The relationship between  
1595 mantle, continental crust and oceanic crust. *Earth and Planetary Science Letters* 90 (3):  
1596 297-314.

1597 Horan, M.F., Walker, R.J., Morgan, J.W., Grossman, J.N., and Rubin, A.E., 2003. Highly  
1598 siderophile elements in chondrites. *Chemical Geology* **196** (1-4): 5-20.

1599 Horan, M.F., Carlson, R.W., Walker, R.J., Jackson, M., Garçon, M., and Norman, M., 2018.  
1600 Tracking Hadean processes in modern basalts with <sup>142</sup>Neodymium. *Earth and Planetary*  
1601 *Science Letters* 484: 184-191.

1602 Humayun, M., 2011. A model for osmium isotopic evolution of metallic solids at the core-  
1603 mantle boundary. *Geochemistry Geophysics Geosystems* 12 (3): 1-23.

1604 Huppert, H.E., Sparks, R.S.J., Turner, J.S., and Arndt, N.T., 1984. Emplacement and cooling  
1605 of komatiite lavas. *Nature* 309 (5963): 19-22.

1606 Huppert, H.E. and Sparks, R.S.J., 1985. Cooling and contamination of mafic and ultramafic  
1607 magmas during ascent through continental crust. *Earth and Planetary Science Letters* 74  
1608 (4): 371-386.

1609 Hyung, E. and Jacobsen, S.B., 2020. The <sup>142</sup>Nd/<sup>144</sup>Nd variations in mantle-derived rocks  
1610 provide constraints on the stirring rate of the mantle from the Hadean to the present.  
1611 *Proceedings of the National Academy of Sciences*: 117 (26): 14738-14744.

1612 Ireland, T.J., Walker, R.J., and Garcia, M.O., 2009. Highly siderophile element and <sup>187</sup>Os  
1613 isotope systematics of Hawaiian picrites: Implications for parental melt composition and  
1614 source heterogeneity. *Chemical Geology* 260 (1-2): 112-128.

1615 Ito, E., Kubo, A., Katsura, T., Walter, M.J., 2004. Melting experiments of mantle materials  
1616 under lower mantle conditions with implications for magma ocean differentiation. *Physics*  
1617 *of the Earth and Planetary Interiors* 143: 397-406.

1618 Jackson, M.G. and Carlson, R.W., 2012. Homogeneous superchondritic <sup>142</sup>Nd/<sup>144</sup>Nd in the  
1619 mid-ocean ridge basalt and ocean island basalt mantle. *Geochemistry Geophysics*  
1620 *Geosystems* 13 (6): Q06011.

1621 Jacobsen, S.B., and Wasserburg, G.J., 1980. Sm-Nd isotopic evolution of chondrites. *Earth*  
1622 *and Planetary Science Letters* 50 (1): 139-155.

1623 Jacobsen, S. B., 1988. Isotopic and chemical constraints on mantle-crust evolution.  
1624 *Geochimica et Cosmochimica Acta* **52** (6): 1341-1350.

1625 Jacobsen, S.B. and Yu, G., 2015. Extinct isotope heterogeneities in the mantles of Earth and  
1626 Mars: Implications for mantle stirring rates. *Meteoritics & Planetary Science* 50 (4): 555-  
1627 567.

- Jahn, B.-M., Gruau, G., and Glikson, A.Y., 1982. Komatiites of the Onverwacht Group, South Africa: REE geochemistry, Sm-Nd age and mantle evolution. *Contributions to Mineralogy and Petrology* 80 (1): 25-40.
- Jamais, M., Lassiter, J.C., and Brüggmann, G., 2008. PGE and Os-isotopic variations in lavas from Kohala Volcano, Hawaii: Constraints on PGE behavior and melt/crust interaction. *Chemical Geology* 250 (1-4): 16-28.
- Jenner, F.E. and O'Neill, H.St.C.C.Q., 2012. Major and trace analysis of basaltic glasses by laser-ablation ICP-MS. *Geochemistry, Geophysics, Geosystems* 13 (3): Q03003.
- Jochum, K.P., Arndt, N.T., and Hofmann, A.W., 1991. Nb-Th-La in komatiites and basalts: constraints on komatiite petrogenesis and mantle evolution. *Earth and Planetary Science Letters* 107 (2): 272-289.
- Johnson, T.E., Brown, M., Gardiner, N.J., Kirkland, C.L., and Smithies, R.H., 2017. Earth's first stable continents did not form by subduction. *Nature* 543 (7644): 239-242.
- Kato, T., Ringwood, A.E., and Irifune, T., 1988. Experimental determination of element partitioning between silicate perovskite, garnet and liquid: constraints on early differentiation of the mantle. *Earth and Planetary Science Letters* 89 (1): 123-145.
- Kent, R.W., Hardarson, B.S., Saunders, A.D., and Storey, M., 1996. Plateaux ancient and modern: Geochemical and sedimentological perspectives on Archaean oceanic magmatism. *Lithos* 37 (2-3): 129-142.
- Kimura, G., Ludden, J.N., Desrochers, J.-P., and Hori, R., 1993. A model of ocean-crust accretion for the Superior province, Canada. *Lithos* 30 (3-4): 337-355.
- Kimura, K., Lewis, R.S., Anders, S., 1974. Distribution of gold and rhenium between nickel-iron and silicate melts; implications for abundance of siderophile elements on the Earth and Moon. *Geochimica et Cosmochimica Acta* 38 (5): 683-701.
- Kleine, T., Münker, C., Mezger, K., Palme, H., 2002. Rapid accretion and early core formation on asteroids and the terrestrial planets from Hf-W chronometry. *Nature* 418 (6901): 952-955.
- Kleine, T., Mezger, K., Palme, H., Münker, C., 2004. The W isotope evolution of the bulk silicate Earth: constraints on the timing and mechanisms of core formation and accretion. *Earth and Planetary Science Letters* 228 (1-2): 109-123.
- Kleine, T., Touboul, M., Bourdon, B., Nimmo, F., Mezger, K., Palme, H., Jacobsen, S.B., Yin, Q.-Z., and Halliday, A.N., 2009. Hf-W chronology of the accretion and early evolution of asteroids and terrestrial planets. *Geochimica et Cosmochimica Acta* 73 (17): 5150-5188.
- Kleine, T., Walker, R. J., 2017. Tungsten Isotopes in Planets. *Annual Review of Earth and Planetary Sciences* 45 (1): 389-417.
- König, S., Münker, C., Schuth, S., and Garbe-Schönberg, D., 2008. Mobility of tungsten in subduction zones. *Earth and Planetary Science Letters* 274 (1-2): 89-92.
- König, S., Münker, C., Hohl, S., Paulick, H., Barth, A. R., Lagos, M., Pfander, J., Büchl, A., 2011. The Earth's tungsten budget during mantle melting and crust formation. *Geochimica et Cosmochimica Acta* 75 (8): 2119-2136.
- Koppers, A.A.P., Becker, T.W., Jackson, M.G., Konrad, K., Müller, R.D., Romanowicz, B., Steinberger, B., and Whittaker, J.M., 2021. Mantle plumes and their role in Earth processes. *Nature Reviews* 2: 382-401.



1672 Korenaga, J., 2021. Hadean geodynamics and the nature of early continental crust.  
1673 *Precambrian Research* 359: 106178.

1674 Kruijer, T.S., Kleine, T., Fischer-Gödde, M., Sprung, P., 2015. Lunar tungsten isotopic  
1675 evidence for the late veneer. *Nature* 520 (7548): 534-537.

1676 Kruijer, T. S., Kleine, T., 2017. Tungsten isotopes and the origin of the Moon. *Earth and*  
1677 *Planetary Science Letters* **475** (Supplement C): 15-24.

1678 Kusky, T.M. and Kidd, W.S.F., 1992. Remnants of an Archean oceanic plateau, Belingwe  
1679 greenstone belt, Zimbabwe. *Geology* 20 (1): 43-46.

1680 Labrosse, S., Hernlund, J.W., and Coltice, N., 2007. A crystallizing dense magma ocean at the  
1681 base of the Earth's mantle. *Nature* 450 (7171): 866-869.

1682 Lassiter, J.C. and Hauri, E.H., 1998. Osmium-isotope variations in Hawaiian lavas: evidence  
1683 for recycled oceanic lithosphere in the Hawaiian plume. *Earth and Planetary Science*  
1684 *Letters* 164 (3-4): 483-496.

1685 Lassiter, J.C., 2006. Constraints on the coupled thermal evolution of the Earth's core and  
1686 mantle, the age of the inner core, and the origin of the  $^{186}\text{Os}/^{188}\text{Os}$  "core signal" in plume-  
1687 derived lavas. *Earth and Planetary Science Letters* 250 (1-2): 306-317.

1688 Liebske, C., Corgne, A., Frost, D.J., Rubie, D.C., and Wood, B.J., 2005. Compositional  
1689 effects on element partitioning between Mg-silicate perovskite and silicate melts.  
1690 *Contributions to Mineralogy and Petrology* 149 (1): 113-128.

1691 Liu, J., Touboul, M., Ishikawa, A., Walker, R.J., and Pearson, D.G., 2016. Widespread  
1692 tungsten isotope anomalies and W mobility in crustal and mantle rocks of the Eoarchean  
1693 Saglek Block, northern Labrador, Canada: Implications for early Earth processes and W  
1694 recycling. *Earth and Planetary Science Letters* 448: 13-23.

1695 Loper, D.E., 1991. Mantle plumes. *Tectonophysics* 187 (4): 373-384.

1696 Maier, W.D., Barnes, S.J., Campbell, I.H., Fiorentini, M.L., Peltonen, P., Barnes, S.-J.,  
1697 Smithies, R.H., 2009. Progressive mixing of meteoritic veneer into the early Earth's deep  
1698 mantle. *Nature* 460 (7255): 620-623.

1699 Mallmann, G. and O'Neill, H.St.C., 2007. The effect of oxygen fugacity on the partitioning of  
1700 Re between crystals and silicate melt during mantle melting. *Geochimica et*  
1701 *Cosmochimica Acta* 71 (11): 2837-2857.

1702 Marchi, S., Canup, R.M., Walker, R.J., 2018. Heterogeneous delivery of silicate and metal to  
1703 the Earth by large planetesimals. *Nature Geoscience* 11: 77-81.

1704 Marchi, S., Walker, R.J., and Canup, R.M., 2020. A compositionally heterogeneous martian  
1705 mantle due to late accretion. *Science Advances* 6 (7): eaay2338.

1706 Maya, J.M., Bhutani, R., Balakrishnan, S., and Rajee Sandhya, S., 2017. Petrogenesis of 3.15  
1707 Ga old Banasandra komatiites from the Dharwar craton, India: Implications for early  
1708 mantle heterogeneity. *Geoscience Frontiers* 8 (3): 467-481.

1709 McDonough, W.F. and Sun, S.S., 1995. The composition of the Earth. *Chemical Geology* 120  
1710 (3-4): 223-253.

1711 McKenzie, D. and Bickle, M.J., 1988. The volume and composition of melt generated by  
1712 extension of the lithosphere. *Journal of Petrology* 29 (3): 625-679.

1713 Meisel, T., Walker, R.J., Irving, A.J., Lorand, J.-P., 2001. Osmium isotopic compositions of  
1714 mantle xenoliths: A global perspective. *Geochimica et Cosmochimica Acta* 65 (8): 1311-  
1715 1323.

1716 Michael, P., 1995. Regionally Distinctive Sources of Depleted MORB - Evidence from Trace-  
1717 Elements and H<sub>2</sub>O. *Earth and Planetary Science Letters* 131 (3-4): 301-320.

1718 Mole, D.R., Fiorentini, M.L., Thebaud, N., Cassidy, K.F., McCuaig, T.C., Kirkland, C.L.,  
1719 Romano, S.S., Doublier, M.P., Belousova, E.A., Barnes, S.J., and Miller, J., 2014. Archean  
1720 komatiite volcanism controlled by the evolution of early continents. *Proceedings of the*  
1721 *National Academy of Sciences* 111 (28): 10083-10088.

1722 Montelli, R., Nolet, G., Dahlen, F.A., Masters, G., Engdahl, E.R., and Hung, S.-H., 2004.  
1723 Finite-Frequency Tomography Reveals a Variety of Plumes in the Mantle. *Science* 303  
1724 (5656): 338-343.

1725 Moore, J.G., 1970. Water Content of Basalt Erupted on the ocean floor. *Contributions to*  
1726 *Mineralogy and Petrology* 28 (4): 272-279.

1727 Morino, P., Caro, G., Reisberg, L., and Schumacher, A., 2017. Chemical stratification in the  
1728 post-magma ocean Earth inferred from coupled <sup>146,147</sup>Sm-<sup>142,143</sup>Nd systematics in  
1729 ultramafic rocks of the Saglek block (3.25-3.9 Ga; northern Labrador, Canada). *Earth and*  
1730 *Planetary Science Letters* 463: 136-150.

1731 Mundl, A., Touboul, M., Jackson, M.G., Day, J.M.D., Kurz, M.D., Lekic, V., Helz, R.T., and  
1732 Walker, R.J., 2017. Tungsten-182 heterogeneity in modern ocean island basalts. *Science*  
1733 356 (6333): 66-69.

1734 Mundl, A., Walker, R.J., Reimink, J.R., Rudnick, R.L., and Gaschnig, R.M., 2018. Tungsten-  
1735 182 in the upper continental crust: Evidence from glacial diamictites. *Chemical Geology*  
1736 494: 144-152.

1737 Mundl-Petermeier, A., Walker, R.J., Jackson, M.G., Blichert-Toft, J., Kurz, M.D., and  
1738 Haldórsson, S.A. (2019) Temporal evolution of primordial tungsten-182 and <sup>3</sup>He/<sup>4</sup>He  
1739 signatures in the Iceland mantle plume. *Chemical Geology* 525, 245-259.

1740 Mundl-Petermeier, A., Walker, R.J., Fischer, R.A., Lekic, V., Jackson, M.G., and Kurz, M.D.,  
1741 2020. Anomalous μ<sup>182</sup>W signatures in high <sup>3</sup>He/<sup>4</sup>He ocean island basalts – fingerprints of  
1742 Earth's core? *Geochimica et Cosmochimica Acta* 271: 194-211.

1743 Murphy, D.T., Brandon, A.D., Debaille, V., Burgess, R., and Ballentine, C., 2010. In search  
1744 of a hidden long-term isolated sub-chondritic <sup>142</sup>Nd/<sup>144</sup>Nd reservoir in the deep mantle:  
1745 Implications for the Nd isotope systematics of the Earth. *Geochimica et Cosmochimica*  
1746 *Acta* 74 (2): 738-750.

1747 Murphy, D., Rizo, H., O'Neil, J., Hepple, R., Wiemer, D., Kemp, A., and Vervoort, J., 2021.  
1748 Combined Sm-Nd, Lu-Hf, and <sup>142</sup>Nd study of Paleoarchean basalts from the East Pilbara  
1749 Terrane, Western Australia. *Chemical Geology* 578: 120301.

1750 Nakagawa, T., 2020. A coupled core-mantle evolution: review and future prospects. *Progress*  
1751 *in Earth and Planetary Science* 7 (1): 57.

1752 Nakanishi, N., Giuliani, A., Carlson, R.W., Horan, M.F., Woodhead, J., Pearson, D. G., and  
1753 Walker, R.J., 2021. Tungsten-182 evidence for an ancient kimberlite source. *Proceedings*  
1754 *of the National Academy of Sciences* 118 (23): e2020680118.

1755 Newsom, H.E., Sims, K.W.W., Noll, P.D., Jaeger, W.L., Maehr, S.A., and Beserra, T.B.,  
1756 1996. The depletion of tungsten in the bulk silicate Earth: Constraints on core formation.  
1757 *Geochimica et Cosmochimica Acta* 60 (5): 1155-1169.

1758 Nicklas, R.W., Puchtel, I.S., and Ash, R.D., 2018. The Redox Evolution of the Archean  
1759 Mantle: Evidence from Komatiites. *Geochimica et Cosmochimica Acta* 222: 447-466.

1760 Nicklas, R.W., Puchtel, I.S., Ash, R.D., Piccoli, P.M., Hanski, E., Nisbet, E.G., Waterton, P.,  
 1761 Pearson, D.G., and Anbar, A.D., 2019. Secular mantle oxidation across the Archean-  
 1762 Proterozoic boundary: Evidence from V partitioning in komatiites and picrites.  
 1763 *Geochimica et Cosmochimica Acta* 250: 49-75.  
 1764 Nesbitt, R.W., Sun, S.S., and Purvis, A.C., 1979. Komatiites: geochemistry and genesis.  
 1765 *Canadian Mineralogist* 17 (2): 165-186.  
 1766 Nisbet, E.G., Cheadle, M.J., Arndt, N.T., and Bickle, M.J., 1993. Constraining the potential  
 1767 temperature of the Archaean mantle: a review of the evidence from komatiites. *Lithos* 30:  
 1768 291-307.  
 1769 Ohtani, E., 1984. Generation of komatiite magma and gravitational differentiation in the deep  
 1770 upper mantle. *Earth and Planetary Science Letters* 67 (2): 261-272.  
 1771 O'Neil, J., Carlson, R.W., Francis, D., and Stevenson, R.K., 2008. Neodymium-142 evidence  
 1772 for Hadean mafic crust. *Science* 321 (5897): 1828-1831.  
 1773 O'Neil, J., Carlson, R.W., Paquette, J.-L., and Francis, D., 2012. Formation age and  
 1774 metamorphic history of the Nuvvuagittuq Greenstone Belt. *Precambrian Research* 220-  
 1775 221: 23-44.  
 1776 O'Neil, J., Rizo, H., Boyet, M., Carlson, R.W., Rosing, M.T., 2016. Geochemistry and Nd  
 1777 isotopic characteristics of Earth's Hadean mantle and primitive crust. *Earth and Planetary*  
 1778 *Science Letters* 442: 194-205.  
 1779 O'Neill, C. and Debaille, V., 2014. The evolution of Hadean-Eoarchaeon geodynamics. *Earth*  
 1780 *and Planetary Science Letters* 406: 49-58.  
 1781 Parman, S.W., Dann, J.C., Grove, T.L., and de Wit, M.J., 1997. Emplacement conditions of  
 1782 komatiite magmas from the 3.49 Ga Komati Formation, Barberton greenstone belt, South  
 1783 Africa. *Earth and Planetary Science Letters* 150 (3-4): 303-323.  
 1784 Parman, S.W., Grove, T.L., and Dann, J.C., 2001. The production of Barberton komatiites in  
 1785 an Archean subduction zone. *Geophysical Research Letters* 28 (13): 2513-2516.  
 1786 Parman, S.W., Grove, T.L., Dann, J.C., and de Wit, M.J., 2004. *South African Journal of*  
 1787 *Geology* 107 (1-2): 107-118.  
 1788 Patchett, P.J. and Tatsumoto, M., 1980. Hafnium isotope variations in oceanic basalts.  
 1789 *Geophysical Research Letters* 7 (12): 1077-1080.  
 1790 Patchett, P.J., Kauvo, O., Hedge, C.E., and Tatsumoto, M., 1981. Evolution of continental  
 1791 crust and mantle heterogeneity: evidence from Hf isotopes. *Contributions to Mineralogy*  
 1792 *and Petrology* 78 (3): 279-297.  
 1793 Patchett, P. J., White, W. M., Feldmann, H., Kielinczuk, S., Hofmann, A. W., 1984.  
 1794 Hafnium/rare earth element fractionation in the sedimentary system and crustal recycling  
 1795 into the Earth's mantle. *Earth and Planetary Science Letters* 69 (2): 365-378.  
 1796 Peters, B.J., Carlson, R.W., Day, J.M.D., and Horan, M.F., 2018. Hadean silicate  
 1797 differentiation preserved by anomalous <sup>142</sup>Nd/<sup>144</sup>Nd ratios in the Réunion hotspot source.  
 1798 *Nature* 555: 89-106.  
 1799 Peters, B.J., Mundl-Petermeier, A., Carlson, R.W., Walker, R.J., and Day, J.M.D., 2021.  
 1800 Combined lithophile-siderophile isotopic constraints on Hadean processes preserved in  
 1801 ocean island basalt sources. *Geochemistry, Geophysics, Geosystems* 22 (3):  
 1802 e2020GC009479.

1803 Puchtel, I.S., Hofmann, A.W., Mezger, K., Jochum, K.P., Shchipansky, A.A., and Samsonov,  
1804 A.V., 1998. Oceanic plateau model for continental crustal growth in the Archaean: A case  
1805 study from the Kostomuksha greenstone belt, NW Baltic Shield. *Earth and Planetary*  
1806 *Science Letters* 155 (1-2): 57-74.

1807 Puchtel, I.S. and Humayun, M., 2000. Platinum group elements in Kostomuksha komatiites  
1808 and basalts: Implications for oceanic crust recycling and core-mantle interaction.  
1809 *Geochimica et Cosmochimica Acta* 64 (24): 4227-4242.

1810 Puchtel, I.S., Brandon, A.D., and Humayun, M., 2004a. Precise Pt-Re-Os isotope systematics  
1811 of the mantle from 2.7-Ga komatiites. *Earth and Planetary Science Letters* 224 (1-2): 157-  
1812 174.

1813 Puchtel, I.S., Humayun, M., Campbell, A., Sproule, R., and Lesher, C.M., 2004b. Platinum  
1814 group element geochemistry of komatiites from the Alexo and Pyke Hill areas, Ontario,  
1815 Canada. *Geochimica et Cosmochimica Acta* 68 (6): 1361-1383.

1816 Puchtel, I.S. and Humayun, M., 2005. Highly siderophile element geochemistry of <sup>187</sup>Os-  
1817 enriched 2.8-Ga Kostomuksha komatiites, Baltic Shield. *Geochimica et Cosmochimica*  
1818 *Acta* 69 (6): 1607-1618.

1819 Puchtel, I.S., Brandon, A.D., Humayun, M., and Walker, R.J., 2005. Evidence for the early  
1820 differentiation of the core from Pt-Re-Os isotope systematics of 2.8-Ga komatiites. *Earth*  
1821 *and Planetary Science Letters* 237 (1-2): 118-134.

1822 Puchtel, I.S., Humayun, M., and Walker, R.J., 2007. Os-Pb-Nd isotope and highly siderophile  
1823 and lithophile trace element systematics of komatiitic rocks from the Volotsk suite, SE  
1824 Baltic Shield. *Precambrian Research* 158 (1-2): 119-137.

1825 Puchtel, I.S., Walker, R.J., Brandon, A.D., and Nisbet, E.G., 2009a. Pt-Re-Os and Sm-Nd  
1826 isotope and HSE and REE systematics of the 2.7 Ga Belingwe and Abitibi komatiites.  
1827 *Geochimica et Cosmochimica Acta* 73 (20): 6367-6389.

1828 Puchtel, I. S., Walker, R. J., Anhaeusser, C. R., Gruau, G., 2009b. Re-Os isotope systematics  
1829 and HSE abundances of the 3.5 Ga Schapenburg komatiites, South Africa: Hydrous  
1830 melting or prolonged survival of primordial heterogeneities in the mantle? *Chemical*  
1831 *Geology* **262** (3-4): 355-369.

1832 Puchtel, I.S., Blichert-Toft, J., Touboul, M., Walker, R.J., Byerly, G., Nisbet, E.G., and  
1833 Anhaeusser, C.R., 2013. Insights into early Earth from Barberton komatiites: Evidence  
1834 from lithophile isotope and trace element systematics. *Geochimica et Cosmochimica Acta*  
1835 108: 63-90.

1836 Puchtel, I.S., Walker, R.J., Touboul, M., Nisbet, E.G., and Byerly, G.R., 2014. Insights into  
1837 early Earth from the Pt-Re-Os isotope and highly siderophile element abundance  
1838 systematics of Barberton komatiites. *Geochimica et Cosmochimica Acta* 125: 394-413.

1839 Puchtel, I.S., Blichert-Toft, J., Touboul, M., Horan, M.F., and Walker, R.J., 2016a. The  
1840 coupled <sup>182</sup>W-<sup>142</sup>Nd record of early terrestrial mantle differentiation. *Geochemistry,*  
1841 *Geophysics, Geosystems* 17 (6): 2168-2193.

1842 Puchtel, I.S., Touboul, M., Blichert-Toft, J., Walker, R.J., Brandon, A.D., Nicklas, R.W.,  
1843 Kulikov, V.S., and Samsonov, A.V., 2016b. Lithophile and siderophile element  
1844 systematics of the mantle at the Archean-Proterozoic boundary: Evidence from 2.4 Ga  
1845 komatiites. *Geochimica et Cosmochimica Acta* 180: 227-255.

1846 Puchtel, I.S., Blichert-Toft, J., Touboul, M., and Walker, R.J., 2018.  $^{182}\text{W}$  and HSE  
1847 constraints from 2.7 Ga komatiites on the heterogeneous nature of the Archean mantle.  
1848 *Geochimica et Cosmochimica Acta* 228: 1-26.

1849 Puchtel, I.S., Mundl-Petermeier, A., Horan, M., Hanski, E.J., Blichert-Toft, J., and Walker,  
1850 R.J., 2020. Ultra-depleted 2.05 Ga komatiites of Finnish Lapland: Products of grainy late  
1851 accretion or core-mantle interaction? *Chemical Geology* 554: 119801.

1852 Puchtel I.S., Nicklas R.W., Slagle J., Horan M., Walker R.J., Nisbet E.G., and Locmelis M.,  
1853 2022. Early global mantle chemical and isotope heterogeneity revealed by the komatiite-  
1854 basalt record: The Western Australia connection. *Geochimica et Cosmochimica Acta* (in  
1855 press).

1856 Rehkämper, M., Halliday, A.N., Fitton, J.G., Lee, D.-C., Wieneke, M., and Arndt, N.T., 1999.  
1857 Ir, Ru, Pt and Pd in basalts and komatiites: New constraints for the geochemical behavior  
1858 of the platinum group elements in the mantle. *Geochimica et Cosmochimica Acta* 63 (22):  
1859 3915-3934.

1860 Reimink, J.R., Chacko, T., Carlson, R.W., Shirey, S.B., Liu, J., Stern, R.A., Bauer, A.M.,  
1861 Pearson, D.G., and Heaman, L.M., 2018. Petrogenesis and tectonics of the Acasta Gneiss  
1862 Complex derived from integrated petrology and  $^{142}\text{Nd}$  and  $^{182}\text{W}$  extinct nuclide-  
1863 geochemistry. *Earth and Planetary Science Letters* 494: 12-22.

1864 Reimink, J.R., Mundl-Petermeier, A., Carlson, R. W., Shirey, S.B., Walker, R.J., and Pearson,  
1865 D.G., 2020. Tungsten isotope composition of Archean crustal reservoirs and implications  
1866 for terrestrial  $\mu^{182}\text{W}$  evolution. *Geochemistry, Geophysics, Geosystems* 21 (7):  
1867 e2020GC009155.

1868 Richard, D., Marty, B., Chaussidon, M., and Arndt, N.T., 1996. Helium isotopic evidence for  
1869 a lower mantle component in depleted Archean komatiite. *Science* 273 (5271): 93-95.

1870 Richards, M.A., Jones, D.L., Duncan, R.A., and DePaolo, D.J., 1991. A mantle plume  
1871 initiation model for the Wrangellia flood basalt and other oceanic plateaus. *Science* 254  
1872 (5029): 263-265.

1873 Richter, F.M., 1985. Models for the Archean Thermal Regime. *Earth and Planetary Science*  
1874 *Letters* 73 (2-4): 350-360.

1875 Richter, F.M., 1988. A major change in the thermal state of the Earth at the Archean-  
1876 Proterozoic boundary: Consequences for the nature and preservation of continental  
1877 lithosphere. *Journal of Petrology, Special Lithosphere Issue*: 39-52.

1878 Righter, K. and Drake, M.J., 1997. Metal-silicate equilibrium in a homogeneously accreting  
1879 earth: new results for Re. *Earth and Planetary Science Letters* 146 (3-4): 541-553.

1880 Righter, K., Walker, R.J., and Warren, P.H., 2000. Significance of highly siderophile  
1881 elements and osmium isotopes in the lunar and terrestrial mantles. In: Righter, K. and  
1882 Canup, R.M. (Eds.). *Origin of the Earth and Moon*. University of Arizona Press. Tucson,  
1883 AZ, 291-322.

1884 Rizo, H., Boyet, M., Blichert-Toft, J., Rosing, M., 2011. Combined Nd and Hf isotope  
1885 evidence for deep-seated source of Isua lavas. *Earth and Planetary Science Letters* 312 (3-  
1886 4): 267-279.

1887 Rizo, H., Boyet, M., Blichert-Toft, J., O'Neil, J., Rosing, M.T., and Paquette, J.-L., 2012. The  
1888 elusive Hadean enriched reservoir revealed by  $^{142}\text{Nd}$  deficits in Isua Archaean rocks.  
1889 *Nature* 491 (7422): 96-100.

1890 Rizo, H., Boyet, M., Blichert-Toft, J., and Rosing, M.T., 2013. Early mantle dynamics  
1891 inferred from  $^{142}\text{Nd}$  variations in Archean rocks from southwest Greenland. *Earth and*  
1892 *Planetary Science Letters* 377-378: 324-335.

1893 Rizo, H., Walker, R.J., Carlson, R.W., Touboul, M., Horan, M.F., Puchtel, I.S., Boyet, M.,  
1894 and Rosing, M.T., 2016. Early Earth differentiation investigated through  $^{142}\text{Nd}$ ,  $^{182}\text{W}$ , and  
1895 highly siderophile element abundances in samples from Isua, Greenland. *Geochimica et*  
1896 *Cosmochimica Acta* **175**: 319-336.

1897 Rizo H., Andrault D., Bennett N.R., Humayun M., Brandon A.D., Vlastelic I., Moine B.,  
1898 Poirier A., Bouhifd M.A., and Murphy D.T., 2019.  $^{182}\text{W}$  evidence for core-mantle  
1899 interaction in the source of mantle plumes. *Geochemical Perspectives Letters* 11: 6-11.

1900 Rosas, J.C. and Korenaga, J., 2018. Rapid crustal growth and efficient crustal recycling in the  
1901 early Earth: Implications for Hadean and Archean geodynamics. *Earth and Planetary*  
1902 *Science Letters* 494: 42-49.

1903 Roth, A.S.G., Bourdon, B., Mojzsis, S.J., Touboul, M., Sprung, P., Guitreau, M., and  
1904 Blichert-Toft, J., 2013. Inherited  $^{142}\text{Nd}$  anomalies in Eoarchean protoliths. *Earth and*  
1905 *Planetary Science Letters* 361: 50-57.

1906 Roth, A.S.G., Bourdon, B., Mojzsis, S.J., Rudge, J.F., Guitreau, M., and Blichert-Toft, J.,  
1907 2014. Combined  $^{147,146}\text{Sm}$ - $^{143,142}\text{Nd}$  constraints on the longevity and residence time of  
1908 early terrestrial crust. *Geochemistry, Geophysics, Geosystems* 15 (6): 2329-2345.

1909 Roy-Barman, M. and Allègre, C.-J., 1995.  $^{187}\text{Os}/^{186}\text{Os}$  in oceanic island basalts: tracing  
1910 oceanic crust recycling in the mantle. *Earth and Planetary Science Letters* 129 (1-4): 145-  
1911 161.

1912 Rubie, D.C., Frost, D.J., Mann, U., Asahara, Y., Nimmo, F., Tsuno, K., Kegler, P., Holzheid,  
1913 A., and Palme, H., 2011. Heterogeneous accretion, composition and core-mantle  
1914 differentiation of the Earth. *Earth and Planetary Science Letters* 301 (1-2): 31-42.

1915 Rudnick, R.L., Barth, M., Horn, I., and McDonough, W.F., 2000. Rutile-bearing refractory  
1916 eclogites: missing link between continents and depleted mantle. *Science* 287 (5451): 278-  
1917 281.

1918 Rudnick, R.L. and Gao, S., 2014. Composition of the Continental Crust. *Treatise on*  
1919 *Geochemistry*: 1-51.

1920 Ryder, G., 2002. Mass flux in the ancient Earth-Moon system and benign implications for the  
1921 origin of life on Earth. *Journal of Geophysical Research* 107 (E4): 6.1-6.13.

1922 Saal, A.E., Hauri, E.H., Langmuir, C.H., and Perfit, M.R., 2002. Vapour undersaturation in  
1923 primitive mid-ocean-ridge basalt and the volatile content of Earth's upper mantle. *Nature*  
1924 419 (6906): 451-455.

1925 Saji, N.S., Larsen, K., Wielandt, D., Schiller, M., Costa, M.M., Whitehouse, M.J., Rosing,  
1926 M.T., and Bizzarro, M., 2018. Hadean geodynamics inferred from time-varying  
1927  $^{142}\text{Nd}/^{144}\text{Nd}$  in the early Earth rock record. *Geochemical Perspectives Letters* 7: 43-48.

1928 Salters, V. J. M., White, W. M., 1998. Hf isotope constraints on mantle evolution. *Chemical*  
1929 *Geology* **145** (3-4): 447-460.

1930 Schneider, K.P., Hoffmann, J.E., Boyet, M., Münker, C., and Kröner, A., 2018. Coexistence  
1931 of enriched and modern-like  $^{142}\text{Nd}$  signatures in Archean igneous rocks of the eastern  
1932 Kaapvaal Craton, southern Africa. *Earth and Planetary Science Letters* 487: 54-66.

- 1933 Schoenberg, R., Kamber, B. S., Collerson, K. D., Eugster, O., 2002. New W-isotope evidence  
1934 for rapid terrestrial accretion and very early core formation. *Geochimica et Cosmochimica*  
1935 *Acta* **66** (17): 3151-3160.
- 1936 Schubert, G. and Sandwell, D., 1989. Crustal volumes of the continents and of oceanic and  
1937 continental submarine plateaus. *Earth and Planetary Science Letters* **92** (2): 234-246.
- 1938 Shirey, S.B. and Hanson, G.N., 1986. Mantle heterogeneity and crustal recycling in Archean  
1939 granite-greenstone belts: Evidence from Nd isotopes and trace elements in the Rainy Lake  
1940 area, Superior Province, Ontario, Canada. *Geochimica et Cosmochimica Acta* **50** (12):  
1941 2631-2651.
- 1942 Shirey, S. B., Walker, R. J., 1998. The Re-Os isotope system in cosmochemistry and high-  
1943 temperature geochemistry. *Annual Reviews of Earth and Planetary Sciences* **26**: 423-500.
- 1944 Shirey, S.B., Kamber, B.S., Whitehouse, M.J., Mueller, P.A., and Basu, A.R., 2008. A review  
1945 of the isotopic and trace element evidence for mantle and crustal processes in the Hadean  
1946 and Archean: Implications for the onset of plate tectonic subduction. In: Condie, K.C. and  
1947 Pease, V. (Eds.), *When Did Plate Tectonics Begin on Planet Earth?* Geological Society of  
1948 America Special Paper 440: 1-29.
- 1949 Sivell, W.J. and McCulloch, M.T., 1991. Neodymium isotope evidence for ultra-depleted  
1950 mantle in the early Proterozoic. *Nature* **354** (6352): 384-387.
- 1951 Sizova, E., Gerya, T., Stüwe, K., and Brown, M., 2015. Generation of felsic crust in the  
1952 Archean: A geodynamic modeling perspective. *Precambrian Research* **271**: 198-224.
- 1953 Smithies, R.H., Champion, D.C., Van Kranendonk, M.J., and Hickman, A.H., 2007.  
1954 Geochemistry of volcanic rocks of the northern Pilbara Craton, Western Australia.  
1955 Geological Survey of Western Australia, Report 104. Perth, 47 pp.
- 1956 Sobolev, A.V., Asafov, E.V., Gurenko, A.A., Arndt, N.T., Batanova, V.G., Portnyagin, M.V.,  
1957 Garbe-Schönberg, D., and Krashennnikov, S.P., 2016. Komatiites reveal a hydrous  
1958 Archean deep-mantle reservoir. *Nature* **531** (7596): 628-632.
- 1959 Sobolev, A.V., Asafov, E.V., Gurenko, A.A., Arndt, N.T., Batanova, V.G., Portnyagin, M.V.,  
1960 Garbe-Schönberg, D., Wilson, A.H., and Byerly, G.R., 2019. Deep hydrous mantle  
1961 reservoir provides evidence for crustal recycling before 3.3 billion years ago. *Nature* **571**  
1962 (7766): 555-559.
- 1963 Sossi, P.A., Eggins, S.M., Nesbitt, R.W., Nebel, O., Hergt, J.M., Campbell, I.H., O'Neill,  
1964 H.St.C., Van Kranendonk, M., and Davies, D.R., 2016. Petrogenesis and Geochemistry of  
1965 Archean Komatiites. *Journal of Petrology* **57** (1): 147-184.
- 1966 Storey, M., Mahoney, J.J., Kroenke, L.W., and Saunders, A.D., 1991. Are oceanic plateaus  
1967 sites of komatiite formation? *Geology* **19** (4): 376-379.
- 1968 Strom, R.G., Malhotra, R., Ito, T., Yoshida, F., and Kring, D.A., 2005. The origin of planetary  
1969 impactors in the inner Solar system. *Science* **309** (5742): 1847-1850.
- 1970 Tonks, W.B. and Melosh, H.J., 1993. Magma Ocean Formation Due to Giant Impacts. *Journal*  
1971 *of Geophysical Research* **98** (E3): 5319-5333.
- 1972 Torsvik, T.H., Steinberger, B., Ashwal, L.D., Doubrovine, P.V., and Trønnes, R.G., 2016.  
1973 Earth evolution and dynamics - a tribute to Kevin Burke. *Canadian Journal of Earth*  
1974 *Sciences* **53** (11): 1073-1087.
- 1975 Touboul, M., Puchtel, I.S., and Walker, R.J., 2012. <sup>182</sup>W Evidence for Long-Term  
1976 Preservation of Early Mantle Differentiation Products. *Science* **335**: 1065-1069.

1977 Touboul, M., Liu, J., O'Neil, J., Puchtel, I.S., and Walker, R.J., 2014. New Insights into the  
1978 Hadean Mantle Revealed by  $^{182}\text{W}$  and Highly Siderophile Element Abundances of  
1979 Supracrustal Rocks from the Nuvvuagittuq Greenstone Belt, Quebec, Canada. *Chemical*  
1980 *Geology* 383: 63-75.

1981 Touboul, M., Puchtel, I.S., and Walker, R.J., 2015. Tungsten isotopic evidence for  
1982 disproportional late accretion to the Earth and Moon. *Nature* 520 (7548): 530-533.

1983 Trønnes, R.G. and Frost, D.J., 2002. Peridotite melting and mineral-melt partitioning of major  
1984 and minor elements at 22-24.5 GPa. *Earth and Planetary Science Letters* 197 (1-2): 117-  
1985 131.

1986 Turekian, K.K. and Clark, S.P., 1969. Inhomogeneous accumulation of the earth from the  
1987 primitive solar nebula. *Earth and Planetary Science Letters* 6 (5): 346-348.

1988 Tusch, J., Sprung, P., van de Löcht, J., Hoffmann, J.E., Boyd, A.J., Rosing, M.T., and  
1989 Münker, C., 2019. Uniform  $^{182}\text{W}$  isotope compositions in Eoarchean rocks from the Isua  
1990 region, SW Greenland: The role of early silicate differentiation and missing late veneer.  
1991 *Geochimica et Cosmochimica Acta* 257: 284-310.

1992 Tusch, J., Münker, C., Hasenstab, E., Jansen, M., Marien, C. S., Kurzweil, F., Van  
1993 Kranendonk, M. J., Smithies, H., Maier, W., and Garbe-Schönberg, D., 2021. Convective  
1994 isolation of Hadean mantle reservoirs through Archean time. *Proceedings of the National*  
1995 *Academy of Sciences* 118 (2): e2012626118.

1996 Van Kranendonk, M.J., 2008. Two types of Archean continental crust: Plume and plate  
1997 tectonics on early Earth. *American Journal of Science* 310 (10): 1187-1210.

1998 Vervoort, J.D. and Blichert-Toft, J., 1999. Evolution of the depleted mantle: Hf isotope  
1999 evidence from juvenile rocks through time. *Geochimica et Cosmochimica Acta* 63 (3-4):  
2000 533-556.

2001 Vervoort, J.D., Patchett, P.J., Blichert-Toft, J., and Albarède, F., 1999. Relationships between  
2002 Lu-Hf and Sm-Nd isotopic systems in the global sedimentary system. *Earth and Planetary*  
2003 *Science Letters* 168 (1-2): 79-99.

2004 Vervoort, J.D., Patchett, P.J., Albarède, F., Blichert-Toft, J., Rudnick, R., and Downes, H.,  
2005 2000. Hf-Nd isotopic evolution of the lower crust. *Earth and Planetary Science Letters*  
2006 181 (1-2): 115-129.

2007 Viljoen, M.J. and Viljoen, R.P., 1969. The geology and geochemistry of the Lower  
2008 Ultramafic Unit of the Onverwacht Group and a proposed new class of igneous rocks.  
2009 *Geological Society of South Africa Special Publication* 2: 55-86.

2010 Wade, J. and Wood, B.J., 2005. Core formation and the oxidation state of the Earth. *Earth and*  
2011 *Planetary Science Letters* 236 (1-2): 78-95.

2012 Walker, R.J., Shirey, S.B., and Stecher, O., 1988. Comparative Re-Os, Sm-Nd and Rb-Sr  
2013 isotope and trace element systematics for Archean komatiite flows from Munro Township,  
2014 Abitibi belt, Ontario. *Earth and Planetary Science Letters* 87 (1-2): 1-12.

2015 Walker, R.J., Morgan, J.W., and Horan, M.F., 1995.  $^{187}\text{Os}$  enrichment in some plumes:  
2016 evidence for core-mantle interaction? *Science* 269 (5225): 819-822.

2017 Walker, R.J., Morgan, J.W., Beary, E.S., Smoliar, M.I., Czamanske, G.K., and Horan, M.F.,  
2018 1997. Applications of the  $^{190}\text{Pt}$ - $^{186}\text{Os}$  isotope system to geochemistry and cosmochemistry.  
2019 *Geochimica et Cosmochimica Acta* 61 (22): 4799-4807.



Walker, R. J., Horan, M. F., Morgan, J. W., Becker, H., Grossman, J. N., Rubin, A. E., 2002. Comparative  $^{187}\text{Re}$ - $^{187}\text{Os}$  systematics of chondrites: Implications regarding early solar system processes. *Geochimica et Cosmochimica Acta* **66** (23): 4187-4201.

Walker, R.J., Horan, M.F., Shearer, C.K., and Papike, J.J., 2004. Low abundances of highly siderophile elements in the lunar mantle: Evidence for prolonged late accretion. *Earth and Planetary Science Letters* **224** (3-4): 399-413.

Walker, R.J., 2009. Highly siderophile elements in the Earth, Moon and Mars: Update and implications for planetary accretion and differentiation. *Chemie der Erde - Geochemistry* **69** (2): 101-125.

Walker, R.J., 2014. Siderophile element constraints on the origin of the Moon. *Philosophical Transactions of the Royal Society of London* **372**: 20130258.

Walker, R.J., 2016. Siderophile Elements in Tracing Planetary Formation and Evolution. *Geochemical Perspectives* **5** (1): 1-145.

Walter, M.J., Nakamura, E., Trønnes, R.G., and Frost, D.J., 2004. Experimental constraints on crystallization differentiation in a deep magma ocean. *Geochimica et Cosmochimica Acta* **68** (20): 4267-4284.

White, W.M. and Patchett, J., 1984. Hf-Nd-Sr isotopes and incompatible element abundances in island arcs: implications for magma origins and crust-mantle evolution. *Earth and Planetary Science Letters* **67** (2): 167-185.

Widom, E., 1997. Sources of ocean island basalts: A review of the osmium isotope evidence. *Physica A: Statistical Mechanics and its Applications* **244** (1-4): 484-496.

Willbold, M., Elliott, T., and Moorbath, S., 2011. The tungsten isotopic composition of the Earth's mantle before the terminal bombardment. *Nature* **477** (7363): 195-198.

Willbold, M., Mojzsis, S.J., Chen, H.W., and Elliott, T., 2015. Tungsten isotope composition of the Acasta Gneiss Complex. *Earth and Planetary Science Letters* **419**: 168-177.

Willig, M. and Stracke, A., 2019. Earth's chondritic light rare earth element composition: Evidence from the Ce-Nd isotope systematics of chondrites and oceanic basalts. *Earth and Planetary Science Letters* **509**: 55-65.

Willig, M., Stracke, A., Beier, C., and Salters, V.J.M., 2020. Constraints on mantle evolution from Ce-Nd-Hf isotope systematics. *Geochimica et Cosmochimica Acta* **272**: 36-53.

Wilson, A.H. and Carlson, R.W., 1989. A Sm-Nd and Pb isotope study of Archaean greenstone belts in the southern Kaapvaal Craton, South Africa. *Earth and Planetary Science Letters* **96** (1-2): 89-105.

Wyman, D.A., 2013. A critical assessment of Neoarchean "plume only" geodynamics: Evidence from the Superior Province. *Precambrian Research* **229**: 3-19.

Wyman, D., 2019. Do cratons preserve evidence of stagnant lid tectonics? *Geoscience Frontiers* **9** (1): 3-17.

Wyman, D., 2020. Komatiites From Mantle Transition Zone Plumes. *Frontiers in Earth Science* **8** (383): 540744.

Yin, Q., Jacobsen, S.B., Yamashita, K., Blichert-Toft, J., Telouk, P., Albarede, F., 2002. A short timescale for terrestrial planet formation from Hf-W chronometry of meteorites. *Nature* **418** (6901): 949-952.

Yokoyama, T., Walker, D., and Walker, R.J., 2009. Low osmium solubility in silicate at high pressures and temperatures. *Earth and Planetary Science Letters* **279** (3-4): 165-173.

2064 Young, E.D., Kohl, I.E., Warren, P.H., Rubie, D.C., Jacobson, S.A., and Morbidelli, A., 2016.  
 2065 Oxygen isotopic evidence for vigorous mixing during the Moon-forming giant impact.  
 2066 Science 351 (6272): 493-496.  
 2067 Zindler, A., Jagoutz, E., Goldstein, S. L., 1982. Nd, Sr and Pb isotopic systematics in a three-  
 2068 component mantle: a new perspective. Nature **298** (5874): 519-523.  
 2069 Zindler, A., Hart, S. R., 1986. Chemical Geodynamics. Annual Reviews of Earth and  
 2070 Planetary Sciences **14**: 493-571.  
 2071  
 2072

## Figure captions

**Fig. 1.** Variations of model-specific (see the references below for the specific models used), time-integrated Sm/Nd and Lu/Hf ratios in the mantle sources of Archean and Proterozoic komatiite-basalt systems studied to date. The individual models assume a minimum-degree fractionation of Sm/Nd and Lu/Hf in the particular mantle domains from either the chondritic values or values defined by the combined  $^{142,143}\text{Nd}/^{144}\text{Nd}$  systematics (where available) to those required to bring the  $\epsilon^{143}\text{Nd}$  and  $\epsilon^{176}\text{Hf}$  in the mantle sources to the initial  $\epsilon^{143}\text{Nd}$  and  $\epsilon^{176}\text{Hf}$  by the times of the respective komatiite formation. The solid line connects Sm/Nd and Lu/Hf ratios inferred for the chondritic uniform reservoir (CHUR) and modern depleted mantle (DMM). Data are from: Ottawa – Blichert-Toft and Arndt (1999); 2.05 Ga Lapland – Puchtel et al. (2020); 2.41 Ga Vetreny – Puchtel et al. (2016b); 2.72 Ga Pyke Hill and Alexo – Dupre et al. (1984), Walker et al. (1988), Blichert-Toft and Arndt (1999); 2.72 Ga Boston Creek – Puchtel et al. (2018); 2.82 Ga Kostomuksha – Puchtel et al. (1998), Blichert-Toft and Puchtel (2010); 3.48 Ga Komati and 3.26 Ga Weltevreden – Puchtel et al. (2013); 3.32 Ga Comondale – Wilson and Carlson (1989), Hoffmann and Wilson (2017); 3.55 Ga Schapenburg – Puchtel et al. (2009a, 2016a); 3.53 Ga Coonterunah, 3.34 Ga Kelly, and 3.18 Ga Ruth Well and Regal – Puchtel et al. (2022). The CHUR and DMM parameters are from Jacobsen and Wasserburg (1980), Hamilton et al. (1983), Goldstein et al. (1984), Vervoort and Blichert-Toft (1999), and Bouvier et al. (2008). All uncertainties are 2SD of the mean.

**Fig. 2. (a)** Initial  $^{187}\text{Os}/^{188}\text{Os}$  expressed as  $\gamma^{187}\text{Os}$  and **(b)** initial  $^{186}\text{Os}/^{188}\text{Os}$  expressed as  $\mu^{186}\text{Os}$  of Archean komatiite systems studied to date, plotted as a function of their age. The blue bars for the modern BSE estimates represent the 2SD of the mean from Meisel et al. (2001) and Brandon et al. (2006) for (a) and (b), respectively. Data are from: 2.05 Ga Lapland – Puchtel et al. (2020); 2.41 Ga Vetreny – Puchtel et al. (2016b); 2.69 Ga Belingwe and 2.72 Ga Pyke Hill – Puchtel et al. (2009a); 2.72 Ga Boston Creek – Puchtel et al. (2018); 2.82 Ga Kostomuksha – Puchtel et al. (2005); 2.88 Ga Volotsk – Puchtel et al. (2007); 3.48 Ga Komati and 3.26 Ga Weltevreden – Puchtel et al. (2014); 3.55 Ga Schapenburg – Puchtel et al. (2009b, 2016a); 3.34 Ga Kelly and 3.18 Ga Ruth Well and Regal – Puchtel et al. (2022). The data for chondritic meteorites are compiled from Walker et al. (2002), Horan et al. (2003), Brandon et al. (2005; 2006), and Fischer-Gödde et al. (2010) and are plotted as an envelope enclosed between the slanting purple lines and corresponding to the entire range of calculated modern  $\gamma^{187}\text{Os}$  and  $\mu^{186}\text{Os}$  values projected back to the Solar System initial  $^{187}\text{Os}/^{188}\text{Os}$  and  $^{186}\text{Os}/^{188}\text{Os}$  ratios. All uncertainties are 2SD of the mean.

**Fig. 3.** Calculated total HSE abundances in the sources of Archean and Paleoproterozoic komatiite systems plotted as *percent* of those in estimates of the modern BSE of Becker et al. (2006). The blue dashed lines correspond to the range for the BSE estimates from Becker et al. (2006). The dark-red arrow represents the regression line through the data. The dark-red vertical arrows represent the projections to the x-axis from the intersections of the regression line with the range for the BSE estimate, thus, illustrating the uncertainties on the average time of homogenization of late accreted materials within the mantle ( $2.5 \pm 0.2$  Ga). Data are

from: 2.05 Ga Lapland – Puchtel et al. (2020); 2.41 Ga Vetreny Belt – Puchtel et al. (2016b); 2.69 Ga Belingwe – Puchtel et al. (2009a); 2.72 Ga Pyke Hill and Alexo – Puchtel et al. (2004b, 2009a); 2.72 Ga Boston Creek – Puchtel et al. (2018); 2.82 Ga Kostomuksha – Puchtel and Humayun (2005); 2.88 Ga Volotsk – Puchtel et al. (2007); 3.26 Ga Weltevreden and 3.48 Ga Komati – Puchtel et al. (2014); 3.55 Ga Schapenburg – Puchtel et al. (2009b, 2016a); 3.53 Ga Coonterunah, 3.34 Ga Kelly, and 3.18 Ga Ruth Well and Regal – Puchtel et al. (2022). Uncertainties are 2SD. The data reveal a broad trend of increasing HSE abundances in komatiite mantle sources over geological time. All uncertainties are 2SD of the mean. See text for additional details and the [Electronic Supplement](#) for the algorithm used to estimate the HSE abundances in the sources of the komatiite systems.

**Fig. 4.** Evolution of the time-integrated  $^{147}\text{Sm}/^{144}\text{Nd}$  and  $^{176}\text{Lu}/^{177}\text{Hf}$  in the calculated sources of the Komati and Weltevreden komatiite systems formed during crystallization of a primordial magma ocean. The differentiation trends (shown by tick marks in percentage) depend on the relative proportions of the fractionating lower mantle mineral phases, *i.e.*, bridgmanite and Ca-Pv. The composition of the magma ocean prior to onset of crystallization is represented by that of the CHUR. The upper part of the panel represents aggregate compositions of magma ocean cumulates, while the lower part of the panel represents compositions of residual liquids after removal of the respective amounts of cumulate bridgmanite and Ca-Pv. All uncertainties are 2SD of the mean. See text for additional details of the model and the [Electronic Supplement](#) for the algorithm used in the calculations.

**Fig. 5.** Values of  $\mu^{182}\text{W}$  versus (A)  $\mu^{186}\text{Os}$  and (B)  $\gamma^{187}\text{Os}$  in the Kostomuksha komatiites illustrating mixing between the modern BSE and a mantle reservoir preserved from an early magma ocean crystallization event. The Re/Os, Pt/Os, and Hf/W ratios were established by high-pressure and -temperature metal-silicate equilibrium, resulting in  $^{187,186}\text{Os}$  and  $^{182}\text{W}$  enrichments at 2.82 Ga (Touboul et al., 2012). The coupled  $^{186,187}\text{Os}$  and  $^{182}\text{W}$  excesses in the source of the Kostomuksha komatiites (yellow circle) are explained by a ~50% contribution from the isotopically enriched reservoir to the modern BSE. All uncertainties are 2SD of the mean. See text for additional details.

**Fig. 6.**  $\mu^{182}\text{W}$  (ppm) versus calculated total HSE abundances in the sources of Archean and Paleoproterozoic komatiite-basalt systems studied to date relative to those in the estimates of the present-day BSE of Becker et al. (2006). This proportion corresponds to the fraction of the total HSE budget of the BSE added during late accretion assuming an HSE-free terrestrial mantle prior to late accretion. The average  $\mu^{182}\text{W}$  value for the Moon of  $+25\pm5$  is from Kruijer et al. (2015) and Touboul et al. (2015). The  $\mu^{182}\text{W}$  of the BSE prior to late accretion is constrained *via Isoplot* regression analysis of the  $\mu^{182}\text{W}$  and HSE compositions of all komatiite-basalt systems except for those of Kostomuksha and Schapenburg and the present-day BSE to be  $+17\pm7$ . The W isotopic data and estimates of the HSE contents for the komatiite systems are from Puchtel and Humayun (2005), Touboul et al. (2012), and Puchtel et al. (2014; 2009b, 2016a,b; 2018; 2020; 2022). All uncertainties are 2SD of the mean. See text for additional details.

**Fig. 7.**  $^{182}\text{W}/^{184}\text{W}$  and  $^{142}\text{Nd}/^{144}\text{Nd}$  data for the terrestrial mafic-ultramafic rock record obtained to date. The colored bands represent the 2SD uncertainty on the mean  $\mu^{182}\text{W}$  and  $\mu^{142}\text{Nd}$  values for each locality. The red arrows illustrate the change in direction and magnitude of the  $^{182}\text{W}$  and  $^{142}\text{Nd}$  anomalies. Note the relative scarcity of data for the period between ~2.7 Ga and present day. Data are from: 3.96 Ga Acasta – Roth et al. (2014), Willbold et al. (2015), Reimink et al. (2018); 3.85 Ga Isua – Willbold et al. (2011), Rizo et al. (2013, 2016), Dale et al. (2017), Tusch et al. (2019), Caro et al. (2006), Bennett et al. (2007), Saji et al. (2018); 3.80 Ga Nuvvuagittuq – O’Neil et al. (2012), Touboul et al. (2014); 3.78 Ga Saglek – Liu et al. (2016), Morino et al. (2017); 3.75 Ga Ukaliq – Caro et al. (2017); 3.72 Ga Isua – Rizo et al. (2011, 2016), Tusch et al. (2019), O’Neil et al. (2016); 3.50 Ga Ameralik – Saji et al. (2018); 3.37 Ga Ameralik – Rizo et al. (2012, 2016), Tusch et al. (2019); 3.55 Ga Schapenburg – Puchtel et al. (2016a); 3.53 Ga Coonterunah – Tusch et al. (2021), Puchtel et al. (2021); 3.48 Ga Komati and 3.26 Weltevreden – Touboul et al. (2012), Caro et al. (2006), Puchtel et al. (2013), Schneider et al. (2018); 3.45 Ga Warrawoona – Archer et al. (2019), Rizo et al. (2019), Murphy et al. (2021); 3.35 Ga Kelly – Puchtel et al. (2022); 3.18 Ga Ruth Well and Regal – Archer et al. (2019), Tusch et al. (2021), Puchtel et al. (2022); 3.14 Ga Banasandra – Maya et al. (2017); 2.82 Ga Kostomuksha and 2.69 Ga Belingwe – Touboul et al. (2012), Boyet and Carlson (2006); 2.72 Ga Boston Creek – Puchtel et al. (2018); 2.72 Ga Theo’s Flow – Debaille et al. (2013); 2.41 Ga Vetreny Belt – Puchtel et al. (2016b); 2.05 Ga Lapland – Puchtel et al. (2020); modern OIB – Caro et al. (2006), Andreasen et al. (2008), Murphy et al. (2010), Touboul et al. (2012), Mundl et al. (2017), Mundl-Petermeier et al. (2019, 2020), Rizo et al. (2019), Horan et al. (2018), Saji et al. (2018), Peters et al. (2018), Hyung and Jacobsen (2020); modern MORB – Caro et al. (2006), Mundl et al. (2017), Hyung and Jacobsen (2020).

2179 **Table 1.** Summary of ages, thermodynamic parameters, and chemical features of the komatiite systems considered in this review.

Komatiite-basalt system	Age, Ga	MgO <sub>liq</sub>	T <sub>liq</sub> °C	T <sub>p</sub> °C	D <sub>melt init</sub> , km	D <sub>plume init</sub> , km	Al <sub>2</sub> O <sub>3</sub> /TiO <sub>2</sub>	(La/Sm) <sub>N</sub>	(Gd/Yb) <sub>N</sub>	Nb/Nb*	W/Th
<i>Kaapvaal Craton, South Africa</i>											
Schapenburg	3.55	29.1±2.8	1582	1811	443	LM	10.0±0.8	0.93±0.04	1.57±0.10	1.2±0.1	9.7±5.5
Komati	3.48	29.9±0.5	1591	1822	494	LM	10.1±0.7	0.97±0.24	1.39±0.05	1.1±0.2	0.25±0.18
Weltevreden	3.26	31.4±0.9	1606	1841	605	LM	29.2±1.1	0.68±0.06	0.84±0.03	1.4±0.1	1.5±1.4
<i>Pilbara Craton, Western Australia</i>											
Coonterunah	3.53	23.0±0.3	1498	1705	203	MTZ	23.8±1.7	0.80±0.04	0.96±0.04	1.08±0.02	0.91±0.62
Kelly	3.34	27.4±1.0	1561	1786	351	MTZ	22.1±1.7	0.65±0.02	0.91±0.04	1.03±0.04	0.81±0.69
Ruth Well	3.18	29.3±0.7	1584	1814	455	MTZ	11.0±0.5	0.55±0.09† 0.77±0.09	1.31±0.04† 1.32±0.04	1.0±0.1† 0.51±0.05	3.4±2.3
Regal	3.18	29.3±0.7	1584	1814	455	MTZ	11.9±0.8	0.61±0.11† 0.83±0.11	1.28±0.12† 1.31±0.12	1.0±0.1† 0.55±0.09	3.5±2.8
<i>Fennoscandian Shield, northern Europe</i>											
Kostomuksha	2.82	27.6±1.0	1564	1789	361	LM	17.2±1.2	0.48±0.13	1.16±0.02	1.2±0.1	0.84±0.32
Vetreny	2.41	27.0±1.0	1556	1779	333	MTZ	19.7±0.5	0.41±0.10† 2.2±0.1	1.2±0.1† 1.3±0.1	1.0±0.1† 0.29±0.03	0.05±0.02
Lapland	2.05	25.2±0.5	1532	1748	264	LM	13.9±0.4	0.14±0.02† 0.26±0.01	1.48±0.02† 1.49±0.02	1.0±0.1† 0.58±0.01	0.16±0.06
<i>Superior Craton, Canada</i>											
Boston Creek	2.72					MTZ	5.1±0.8	1.9±0.3	2.0±0.2	1.2±0.2	0.9±1.4
Pyke Hill-Alexo	2.72	28.2±0.5	1571	1789	392	MTZ	20.4±0.6	0.53±0.16	0.98±0.03	1.0±0.1	0.15±0.06
<i>Rhodesian Craton, Zimbabwe</i>											
Belingwe	2.69	25.6±0.5	1537	1755	277	MTZ	19.8±0.6	0.68±0.02	1.02±0.04	0.97±0.05	0.20±0.06

†Values corrected for AFC. The italicized values are those measured in the emplaced lavas, before correction for AFC. All uncertainties are 2SD of the mean. **MgO<sub>liq</sub>** – the MgO content of the original emplaced komatiite magma for each komatiite system compiled from Nicklas et al. (2018, 2019) and Puchtel et al. (1998, 2016a, 2020, 2022). T<sub>liq</sub> °C, T<sub>p</sub> °C – liquidus temperatures of the emplaced komatiite magmas and mantle potential temperatures for the studied komatiite systems. D<sub>melt init</sub> – depths of melting initiation. D<sub>plume init</sub> – inferred depths of plume initiation for the studied komatiite systems. Nb/Nb\* = Nb<sub>N</sub>/√(Th<sub>N</sub>×La<sub>N</sub>), where N are the BSE normalizing values from Hofmann (1988). For sources of the data see Table 2. See text and the **Electronic Supplement** for details.

2186

**Table 2.** Summary of isotopic features and HSE abundances of the komatiite systems considered in this review

Komatiite-basalt system	$\epsilon^{143}\text{Nd}(\text{T})$	$\epsilon^{176}\text{Hf}(\text{T})$	$\mu^{142}\text{Nd}$	$\mu^{182}\text{W}$	$\gamma^{187}\text{Os}(\text{T})$	$\mu^{186}\text{Os}(\text{T})$	$\Sigma\text{HSE}$	Data source
<i>Kaapvaal Craton, South Africa</i>								
Schapenburg	+2.4±0.5	+5.8±0.8	-5.0±2.8	-8.4±4.1	+3.7±0.3		29±9	[1 – 2]
Komati	+0.46±0.39	+1.9±1.0	-0.9±2.7	+2.7±4.5	+0.3±0.3	-12±8	60±8	[3 – 5]
Weltevreden	+0.54±0.40	+4.7±2.1	+2.5±3.8		-0.1±0.2	+22±7	65±6	[3 – 4]
<i>Pilbara Craton, Western Australia</i>								
Coonterunah	+2.4±0.5	+4.4±0.3		+11.4±4.6			29±6	[6]
Kelly	+0.5±0.6	+1.7±0.6		+8.2±3.3	+0.8±0.4		38±7	[6]
Ruth Well	+1.3±0.7† <i>+0.6±0.7</i>	+2.4±0.4† <i>+1.7±0.4</i>	-1.8±3.8	+7.7±5.0	-0.4±0.4† <i>-0.4±0.4</i>		55±4	[6]
Regal	+1.9±0.3† <i>+1.0±0.3</i>	+4.6±0.8† <i>+4.1±0.8</i>		+7.7±5.0	+0.9±0.3† <i>+0.9±0.3</i>		70±5	[6]
<i>Fennoscandian Shield, northern Europe</i>								
Kostomuksha	+3.0±0.4	+4.9±0.3	+0.4±0.9	+15.0±4.8	+2.5±0.6	+22±6	79±6	[7 – 11]
Vetreny	+3.7±0.4† <i>-0.9±0.4</i>	+6.3±0.9† <i>+0.4±0.9</i>	+0.5±2.1	-0.5±5.2† <i>+7.5±5.2</i>	+1.3±0.2† <i>+1.7±0.2</i>	+3.2±1.7	66±10	[12]
Lapland	+4.9±0.3† <i>+3.7±0.3</i>	+10.2±0.7† <i>+8.7±0.7</i>		-10.0±5.0† <i>+1.5±3.3</i>	-0.2±0.3† <i>-0.2±0.3</i>	+29±2	120±5	[13]
<i>Superior Craton, Canada</i>								
Boston Creek	+2.5±0.2	+4.3±0.9	-3.8±2.8	+11.7±4.5	+0.1±0.3		35±10	[14]
Pyke Hill-Alexo	+3.0±0.5	+5.5±0.6	+6.8±2.5		+0.4±0.1	-0.1±4.2	85±5	[15 – 19]
<i>Rhodesian Craton, Zimbabwe</i>								
Belingwe	+2.9±0.2		+3.7±7.0		+0.1±0.2	+0.6±2.5	57±7	[20 – 21]

2187

2188

2189

2190

2191

2192

†Values corrected for AFC. The italicized values are those measured in the emplaced lavas, before correction for AFC. All uncertainties are 2SD of the mean. Data sources are as follows: [1] - Puchtel et al. (2009a); [2] - Puchtel et al. (2016a); [3] - Puchtel et al. (2013); [4] - Puchtel et al. (2014); [5] - Touboul et al. (2012); [6] - Puchtel et al. (2022); [7] - Puchtel et al. (1998); [8] - Boyet and Carlson (2006); [9] - Touboul et al. (2012); [10] - Puchtel et al. (2005); [11] - Puchtel and Humayun (2005); [12] - Puchtel et al. (2016b); [13] - Puchtel et al. (2020); [14] - Puchtel et al. (2018); [15] - Blichert-Toft and Arndt (1999); [16] - Puchtel et al. (2004a); [17] - Puchtel et al. (2004b); [18] - Puchtel et al. (2009b); [19] - Debaille et al. (2013); [20] - Puchtel et al. (2009b); [21] - Boyet and Carlson (2006).

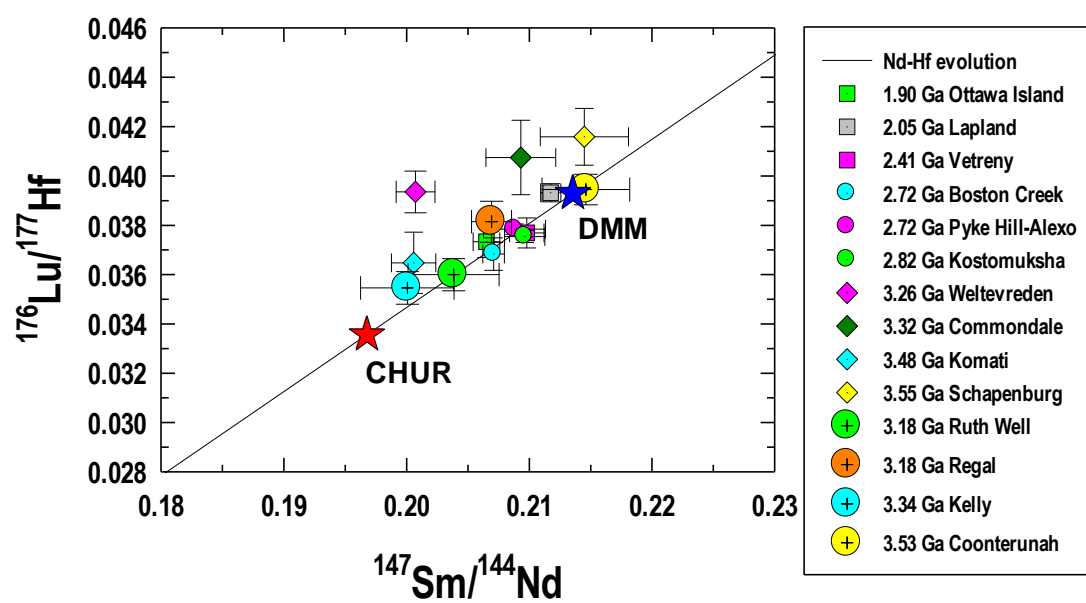


**Fig. 1**



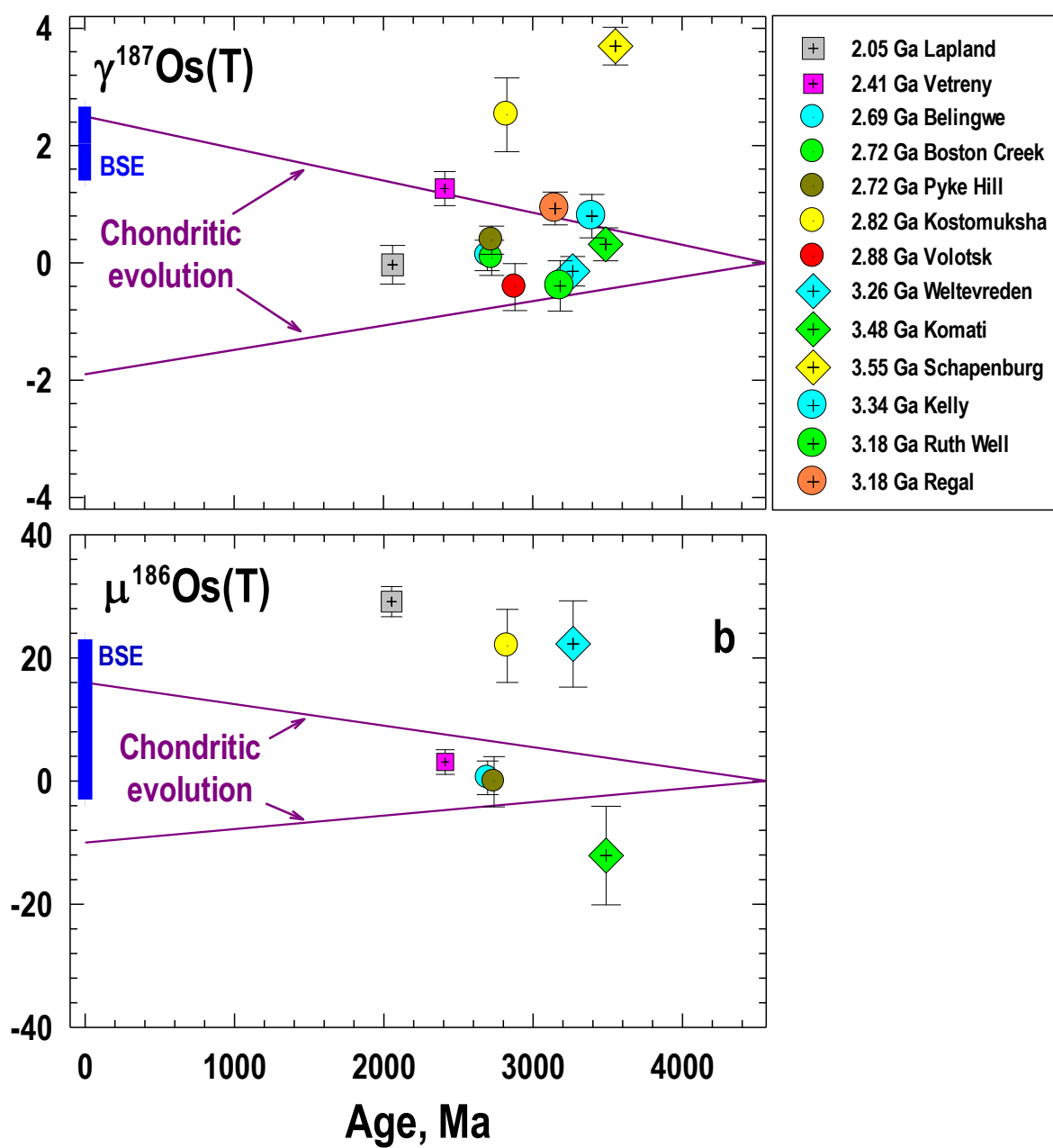


**Fig. 2**

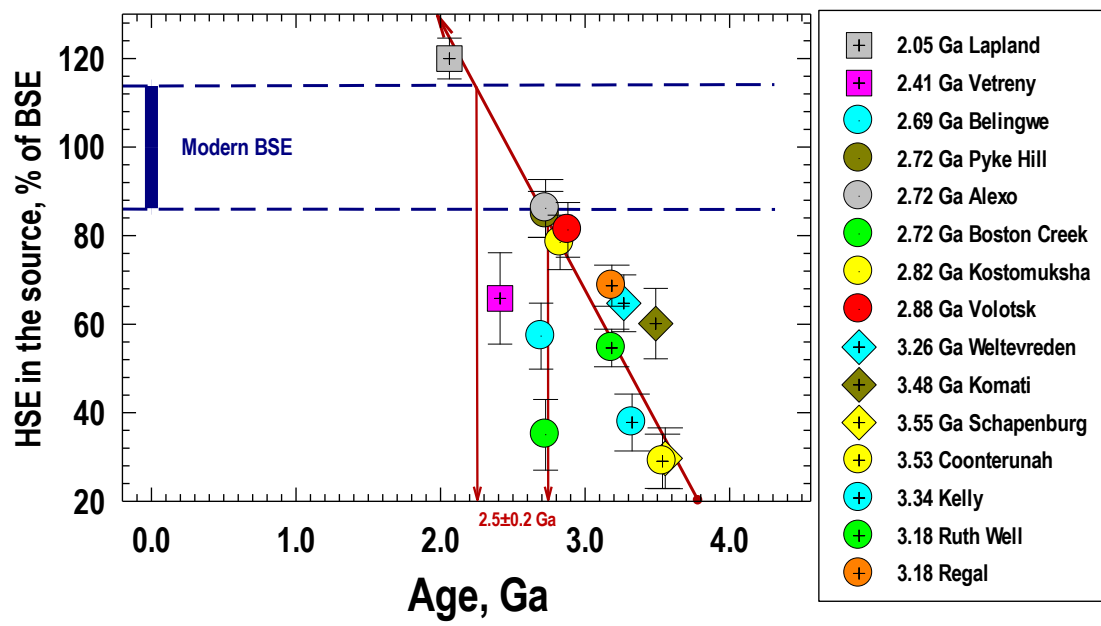
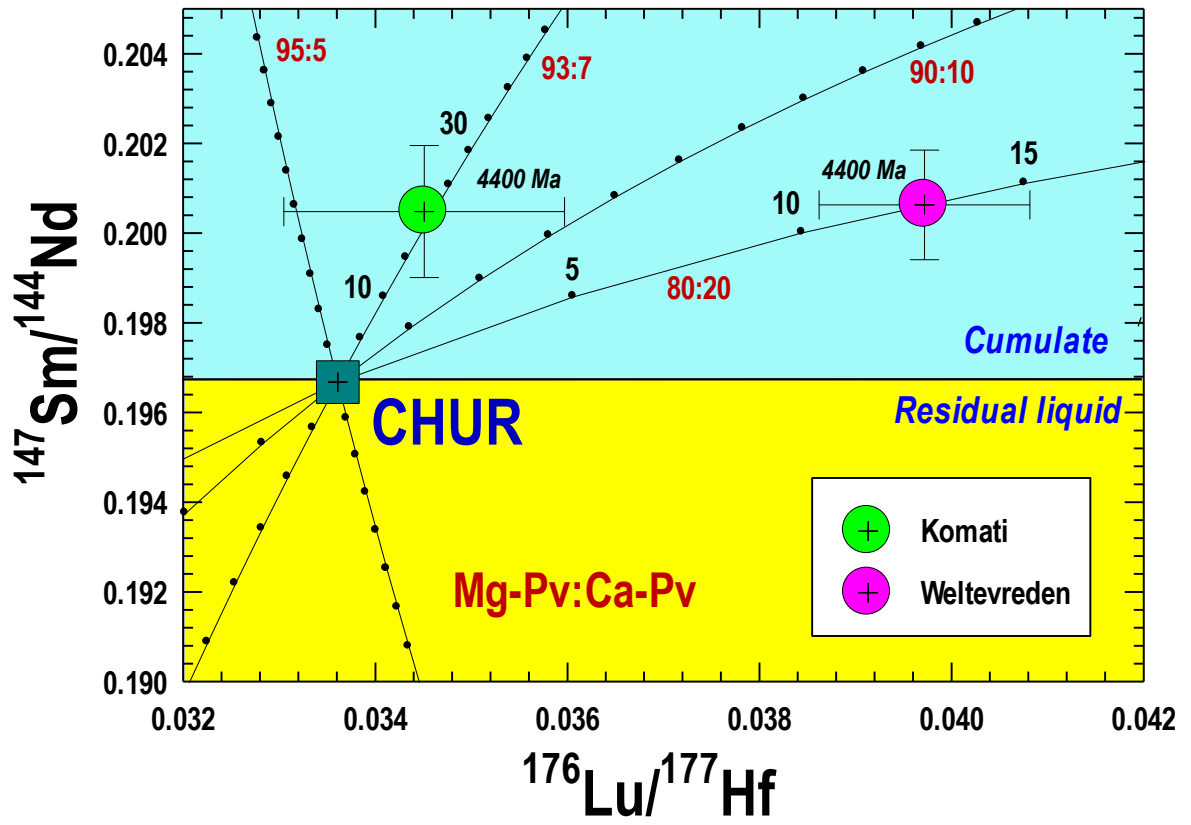


Fig. 3



2204  
2205

2206 Fig. 4

2207

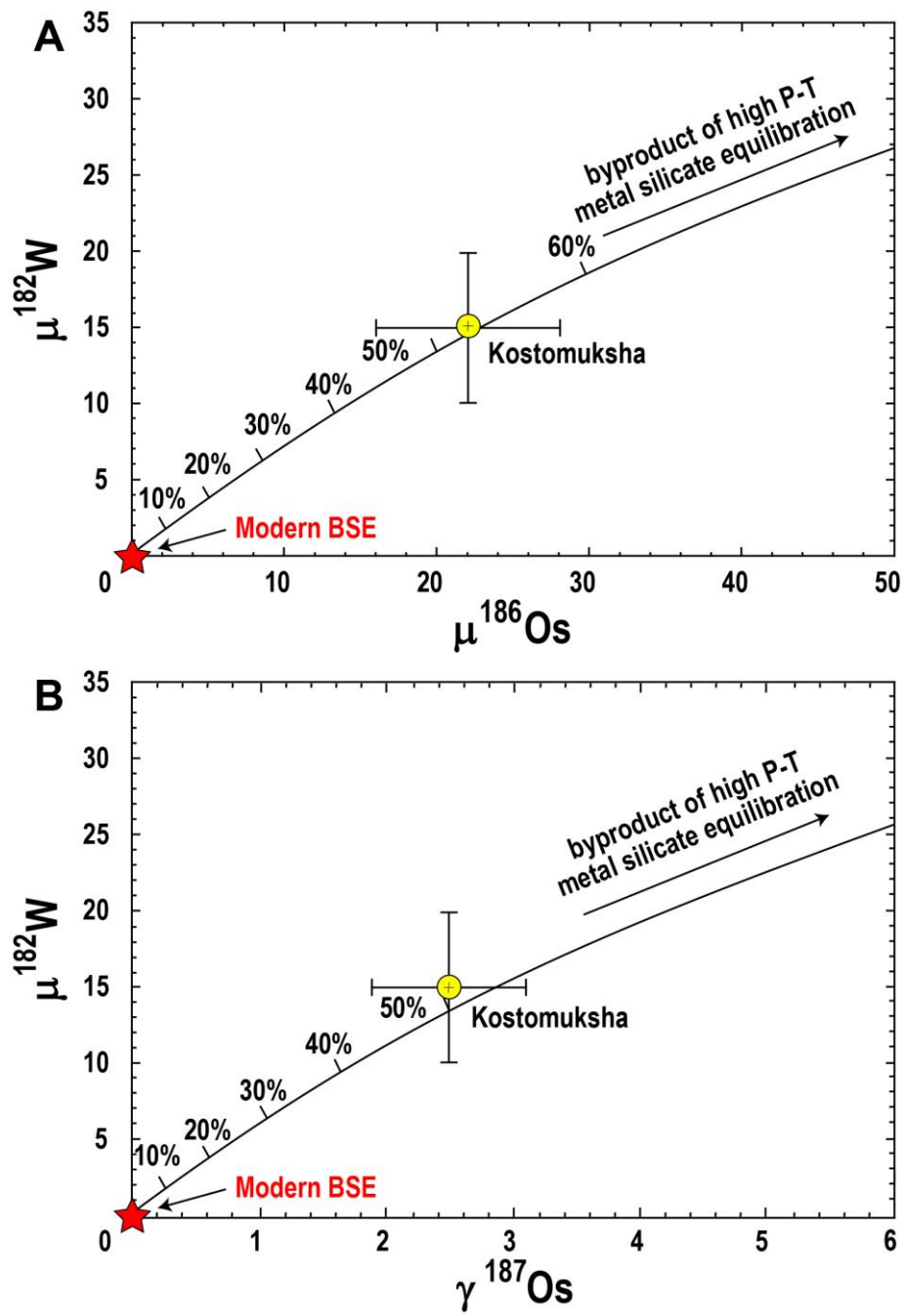


**Fig. 5.**

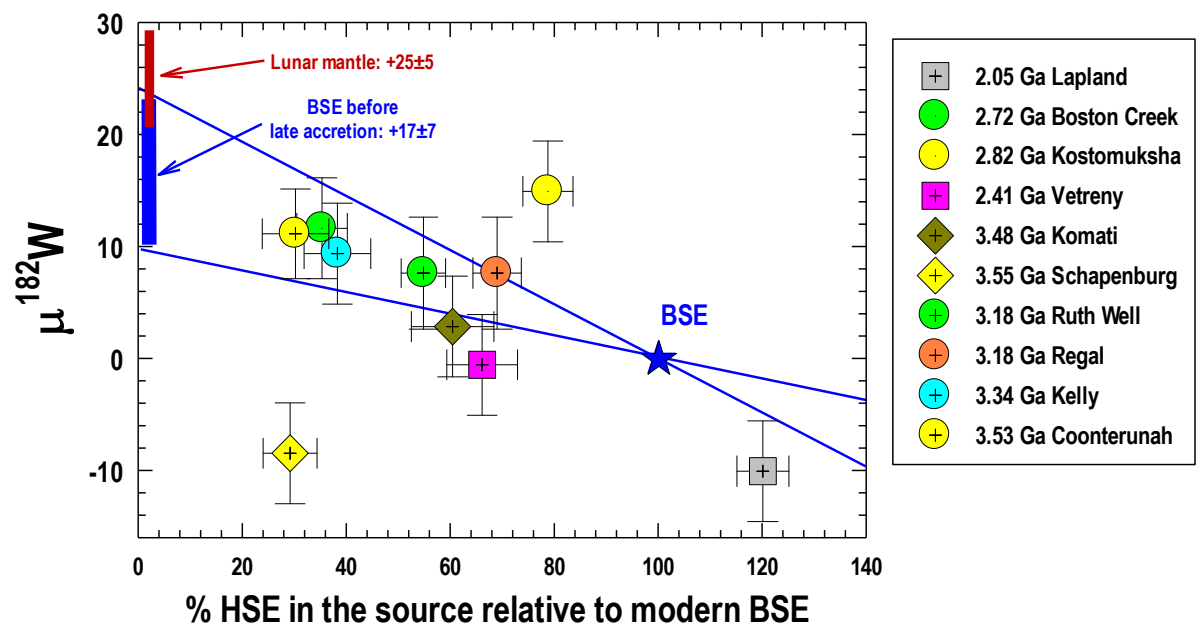
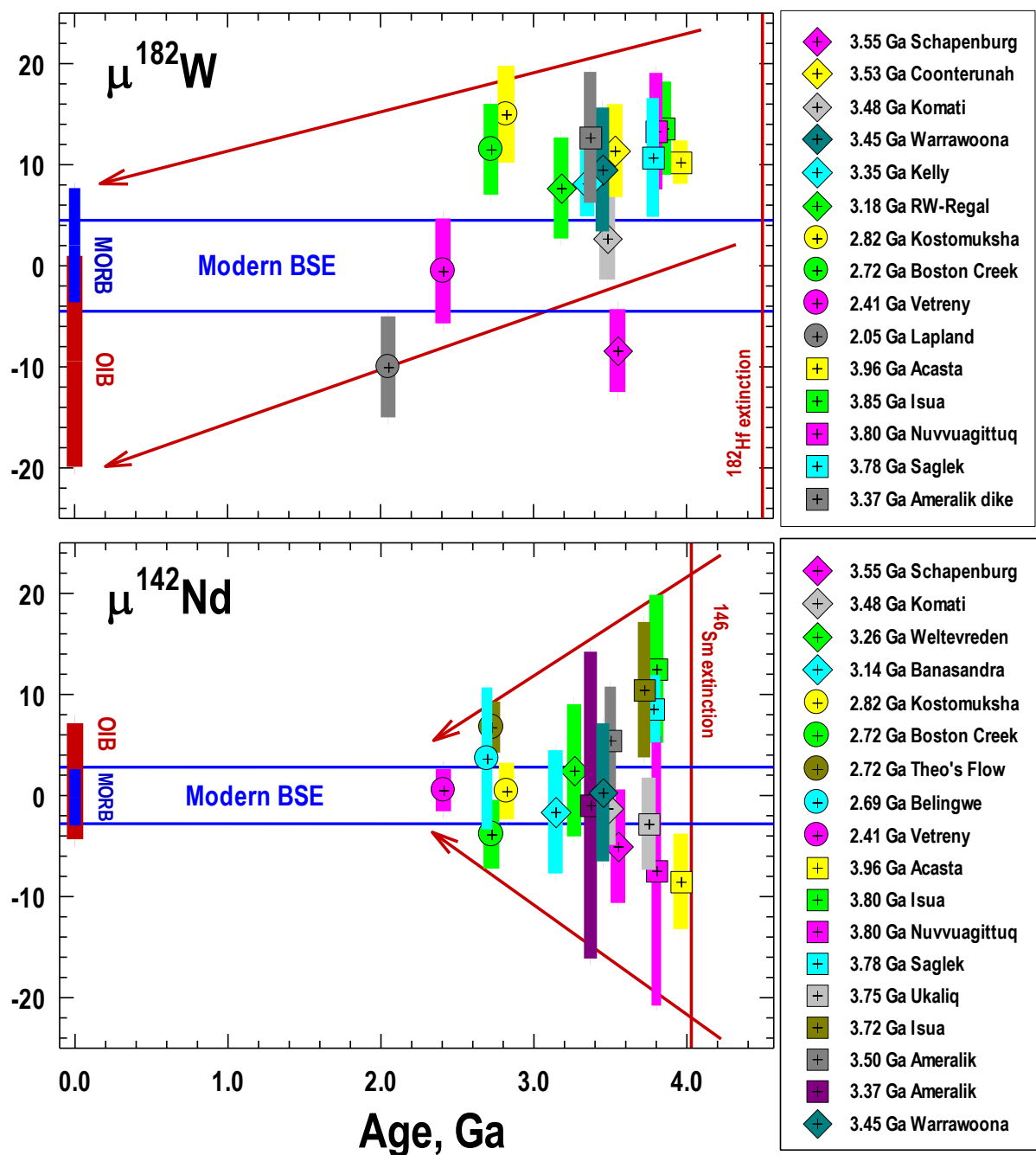


**Fig. 6.**



2215  
2216  
2217

2218 **Fig. 7**